A High Resolution Wide-Band Sonar Using Coded Noise-Like Waveforms And a Parametric Transmit Array

by

John Anthony Halsema

B.S Biomedical Eng Marquette University

(1978)

Submitted To The Department Of
Ocean Engineering
In Partial Fulfillment Of The Requirements
For The Degree Of

Ocean Engineer

at the

Massachusetts Institute Of Technology
February, 1992

Signature of Author.....
Department of Ocean Engineering Oct, 1991

Certified by.....
Arthur B. Baggeroer
Professor of Electrical and Ocean Engineering

Accepted by.....
A. Douglas Carmichael, Chairman
Department Graduate Committee
Department of Ocean Engineering

This report was prepared at the Charles Stark Draper Laboratory, Inc. under IR&D Project 341.

Publication of this report does not constitute approval by the Draper Laboratory or the sponsoring agency of the findings or conclusions contained herein. It is published for the exchange and stimulation of ideas.

I hereby consign my copyright of this thesis to the Charles Stark Draper Laboratory, Inc. Cambridge, Massachusetts.

.....

Permission is hereby granted by the Charles Stark Draper Laboratory, Inc. to the U.S. Navy and to the Massachusetts Institute of Technology to reproduce any or all of this thesis.

A High Resolution Wide-Band Sonar Using Coded Noise-Like Waveforms And a Parametric Transmit Array

by

John Anthony Halsema

Submitted to the Department of Ocean Engineering in partial fulfillment of the requirements for the degree of Ocean Engineer at the Massachusetts Institute Of Technology February, 1992

Abstract

A wide-band sonar has been developed which is capable of producing high resolution single beam images. The sonar uses pseudorandom broadband pulses with a bandwidth of 10 kHz to achieve a range resolution on the order of 16 cm. The active signal is centered at 10 kHz. Long range sound propagation is possible because of the low absorption loss at this frequency. A parametric transmit array is used to achieve azimuthal resolution and to eliminate the sidelobes from the active projector. This technique allows small physical arrays to produce very narrow beams. Because of this, the 330 mm diameter transducer produces a two degree beam at 10 kHz. In addition, the array has no measurable sidelobes which significantly enhances its performance in shallow water experiments.

This thesis discusses the basic theory behind pseudorandom broadband signals and parametric arrays. It then describes the system which was designed and built to support this research effort. A detailed account of the design process and the experimental program is provided. Finally, the results of an experiment which produced a high resolution single beam image of a vessel moored in less than 13 meters of water are discussed.

Thesis Supervisor: Arthur Baggeroer

Title: Professor of Electrical and Ocean Engineering

Acknowledgements

To begin, I would like to thank my advisor, Arthur Baggeroer, for his sage advice and enormous patience throughout this endeavor. Tom Muir at ARL provided the encouragement to attempt the experiment.

John Irza of the Charles Stark Draper Laboratory deserves special recognition for the many sleepless cold nights he spent watching my experiments and listening to my ideas. A special thanks to his wife, Ann, who provided moral support.

I would be remiss if I did not thank my wife, Terry, and my children, Maureen and Joey, for their support, patience, and understanding while 'Dad' was a graduate student.

I owe a great deal to many of the other students at MIT. In particular, Ken Rolt spent many long nights assisting with the Boston Harbor work. Ken also devoted a great deal of time in developing transducer models. Brian Tracey helped set up the hardware and assisted with data collection. Dave Mackovjak read, critiqued, and assisted in producing this thesis. Finally, I greatly appreciate the work Jerry Akerson did in reviewing my work and providing continuing encouragement.

Dedicated to my wife, Terry,

and my children, Maureen and Joey

Table of Contents

List of Figures

List of Tables

Chapter 1

Introduction

1.0 Purpose

The classification and identification of active sonar targets can be improved significantly by employing advanced signal processing hardware, wide-band pseudorandom noise waveforms, and parametric arrays. This thesis describes the design of such a system and the results of a series of experiments conducted to evaluate its capabilities.

1.1 The Need for High Resolution Active Sonars

Although the ability of active sonars to detect underwater objects has improved considerably, the poor classification capabilities of these systems has significantly degraded their usefulness. This limitation is particularly severe when the object being searched for is in the vicinity of a reflective boundary such as the surface or bottom. Under these conditions the sonar may well be able to detect the object, but the operators will be unable to separate the valid detection from the "clutter" of the boundary reflections. Recent examples of sonar searches for objects close to a boundary include the search for parts from the ill-fated space shuttle Challenger, which were scattered over various types of terrain on the Atlantic sea floor, and the search for mines which were tethered close to the surface and bottom in the shallow waters of the Persian Gulf. In both of these cases, the extremely high false

alarm rate caused by the adjacent boundaries greatly degraded the search effectiveness. In fact, many detections of potential objects of interest had to be classified visually by either underwater towed cameras or by personnel in manned submersibles. These particular cases illustrate the need for high resolution systems capable of providing acoustic "images" of sonar detections.

1.2 Overview of High Resolution Sonar Methods

Several methods have been investigated to improve active sonar resolution. Generally all of these methods rely on forming very narrow acoustic beams coupled with the use of wide-band waveforms. Narrow beams, which are necessary to improve azimuthal resolution, can be formed by several methods; including the use of high frequency arrays operating in the hundreds of kilohertz region, the formation of synthetic apertures, or employing interferometry techniques. Wide-band waveforms can improve the range resolution as well as potentially providing additional information about the target from the echo characteristics.

The primary reason for implementing a narrow beam system is that it can be used to ensonify different regions of the target to form an acoustic image. In addition to providing the ability to discriminate various parts of the target for imagery, narrow beam systems can also eliminate some multipath interference problems. Ideally the beam should be narrow enough to exploit a single direct acoustic path from the sonar to the target, thereby eliminating multipath target returns. Most conventional sonars receive target

echoes from several propagation paths, which causes varying estimates of target range, since the propagation time can be different for each path. When the sonar resolution is sufficient to resolve range differences between the various propagation paths, it becomes essential to eliminate the undesired paths, else the image will be distorted or false targets will be generated. Narrow beamwidths can also enhance system performance by eliminating boundary interactions. Avoiding boundaries such as the surface or the bottom can prevent, or at least substantially reduce, boundary reverberations.

The most common technique used to obtain high resolution sonar images is to form narrow beams with high frequency arrays. High frequency systems permit the use of small arrays, with significantly less weight and size than lower frequency systems. Unfortunately, the attenuation of high frequencies in the water is large in comparison to lower frequencies, therefore these systems are generally only useful for very short range work.

Another approach to the problem of forming a narrow beam is to synthesize a long baseline aperture by using a small physical array which is then moved through a distance equal to the length of the desired baseline. These "synthetic apertures" have performed well in the radar environment but relatively poorly in the sonar world. The principal limitation is related to the low propagation speed of sound in the water column. The impact of this low sound speed can be seen by examining the synthetic aperture formation process. Basically the aperture is formed by sampling the ocean at

many points with the physical array as it moves through the water and then coherently adding the samples after correcting the sample phase for physical array motion. As in a physical array, a sample must be taken at least every one-half wavelength to prevent spatial undersampling and the formation of grating lobes. Since it is generally not possible to discriminate between one pulse and the next in most active systems, the synthetic aperture sonar must wait for the return echo before transmitting again. The large time delay, due to the low propagation speed, can result in significant array motion between transmissions. If the velocity of the platform is excessive, the transmissions are separated in space by greater than one-half wavelength and spatial aliasing of the target position occurs. The velocity restriction imposed to avoid aliasing is often severe. For practical systems, velocities in excess of one knot may cause aliasing.

Finally, interferometry techniques are used to form narrow beams. Typically interferometry is performed by creating an array with the elements spaced sufficiently far apart to form intentional grating lobes and interference patterns. These interference patterns can then be interpreted to provide information about the azimuthal extent of the target. Similarly, if the hydrophones are oriented in the vertical direction, elevation information can be extracted by analyzing the interference pattern. Interferometry works well for bathymetry, but the interference pattern describes the extent of a target within the beam, not the actual structure of the target. Thus this technique defines the shape of larger targets, but it can not

always discriminate against multiple targets contained within the beamwidth.

Broadband pulses are used in high resolution systems primarily for their usefulness in estimating target range. In addition, these pulses also have the potential to improve target echo strength, reduce volumetric reverberation, and to aid in target classification by determining the target form function. In order to use these benefits at long ranges it is necessary to transmit the broadband pulse at a low frequency, which implies a low Q. Unfortunately, typical sonar projectors have high Q's, on the order of at least five to ten, which seriously limits the available bandwidth at lower frequencies.

One method to combine narrow beamwidth and wide bandwidth capabilities at low frequencies is to use a parametric source. This source relies on the nonlinear effects of propagation through the water column to form a virtual endfire array. The parametric array is usually created by using a physical source which radiates two primary frequencies, while the water column, acting as a mixer, produces a difference frequency. The difference frequency beamwidth is approximately the same as the beamwidth of the source at the primary frequencies. By using this technique small transducers with good high frequency directivity characteristics can be used to form narrow low frequency beams which will propagate much farther. In addition, relatively high Q devices can be used to produce broadband signals at the difference frequency. The major limitation in this type of system is the low conversion efficiency of

the mixing process. Typical mixing losses are on the order of -28 to -50 dB. While this might appear to be a severe penalty, the benefits of this type of system can more than offset its limitations.

1.3 Development of an Experimental High Resolution Sonar

The purpose of this research effort was to design, construct, and test an experimental high resolution active sonar system. "High resolution" was defined as a range resolution of less than 30 cm and an azimuthal resolution of less than five degrees. The system was also required to operate at frequencies below 20 kHz to reduce absorption losses and provide long range propagation. Finally, the system had to be capable of operation in less than 15 meters of water.

To achieve the range resolution specification a pseudorandom broadband pulse was selected with a nominal 3 dB bandwidth of 12 kHz. The pulse was generated by modulating a 10 kHz carrier with phase shift keying (PSK) using a 511 point maximal length sequence. A parametric array with a beamwidth of approximately two degrees was used to provide the required beamwidth and adequate transducer bandwidth. The effective Q of the system was less than one. An added benefit of the parametric array was the absence of sidelobes which greatly enhanced shallow water operations. Figure 1.1 illustrates the advantages of using of narrow beam systems without sidelobes in shallow water.

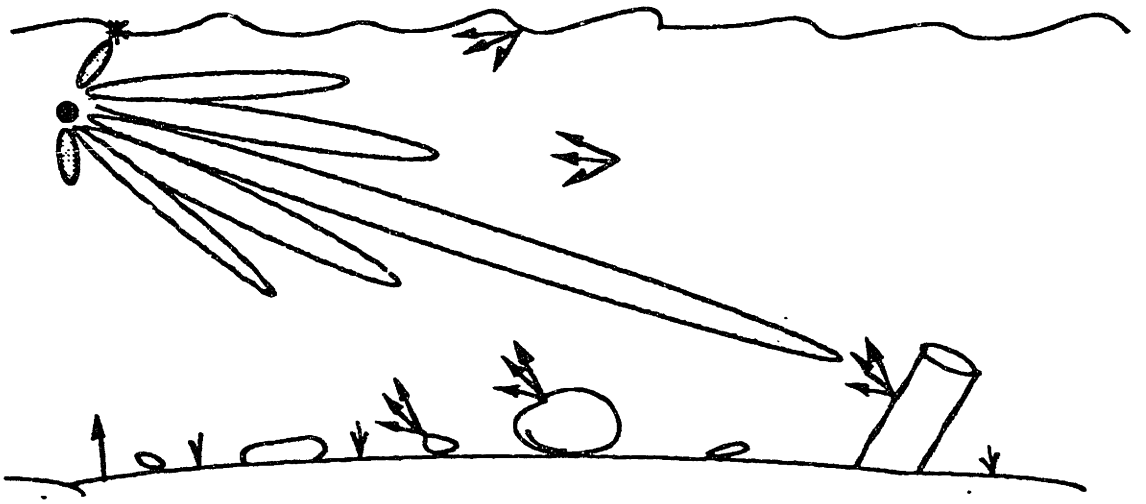

Figure 1.1 a Conventional sonar in shallow water.

This pictorial representation shows what happens when a conventional active sonar source is used in relatively shallow water. The target, represented by the cylindrical object on the bottom, is ensonified by the sonar beam, but the beam pattern sidelobes also cause echoes from numerous other objects, the surface and bottom interfaces, and volumetric scatterers in the water. In very shallow water, the bottom and surface echoes could continue to reflect from these interfaces several times, effectively "blinding" the sonar until the reverberations decay away.

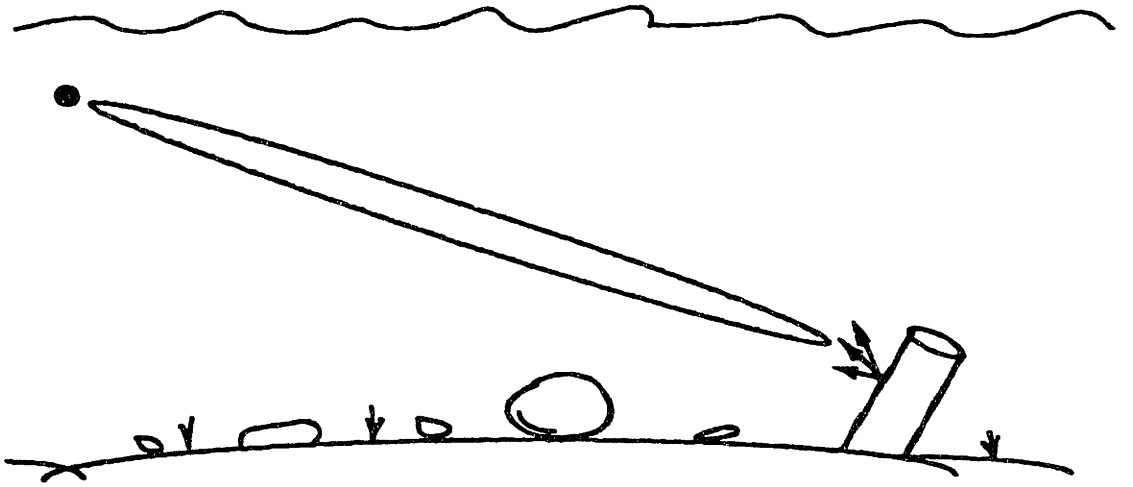

Figure 1.1 b Parametric sonar in shallow water.

In this diagram a parametric array is used as the active source. Note that because of the narrow beamwidth and the absence of sidelobes, the interfering echoes from the bottom, surface, and other targets are eliminated.

The receiver for this system was a standard correlation receiver, except that the signals were not basebanded prior to matched filtering. A Macintosh IIci computer, enhanced with a Spectral Innovations DSP-32c based array processor and data acquisition system, sampled the receive hydrophones and performed most of the receiver functions. The use of a parametric array in the transmitter greatly simplified the receiver design, since the narrow beamwidth ensured only a single acoustic path was used and the absence of sidelobes greatly reduced boundary reverberations. If an array with a large beamwidth had been used it would have been necessary to discriminate against multiple echoes caused by both volumetric and boundary reverberation.

The evaluation of the sonar was performed in Boston Harbor in approximately 12 meters of water. The system performed extremely well even in this adverse shallow water environment. To demonstrate the systems capabilities, a U. S. Coast Guard Seneca class cutter was used as a complex target for some of the experiments. A single beam high resolution image of the stern of the cutter clearly revealed the presence of both propellers, rudders and the skeg (a large planar surface at the center of the vessel). Individual objects on the cutter were resolved to within about 15 cm which clearly meets the range resolution specification.

1.4 Thesis Organization

This thesis is organized into six chapters with appendices. Chapter 1 contains the introduction which motivates the need for

high resolution active sonars. High resolution techniques are briefly discussed and a general description of the experimental system designed for this research effort, as well as a brief statement of its performance, are provided.

Chapter 2 introduces active waveform analysis theory, in the form of the ambiguity function, and the basic theory of a parametric array. In the first part of the chapter, ambiguity functions for narrow-band FM, wide-band FM, and pseudorandom broadband pulses are discussed. The advantages of pseudorandom broadband pulses in high resolution systems are also presented. Following a discussion of maximal length sequences the chapter goes on to discuss parametric array theory. The performance of a parametric array is analyzed using the Mellen-Moffet approach.

Chapter 3 discusses the considerations in designing a receiver for a high resolution system which uses a parametric array in the transmitter. The improvement in the receiver's performance due to the significant reduction in reverberation is discussed.

Chapter 4 presents the detailed design of the experimental system's receiver and transmitter components. The system actually used in the experiments is described in detail in the first part of the chapter. Modifications to the system which were implemented after the completion of the testing are presented at the end of the chapter.

Chapter 5 provides a detailed description of the experimental program. This chapter is the longest in the thesis and provides

detailed information about the evolution of the system throughout the test program. The enormous potential of a system such as this is indicated in the last sections of this chapter, which discuss the results obtained when the stern section of a large vessel was used as the target.

Chapter 6 is the final chapter which offers conclusions, a discussion of planned future experiments, and recommendations for the future development of a more advanced high resolution system.

Chapter 2

Active Waveform and Parametric Array Theory

2.0 Introduction

High quality acoustic images require a sonar system with superior resolution in both azimuth and range. For most existing designs the range resolution is achieved by designing signals which can be "compressed" in a correlation receiver to yield precise time delay estimates. Frequently, this is accomplish by using large time-bandwidth product pulses. This chapter discusses the basic waveform evaluation tools along with the performance of two large time-bandwidth product waveforms. The advantages of a pseudorandom broadband pulse in a high resolution sonar are also presented.

Azimuthal resolution can be achieved by building arrays with large apertures or by using nonconventional techniques such as parametric arrays. Parametric arrays are useful because they allow low frequency high bandwidth signals to be transmitted while simultaneously generating a narrow transmit beam. The basic techniques for predicting the performance of a parametric array are also discussed in this chapter.

2.1 Waveform Analysis Using Ambiguity Functions

Active signals are evaluated with the ambiguity function, defined by Woodward [Stewart, 1959] as:

$$\psi(\tau,\delta) = \int s(t)\, s^*(t-\tau)\, e^{-i\delta t}\, dt,$$

where:

τ is the time delay,

* indicates complex conjugate, and

δ is the Doppler shift using the narrow-band approximation.

This function is the analytical tool for examining the characteristics of a correlator receiver in estimating the delay (range) and Doppler (velocity) of the received signal. Although the Woodward ambiguity function is formulated for narrow-band signals, it can serve as an approximation for large time-bandwidth waveforms if the small Doppler assumption is made. Under this assumption the effects of the signal's time compression or expansion are ignored. That is, only small Doppler values are considered and Doppler is treated as a simple frequency translation of the received spectrum. The small Doppler approximation is useful for quick estimates of a signal's performance in the vicinity of $(\tau,\delta)=(0,0)$, but for some large time-bandwidth product signals it can lead to large errors at even modest Doppler shifts.

For large time-bandwidth product signals, the Woodward ambiguity function can be modified to reflect the true compression or expansion of the signal caused by motion of the target. This wide-band ambiguity function is of the form:

$$\psi(\tau, \phi) = \int s(t)\, s^*(\gamma t - \tau)\, e^{-i\phi t}\, dt$$

where:

γ incorporates the time compression of the waveform, and

ϕ is the true Doppler.

While the wide-band ambiguity function incorporates the true Doppler effect, thus producing a more accurate representation of the characteristics of the correlation receiver, it can be difficult to calculate analytically. For many waveforms a closed form solution may not be available or if one is it may be computationally prohibitive to calculate. A useful approach is to evaluate the wide-band ambiguity function for a general class of signals and then employ the Woodward ambiguity function for specific signals in the class. If the wide-band ambiguity function does not show significant peaks or sidelobes outside the vicinity of $(\tau,\delta)=(0,0)$, the Woodward ambiguity function will be useful in characterizing the performance of the receiver.

2.2 High Resolution Waveforms

There are many types of wide-band waveforms available for high resolution active sonar systems. The most common of these is linear frequency modulated (LFM), also referred to as swept FM, FM slide, or chirp. This waveform is created by sweeping the transmit frequency at a constant rate throughout the transmission period. In addition to LFM there are numerous variations on this concept, such as hyperbolic FM (HFM), where the frequency sweep rate is a function of time during the transmission. Another type of wide-band

waveform, pseudorandom broadband, originates from the spread-spectrum community and is based on a binary sequence modulating either the phase or the frequency-time pattern of the active transmission. This signal has unique characteristics which are useful in high resolution sonars.

One criteria for a 'good' wide-band signal is that it must provide adequate time and Doppler resolution while offering coherent processing gain against noise. Generally this is achieved by designing signals with large time-bandwidth products. However, although an arbitrary signal with a large time-bandwidth product may offer good performance in estimating time delay, it may be a poor estimator of Doppler and vice-versa. Other signals may provide good local estimates of both time delay and Doppler with a single target or propagation path, but poor or erroneous localization information in the case of multiple close reflectors or multiple propagation paths. As discussed in the preceding section, the ambiguity function is used to evaluate the performance of signals under these conditions. In the following sections LFM and pseudorandom broadband waveforms are evaluated using this function.

2.2.1 Linear FM Signals

The well-studied LFM signal, represented by:

$$s_{lfm}(t) = \cos[\,\omega t + 0.5\,\mu t^2\,],$$

where:

μ is the frequency sweep rate,
t is time in seconds, and

ω is radian frequency

has a characteristic ridge in the delay-Doppler plane as shown in Figure 2.1. This ridge creates a delay-Doppler ambiguity condition. If either the target's Doppler or time delay is known, the other parameter can be uniquely determined; otherwise, there is a region of uncertainty which bounds the time delay and Doppler estimation errors. Increasing the time-bandwidth product produces an ambiguity function which no longer has the ridge-like structure, but instead has a well defined local peak with large amplitude sidelobes as shown in Figure 2.2. This is an example of a signal which, due to the high sidelobes, requires the use of the wide-band ambiguity function to properly evaluate the receiver characteristics.

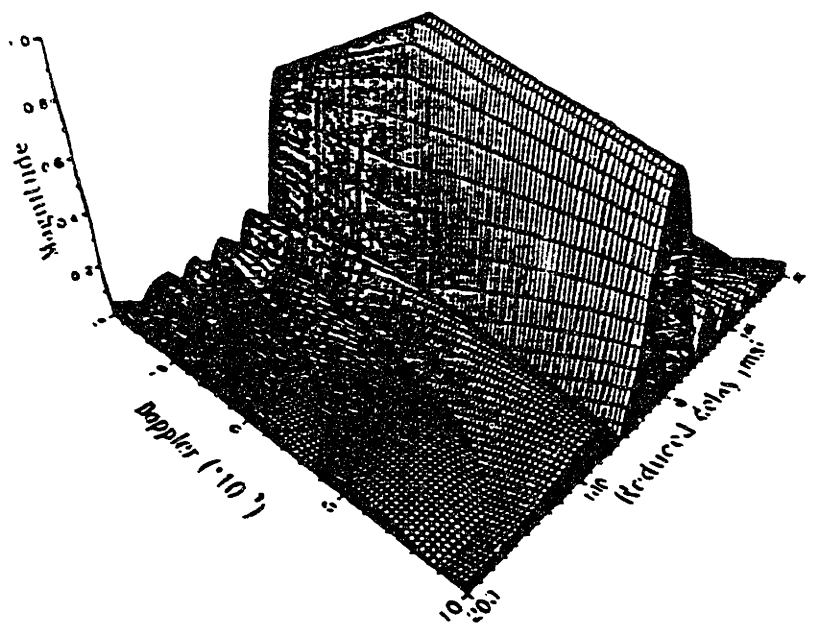

Figure 2.1 Ambiguity surface for narrow-band LFM waveform.

Reproduced from Hermand and Roderick, 1988

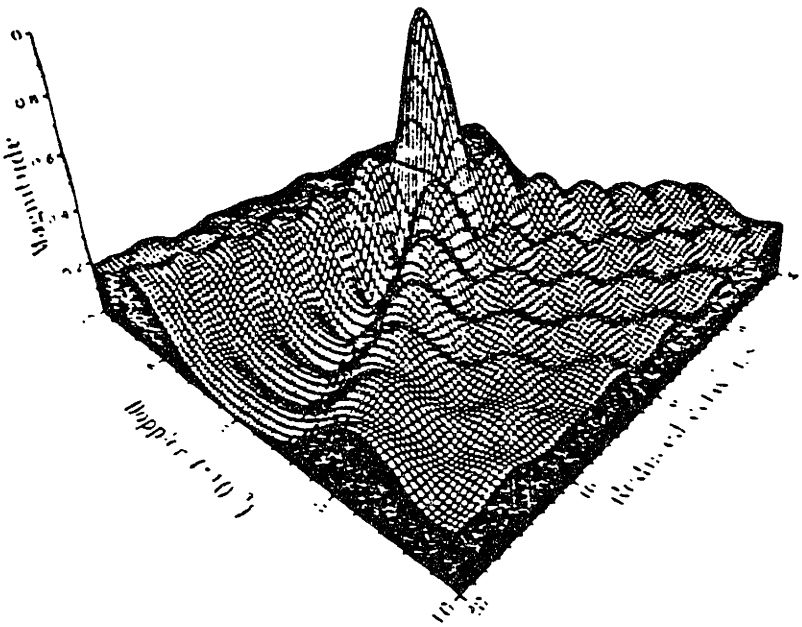

Figure 2.2. Ambiguity surface for wide-band LFM waveform.

Reproduced from Hermand and Roderick, 1988

2.2.2 Pseudorandom Broadband Signals

The pseudorandom broadband bi-phase-modulated signal can be represented as:

$$s_{pn}(t) = \cos[\omega t + \mu c(t)]$$

Where:

μ is the modulation angle, and
c(t) is the modulating sequence normalized to [-1, 1].

If the modulating sequence is composed of a maximal length sequence, the ambiguity function closely approximates the ideal 'thumbtack' response as shown in Figure 2.3. Unlike the LFM case when pseudorandom broadband signals are used the time delay and Doppler dimensions can be tailored independently . The extent of the ambiguity peak on the Doppler axis is primarily controlled by the

pulse width, while on the time delay axis it is determined from the 'chipping' rate. (Chipping rate is defined as the rate at which new digits from the modulating sequence are supplied to the modulator.) As a result of the independence between the dimensions of the ambiguity function, it is a straightforward procedure to design a signal to meet the time delay and Doppler resolution requirements by simply selecting the required pulse length and chipping rate. After these parameters are known, the length of the modulating sequence can be ascertained and an appropriate sequence chosen. Maximal length sequences of various lengths are tabulated in a variety of sources.

The ambiguity function for the pseudorandom broadband signal has several features that are worth noting. First, the sidelobes are essentially flat, forming a pedestal whose size is equal to twice the pulse width in the Doppler direction and twice the bandwidth in the delay direction. Second, the peak to sidelobe ratio is $N^{-1/2}$ where N is the number of digits in the maximal length sequence. Third, the ambiguity function peak has an extent which is the reciprocal of the chipping rate in the time delay direction and the reciprocal of the pulse duration in the Doppler direction. And finally, since large sidelobes are not present outside the vicinity of the origin, the Woodward ambiguity function provides useful estimates of receiver performance. Extensive investigations into the true wide-band ambiguity function have shown that the major sidelobes are close to the Doppler axis (τ=0). The Woodward ambiguity function closely approximates the maximum sidelobes with a sinc function on the

Doppler axis. This is because on the Doppler axis the product $s(t)\ s^*(t-\tau)$ is one, reducing the ambiguity function to the transform of a boxcar, which is of course a sinc function. For most applications this is a suitable representation of the true ambiguity function.

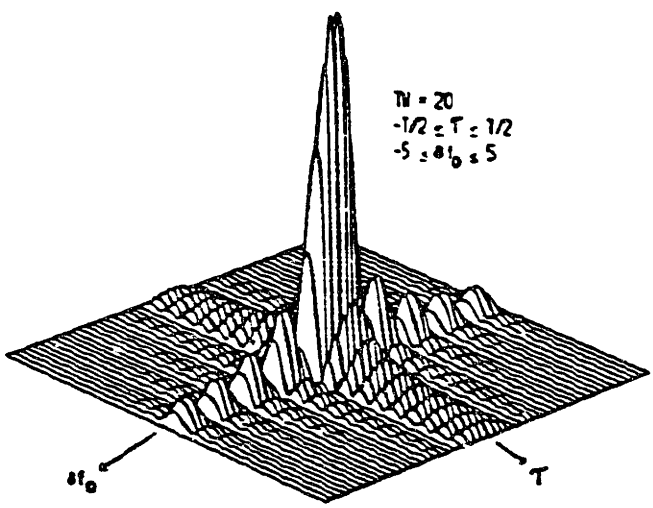

Figure 2.3 Typical ambiguity surface for pseudorandom broadband waveform.

Reproduced from Glisson *et al.*, 1970

2.2.3 Pseudorandom Broadband Advantages

The LFM waveform has historically been the waveform of choice for high resolution systems, but there are several advantages to pseudorandom broadband. Some of the more significant advantages are:

1) Pseudorandom broadband signals produce a well defined peak in the ambiguity surface which has a nearly ideal 'thumbtack' characteristic.

2) The design of pseudorandom broadband signals is greatly simplified by the independence of the time delay and Doppler estimation characteristics of the signal.

3) The pseudorandom broadband signal has lower local sidelobes than the equivalent wide-band LFM. The sidelobes are compressed into a pedestal which surrounds the local maximum.

4) Several maximal length codes with low cross-correlation peaks can exist for a given length sequence. This allows higher data rates to be used or the use of different codes in adjacent beam transmissions.

5) The pseudorandom broadband signal provides a measure of security and could be used under conditions where it is necessary to minimize the probability that the active transmission would be detected.

One potential complication from using the pseudorandom broadband is that the thumbtack nature of the ambiguity surface requires implementing banks of Doppler filters to cover the anticipated range of target velocities. From a detection standpoint, the LFM ambiguity surface has a much higher Doppler tolerance, although the penalty for this increased tolerance is an uncertainty in the targets position. Resolving this uncertainty requires either the

use of additional data from other sensors or estimating the range and Doppler with a target tracker. Thus, while the LFM receiver may be simpler, more post-detection hardware or processing may be required to fully exploit the signal. In the pseudorandom broadband case, all of the information is available in the correlator outputs. Additionally, for applications with stationary targets, it is not necessary to employ a Doppler filter bank since ownship Doppler can be incorporated into a single (zero target Doppler) correlator.

Good Doppler resolution can also be advantageous when higher data rates are required. In cases where it is necessary to transmit at a rate where the target's range becomes ambiguous, the use of coded waveforms which do not interfere with each other can improve global ranging accuracy. For example, if a target is at a range of 750 m the sonar can determine the range without ambiguity if the pulse repetition frequency (PRF) is greater than one transmission per second. Suppose that the required data rate is five updates per second. Now, if an identical waveform is transmitted each time, the returns from one transmission will arrive at the receiver after the next transmission has already occurred. As long as the global range to the target is known this approach will yield the required data rate, but absolute global range cannot be measured and new target detections will have ambiguous ranges. If five different coded waveforms are available and transmitted sequentially, it is possible to still unambiguously resolve range as long as the cross-correlation between the codes is low, as compared with the individual code. This cross-code interference level can be

determined by a straightforward modification to the ambiguity function. The peak interference levels are tabulated for different codes in various references.

Another method to increase the data rate is to use the same code for each transmission, but translate the frequency of subsequent transmissions to points outside the ambiguity function peaks of the previous transmissions. For example, if a given waveform has an ambiguity function main lobe width of 20 Hz in the Doppler direction then translating the next transmission to a center frequency 20 Hz higher than the previous transmission would result in relatively low cross-correlation between the two transmissions. In practice, additional frequency separation between the transmissions would be required to account for the anticipated range of target Dopplers and to allow for equipment tolerances. For high bandwidth signals, this scheme can allow the same code to be used unambiguously in several transmissions with only a slight increase in system bandwidth.

Now consider the use of the pseudorandom broadband and LFM waveforms in the case of a target possessing multiple highlights (perhaps with different Doppler shifts). Both waveforms have a bandwidth of 12 kHz and a center frequency of 10 kHz. The target consists of two closely spaced zero Doppler reflectors. To analyze the LFM case, the wide-band ambiguity function must be used due to the large sidelobes outside the immediate region of the origin. With the LFM waveform, as shown in Figure 2.4, a complex ambiguity surface with numerous false peaks and high sidelobes is generated,

which would confuse the receiver with multiple false targets. In fact, large peaks in the output of the correlator filters may be completely erroneous as a result of near-in constructive and destructive interference between the individual component echoes [Hermand and Roderick, 1988]. When the pseudorandom broadband is used, the higher resolution, in both delay and Doppler, combined with the relatively low sidelobes in the ambiguity surface, separates the individual highlight returns and avoids the generation of false targets.

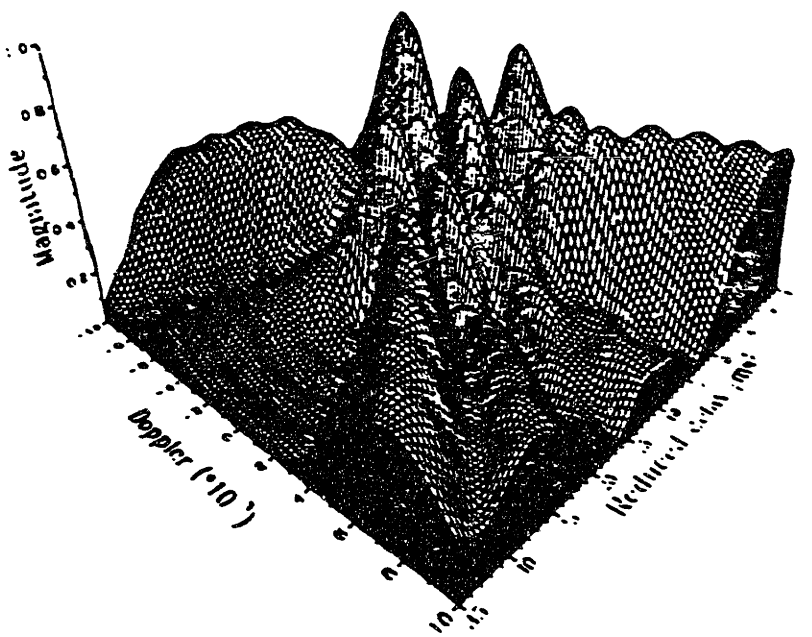

Figure 2.4 Ambiguity surface for LFM waveform with two closely spaced targets. Reproduced from Hermand and Roderick, 1988

Clearly, although the receiver complexity is greater, the improvement in target resolution using the pseudorandom waveform is dramatic. This significant improvement in resolution can support applications such as acoustic imagery. Further, the resolution offered by this class of waveforms improves tracking filter performance during acquisition and while maintaining track.

2.3 Maximal Length Sequences

Maximal length sequences or maximal length shift register sequences are binary sequences which can be generated by shift registers with the appropriate feedback connections. While it is clear that for an N stage shift register the longest possible sequence which can be produced prior to repeating the sequence is 2^N-1, it can also be shown that other sequences exist with a period of 2^N-1. Such sequences are known as maximal length sequences. Since these sequences exhibit the properties which are characteristic of Bernoulli random processes, they are also frequently referred to as pseudorandom sequences. Various publications have tabulated all of the known feedback connections and register seed values which yield a maximal length sequence for values of N.

Maximal length sequences have three interesting properties which enhance their utility in active sonar signal applications. First, the number of ones in the sequence is always exactly one more than the number of zeros. This feature is very useful in generating suppressed carrier signals. When using biphase modulation the

maximum carrier suppression that can be achieved is $(2^N-1)^{-1}$. This is only achievable because of the relative balance between the ones and zeros in the sequence. Second, the distribution of ones and zeros is well known and corresponds closely to a Bernoulli sequence. A run is normally defined as a consecutive group of all ones or zeros. There are exactly $2^{N-(p+2)}$ runs of length p for both ones and zeros in the code sequence, except for some special cases, such as there are no runs of N zeros. Due to the distribution of ones and zeros it can be shown that a maximal length sequence approaches the characteristics of truly random noise. This does not imply that the sequence itself is random, as it is obviously deterministic based on the shift register configuration. It does mean, however, that for small sections of the sequence the distribution appears truly random. Third, the correlation function of a periodic maximal length sequence of infinite extent is -1 everywhere except at the peak where it is 2^N-1. It is the characteristics of this correlation function which lends much of the utility of these sequences in active sonar waveforms.

2.4 Parametric Array Theory And Westervelt's Model

A parametric sonar exploits the weak nonlinear response of the ocean medium to generate a low frequency acoustic source using primary waveforms operating at much higher frequencies. Arrays created in this manner are capable of generating low frequency signals with wide bandwidths, very narrow beamwidths, and essentially no sidelobes. Consider what happens when two discrete frequencies (the primaries) with frequencies f_1 and f_2 are

processed through a nonlinear... (e.g. a mixer). The resultant output consists of the original frequencies, their harmonics (at frequencies nf_1+mf_2, where m and n are positive integers), and their subharmonics (at frequencies nf_1-mf_2). Since absorption in the ocean increases with frequency, the higher harmonics are rapidly attenuated while the lower frequency components, with even less attenuation than the primary signals, can propagate to long ranges. The exponential attenuation with range creates a long baseline exponentially shaded array of virtual sources. This long baseline and the exponential shading are responsible for the unusual parametric array beampattern.

2.4.1 Difference Frequency Generation

The mixer effect of the parametric array is caused by slight nonlinearities in the propagation of sound through water. Linear sound propagation of plane waves in the water is normally described by the linear wave equation.

$$\omega^2\nabla^2 p - k^2\frac{\partial^2 p}{\partial t^2} = 0$$

where:

ω is the radian frequency,
k is the wavenumber which is given by ω/c, and
c is the velocity of sound in the medium which is assumed to be constant.

This linear equation can be derived from the nonlinear Navier-Stokes equations by assuming that the viscosity is zero and by neglecting second and higher order terms in the equations of state. While these

assumptions are reasonably valid for most applications, there is in fact a contribution from these higher order terms.

The more general Navier-Stokes equations, shown here vector form, describe the movement of a particle in a fluid medium.

$$\frac{\partial \mathbf{V}}{\partial t} + (\mathbf{V} \cdot \nabla)\mathbf{V} = -\frac{1}{\rho}\nabla p + \nu \nabla^2 \mathbf{V} + \frac{1}{\rho}\mathbf{F};$$

where:

$\mathbf{V}$ is the velocity vector,
ρ is the density,
p is the pressure,
ν is the viscosity, and
$\mathbf{F}$ is the external force vector..

This nonlinear partial differential equation is difficult to solve except under very simple conditions. Two additional equations are also required; the continuity equation, and the equation of state.

The continuity equation is:

$$\frac{\partial \rho}{\partial t} + \nabla \cdot \rho \mathbf{V} = 0;$$

and the equation of state is:

$$\rho = \rho(p) = \rho_0 + \frac{1}{c_0^2}(p - p_0) - \frac{\varepsilon - 1}{c_0^4 \rho_0}(p - p_0)^2 \ldots;$$

where ε is the parameter of nonlinearity.

The equation of state shown above is a power series expansion of the density in terms of the acoustic pressure and is the key expression for understanding why acoustic propagation is not completely linear. As the acoustic pressure wave passes through a

point the density of the water does, in fact, change. Since sound velocity is dependent on the density of the medium, it also changes. As a result the higher pressure (compression) regions travel faster than the lower pressure (rarefaction) regions. If a sinewave is propagating through a medium with these characteristics the waveform will begin to distort as the high pressure regions "catch up" with the low pressure regions. Figure 2.5 shows a schematic sketch of this effect.

The equation of state also shows why the magnitude of the nonlinearity is dependent on the amplitude of the acoustic wave. At low acoustic pressures the nonlinear term is insignificant and propagation is essentially linear. As the pressure increases the nonlinear term becomes increasingly important and the waveforms begin to distort. If the pressures are high enough and the propagation path sufficiently long, the higher pressure region will actually appear to be overtaking the lower pressure region. Clearly it is not physically meaningful for one to over run the other, but a shock wave begins to form and significant distortion occurs. At this point any additional power at the driving frequency will be converted to energy at harmonically related frequencies.

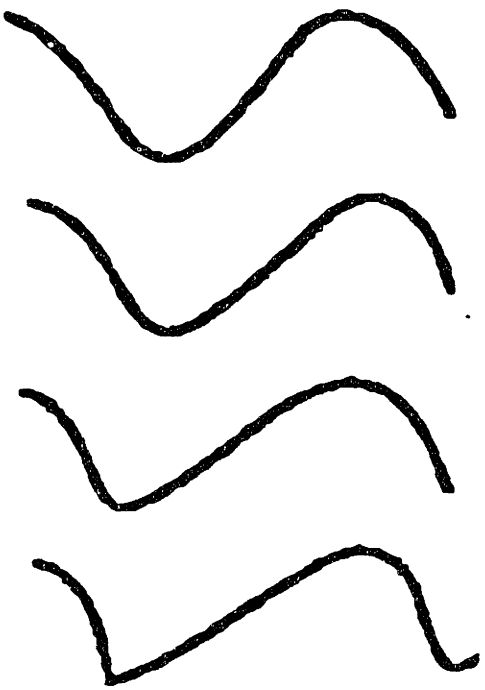

Figure 2.5 Schematic showing the effect of nonlinear sound propagation.

The top sketch shows the original sinewave. The following figures show the progressive distortion as the high pressure regions travel faster than the low pressure regions. Finally the high pressure region "catches up" with the low pressure region and a shock wave forms.

Now if two discrete frequencies are present in the water column at the same time these signals will sum together and create an envelope function which also varies the pressure field. This envelope distorts as the primary frequencies distort, giving rise to the generation of the sum and difference frequencies. The period of the envelope function, in relation to the period of the mean primary frequency, is a factor in determining the amount of difference frequency signal produced. As the period of the envelope function approaches the period of the primaries, the envelope undergoes greater distortion from the primary distortion, thereby increasing

the amount of difference frequency energy produced. The ratio of the difference frequency to the mean primary frequency, (fd/fp), is an important parameter which expresses the relative difference between the primary and secondary periods. The conversion efficiency generally varies as $(fd/fp)^2$ for far-field parametric arrays and $(fd/fp)^4$ for near-field arrays. A far-field array is one in which significant primary to difference frequency conversion takes place in the far-field, while a near-field array converts most of the energy within a Rayleigh length of the physical array.

2.4.2 Parametric Array Bandwidth and Frequency Amplitude Shading

Parametric arrays are capable of transmitting higher bandwidth signals at the difference frequency than conventional transducers. While most conventional sonar transducers have a minimum Q of approximately 10, which limits the bandwidth of these devices, the parametric array is capable of achieving Q's on the order of one. The exceptionally low Q is possible because a small change in the primary frequency, relative to the mean primary frequency, produces a large change at the difference frequency relative to the mean difference frequency. Thus, while the physical array transmits a relatively narrow-band signal, the parametric array output can have wide-band characteristics. In addition, unlike conventional arrays, the difference frequency beamwidth is essentially constant over the bandwidth. This feature greatly simplifies the design of low frequency wide-band active arrays.

When wide-band signals are used as one of the primary components it is possible that the conversion efficiency will vary across the signal's bandwidth. This effect, often called frequency amplitude shading [Noviko, Rudenko, Timoshenko, 1987], occurs when wide-band LFM signals are used. As the frequency of the LFM signal increases the envelope function period decreases, thereby raising conversion efficiency. The difference in conversion efficiency across the bandwidth of the signal can be quite large, leading to undesirable amplitude shaping of the signal's spectrum.

When PSK signals are used as one of the primary components, frequency amplitude shading does not occur. The reason for this is best seen by examining the waveform in Figure 2.6, which is the result of summing a CW component and a PSK modulated signal using a maximal length sequence as the modulation. The difference frequency for this case is the reciprocal of the chipping rate. Whenever the value of the maximal length sequence does not change from one chip to the next the waveform appears to be simply the sum of two CW components. When the sequence does change value there is a shift of $\pi/2$ in the phase of the envelope function as shown in Figure 2.6. Berktay has shown that the difference frequency amplitude is proportional to the first derivative of the square of the envelope function [Berktay, 1965]. Since for the PSK function the first derivative of the square of the envelope function is the same as in the CW case, with the exception of the point where the phase changes, the PSK conversion efficiency should be approximately the same as in the CW case. Another way to look at this is by looking at

the shape of the envelope. Obviously when a digit does not change value the envelope is identical to that of the sum of two CW signals. When the digit does change value the shape of the envelope initially resembles one half of the two frequency CW envelope. As stated previously the distortion of the envelope is what causes the formation of the difference frequency. The portion of the envelope which is caused by the change in the value of the sequence will distort the same way as the leading or trailing edge of the dual CW envelope and therefore the conversion efficiency should remain unchanged.

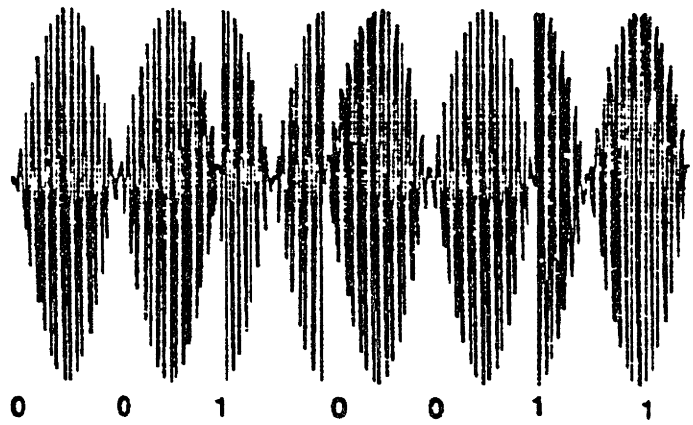

Figure 2.6 Plot of a section of the input waveform to the parametric array.

This waveform consist of a 164 kHz CW component summed with a PSK signal centered at 154 kHz and modulated with a maximal length sequence. The actual value of the sequence is shown below the plot. Note that as long as the sequence does not change value the envelope has the same shape as it would for two CW signals. When the sequence does change value the phase of the envelope abruptly shifts by $\pi/2$.

2.4.3 Parametric Array Beampatterns

The beampattern of a parametric array is unique in that it produces highly collimated beams at low frequencies with virtually no sidelobes. Westervelt was the first to recognize this and proposed a model which resembles an end-fire line array with exponential shading [Westervelt, 1963]. He proposed that the nonlinear conversion process produced a continuum of virtual sources along the axis of the primaries. The acoustic source density along this array is described by:

$$q = \beta \rho^{-2} c^{-4} \frac{\partial p_0^2}{\partial t}$$

where:

β is the parameter of nonlinearity (3.5 in water), and

p_0 is the primary pressure.

From here the acoustic field produced by this array can be computed using Lighthill's equation:

$$P(r,t) = \frac{1}{4\pi} \int dr_x \int dr_y \int dr_z \frac{1}{|R-r|} \frac{\partial}{\partial t} q\left[R, \frac{|R-r|}{c}\right]$$

where:

R is the is the position vector of the observation point,

r is the position vector of the source points,

and the region of integration covers the source volume.

The equations used to model the primaries must include the exponential shading effect from small signal absorption. As a result

of this absorption the array is exponentially tapered and is limited in length by the decreasing source strength. The beampattern generated by such an array contains a narrow main lobe with an almost complete absence of sidelobes.

While the Westervelt approach is somewhat intuitive, it has substantial limitations which must be considered when it is used for performance predictions. These limitations are caused by the assumption that small signal absorption is the predominant factor in determining effective array length and that parametric conversion occurs in the near-field of the physical array. The equation does not account for any nonlinear losses in the primary or for the diffraction i.e. spreading of the primary beam.

There are three general operating regimes for parametric radiators. The first region is one in which the parametric array length is contained in the near-field of the physical array and is limited only by small signal absorption. This first regime is modeled by Westervelt's equations assuming an ideal physical array. When the parametric array length is longer than the physical array's near-field, but still limited only by small signal absorption, the diffraction of the primaries must be considered. This is the second region of operation. As primary power increases shock waves begin to form in the primary and additional energy is rapidly lost to nonlinear attenuation, thereby limiting the length of the parametric array. This is the third region of operation and corresponds to saturation of the array. Shock waves begin to form when the normalized source strength as defined below exceeds 280 dB.

2.5 Performance Predictions

Several methods exist for predicting the performance of a parametric source. Using Westervelt's equations, nomograms [Urick, 1983] can be developed which yield quick, but overly optimistic, performance assessments. There are two limitations in this and similar methods. First is the failure to account for the finite aperture effects of the physical array. Second is the assumption that the effective end-fire array length is controlled by small signal linear absorption of the primary beams within the Rayleigh distance of the real array. Thus these models would never show the effects of phenomena such as array saturation, which is caused by nonlinear absorption within the Rayleigh distance. A good model for predicting far field performance when CW signals are used is the Mellen-Moffet model [Mellen and Moffet, 1976]. The principal weakness in this model is that it assumes that the primary components are plane waves out to the Rayleigh distance and that past this distance the waves undergo spherical spreading. The plane wave assumption introduces some errors into the analysis which have been measured experimentally. Nevertheless, this does not appear to detract significantly from the model as it has historically yielded excellent quality predictions.

To simplify the application of the Mellen-Moffet approach, a series of design curves have been developed and published [Mellen Moffet, 1976 in Scientific and Engineering Studies, Nonlinear Acoustics, 1954 to 1983]. The curves are based on the solution to

the following three equations which describe parametric gain, beam pattern, and directivity gain:

$$g = \frac{\chi}{2}\left(\frac{f}{f_0}\right)^2 \int_0^\infty T^2(r')\left(1 + j\,\frac{f r'}{f_0 R_0}\right)^{-1} \frac{d\,r'}{R_0};$$

$$|D(\theta)|^2 = (\cos\gamma)^2\,|D_{ap}(\theta)|^2 \left\{1 + \left(\frac{2 d_0 f_0}{\chi f}|g|\cos\gamma\right)^2 \left(\sin\frac{\theta}{2}\right)^4\right\}^{-1} + (\sin\gamma)^2\,|D_0(\theta)|^4;$$

$$\delta = \left(\frac{\pi}{4}\frac{\chi}{|g|}\frac{f}{f_0}\cos\gamma + \frac{1}{2}(\sin\gamma)^2\right)^{-1};$$

where:

g is the complex parametric gain,
$\chi = 2\pi\beta_0 P_0 R_0 f_0/\rho c^3$ is a measure of the shock formation in the collimated zone,
f is the difference frequency,
f_0 is the mean primary frequency,
T^2 is the primary wave taper function,
$D(\theta)$ is the difference frequency beam pattern,
$D_{ap}(\theta)$ is the aperture correction factor,
$D_0(\theta)$ is the primary beam pattern,
d_0 is the primary beam directivity factor, and
γ is the phase angle of complex parametric gain

The parametric gain, g, calculated from the above equation is a complex value. The magnitude of this value represents the conversion loss while the phase represents the type of parametric radiator. Although the magnitude of g is positive, this represents conversion loss and does not imply the array has positive gain. Typical conversion losses can range from -20 to -60 dB. Phase

angles near zero represent near-field arrays while those near $\pi/2$ represent far-field arrays.

To use the Mellen and Moffet curves requires the calculation of the following parameters as entering arguments: the normalized primary source strength, L^*; the product of the attenuation coefficient and the Rayleigh distance, αR_0; and the frequency downshift ratio, f_r. The normalized primary source strength is defined as:

$$L^* = L_0 + 20\log(f_0 \times 10^{-3})$$

with L_0 in dB re mPa / meter and f_0 in Hz. The attenuation coefficient should be calculated with Shulkin and Marsh's equation [Shulkin and Marsh, 1963]:

$$\alpha = \left(\frac{2.34\times10^{-6} \times S \times f_T \times f^2}{f_T^2 + f^2} + \frac{3.38\times10^{-6} \times f^2}{f_T} \right) \times \left(1 - 6.54\times10^{-4} \times P\right) 8.686$$

where:

S is the salinity in ppt,

$f_T = 21.9\times 10^{\,6-1520/(T+273)}$ with T in degrees C. f_T in kHz, and 8.686 is the conversion from nepers to dB.

The Rayleigh distance, commonly referred to as the near field distance, is the ratio of the projector area to the wavelength. Finally, the frequency downshift ratio is merely the ratio of the mean primary to secondary frequency.

$$R_0 = A/\lambda_0$$

$$f_r = f_0/f$$

As an example consider an experiment which uses a 50 percent efficient, 30.5 cm piston array, with an electrical peak input power of nominally 1 kW per primary. The proposed system operates with a mean primary frequency of 180 kHz and a difference frequency of 10 kHz. Under these conditions the following values are needed to predict the system performance.

$f_0 = 180 \times 10^3$
$f = 10 \times 10^3$
$R_o = 898.6$ cm
$\alpha R_o = .622$ dB
$D_I = 40.7$ dB
$L^* = 284$ dB

Using these values to enter Figures 2.7-2.9 the performance of the array can be estimated. The figures selected are for an αR_0 of 0.5 dB and represent the closest appropriate figure from the design curves provided by Moffet and Mellen. The calculations can be improved by interpolation, but in general the corrections are relatively small.

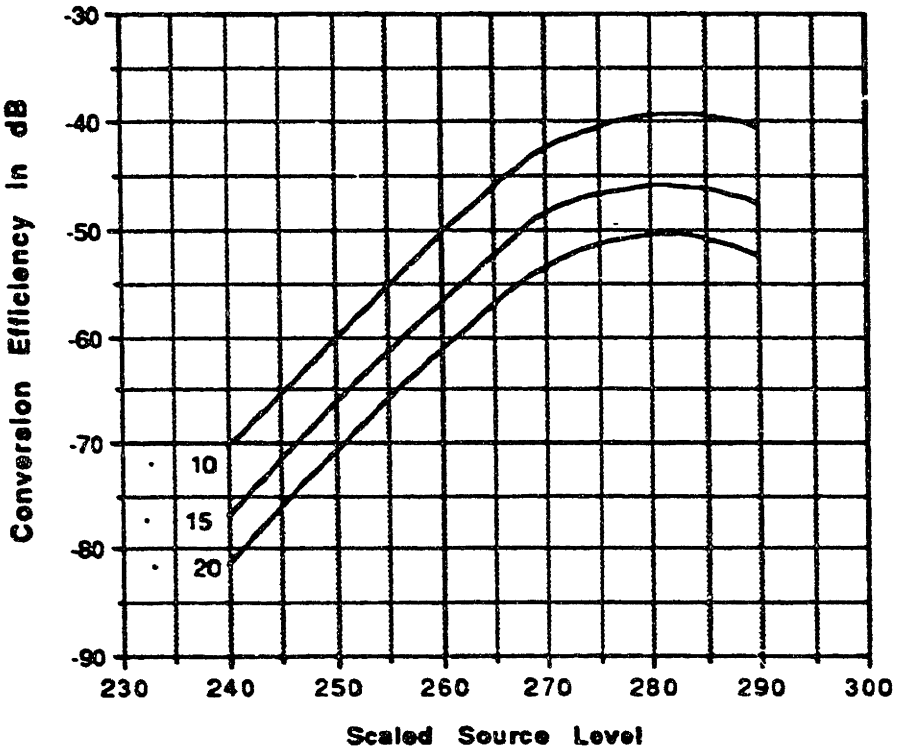

Figure 2.7 Conversion efficiency plot taken from Mellen-Moffett (1976). The abscissa is scaled source level as described in the text. The three curves are for primary-to-difference frequency ratios of 10, 15, and 20. Note the saturation effect, due to shock formation at the primaries, as the scaled source level reaches 280 dB. This curve is for an αR_0 of 0.5 dB.

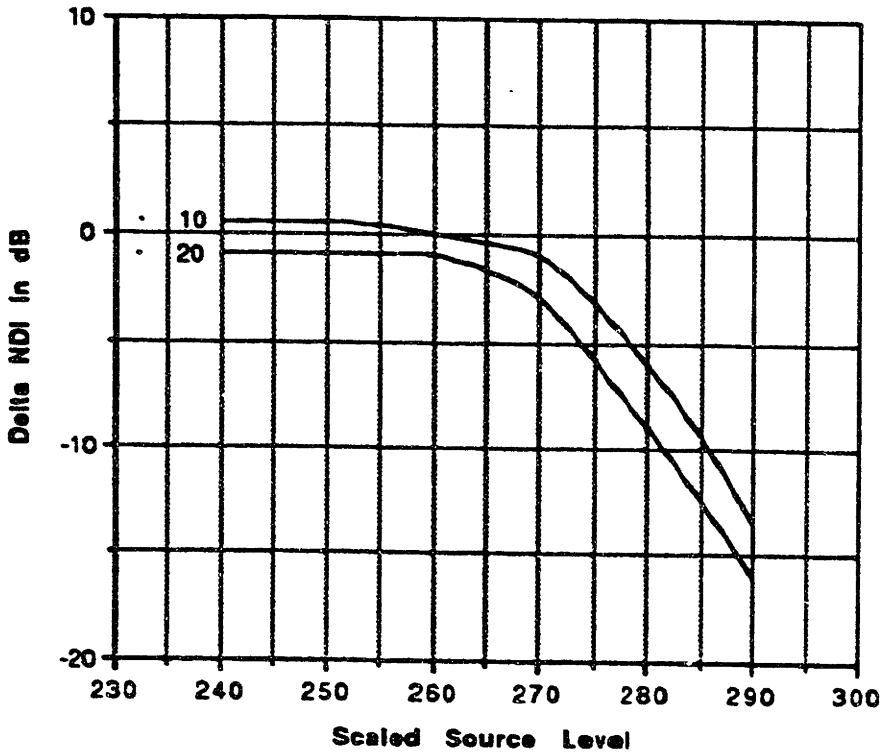

Figure 2.8 Parametric array directivity plot taken from Mellen-Moffett (1976).

The delta NDI refers to the difference between the primary and the secondary NDI. The abscissa is scaled source level as described in the text. The saturation effect at about 280 dB causes the parametric array length to be shorter and the loss in directivity. This curve is for an αR_0 of 0.5 dB.

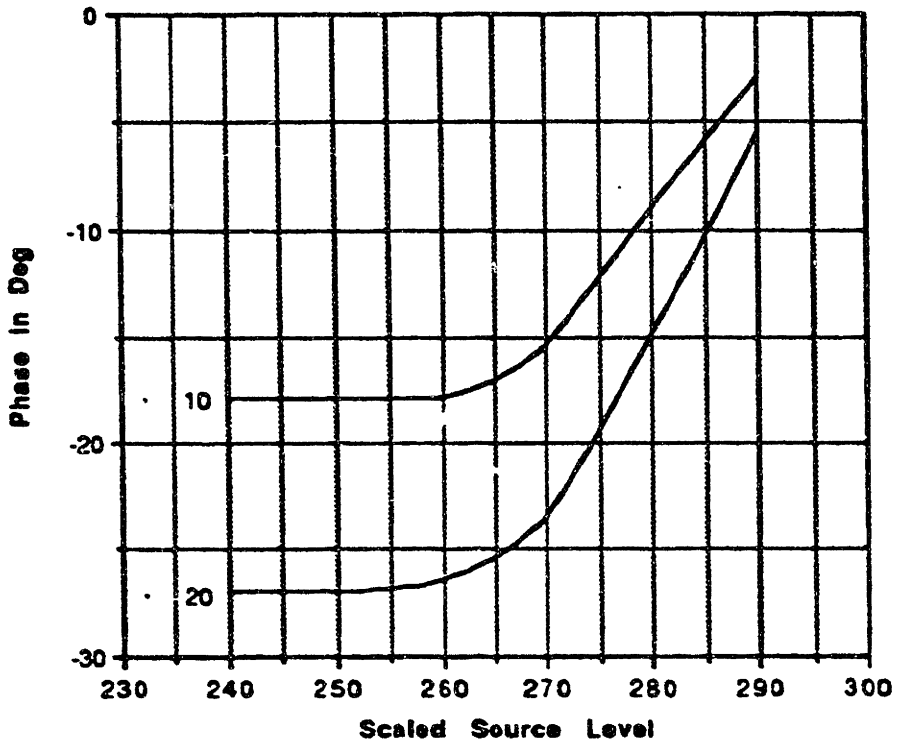

Figure 2.9 Parametric array phase taken from Mellen-Moffett (1976).

The phase determines whether the array is operating as a near-field or far-field radiator.

Using the above curves the following values are obtained for the proposed system:

Parametric Gain	-50 dB;
ΔNDI	-10 dB; and
Phase	8 degrees.

Thus, this is a near-field array operating in the saturation limited region. While the conversion efficiency is very low, this array is capable of producing a 5 degree beam without appreciable sidelobes, and transmitting a bandwidth of at least 10 kHz. A physical projector which could produce this kind of beamwidth at 10 kHz would have a diameter of about 2 meters. In addition, the physical projector would have the usual sidelobes associated with such arrays and a maximum bandwidth of 1 to 2 kHz. The parametric array can effectively transmit wide-band active signals at low frequencies as well as providing narrow beams without sidelobes.

2.6 Conclusion

Pseudorandom broadband pulses and parametric transmit arrays have the potential to improve high resolution active sonar performance. Pseudorandom broadband pulses can yield high resolution range and Doppler estimates and have other advantages due to the maximal length sequence coding. Parametric transmit arrays permit active systems to transmit wide-band pulses, such as pseudorandom broadband, at low frequencies. Azmuthal resolution is enhanced by the characteristic narrow beamwidth and the absence of sidelobes from the parametric array. This allows for exceptionally small arrays to be used even at the lower frequencies which are desireable for long range acoustic propogation.

Parametric array performance can be estimated by using the design curves provided by Mellen and Moffet. These curves were originally produced for two frequency CW parametric systems, but

produce good results when used with parametric arrays transmitting pseudorandom broadband. The analysis also shows that, unlike wide-band LFM, pseudorandom broadband signals should not be subject to frequency amplitude shading.

This Page Intentionally Blank

Chapter 3

Receiver Considerations

3.0 Introduction

The "classic" active sonar receiver is well suited for high resolution sonar systems, although some modifications are appropriate when wide-band waveforms and parametric transmit arrays are used. The active sonar receiver consists of a complex demodulator and replica correlator along with substantial front end and post correlation processing. The "front end" electronics are required to condition the received data and compress the data's dynamic range to within the capabilities of the A/D converters. The post correlation processing is used to detect and track possible targets. This chapter discusses the basic principles behind active sonar receivers as well as the receiver design considerations for an active system which uses wide-band waveforms and parametric transmit arrays.

3.1 Active Sonar Receivers

The heart of the active sonar receiver is the demodulator and replica correlator, or matched filter processor. This type of receiver, shown in Figure 3.1, first complex demodulates the received signal, which reduces the required processor bandwidth, and then performs pulse compression with the replica correlator. The underlying assumption in this receiver is that the echo can be represented by the original signal delayed in time and shifted in

Doppler. Since most active signals meet the narrow-band approximation criteria, i.e. the signal's bandwidth is small compared to the center frequency, it is useful to baseband the signal by using a complex demodulator to reduce the required bandwidth of the subsequent receiver stages. Once the signal is basebanded, a replica correlator provides gain against the noise and generates a function which is used for target detection, as well as estimation of range and Doppler. The locations of the correlation function output peaks correspond to the range and Doppler estimates for the target.

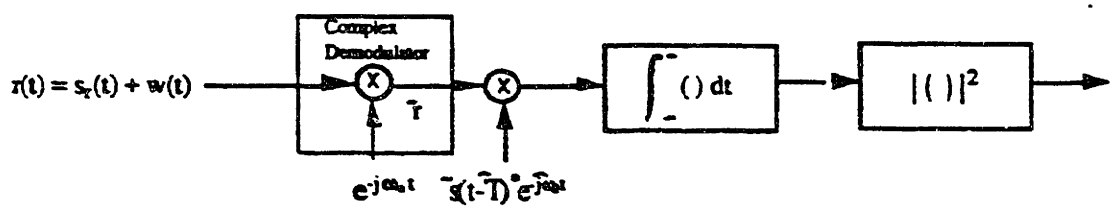

Figure 3.1 Complex demodulator and replica correlator receiver.

The input signal, represented by r(t), is assumed to be a delayed and Doppler shifted version of the transmitted signal summed with white Gaussian noise. The input is basebanded by the complex demodulator. Complex basebanded values are indicated by a ~ and the complex conjugate by an asterisk (*). After basebanding the signal is multiplied by a replica of itself with the appropriate delay and Doppler estimates and the resultant product integrated over all time. Estimated values are indicated by a ^. Since the delay and Doppler can be determined from the envelope, the magnitude squared is used as the output. In practice this receiver is implemented with two channels, the in-phase and quadra-phase channels, representing the real and imaginary parts of the complex demodulator output. Using the magnitude squared reduces the post correlation processing load to a single channel.

The replica correlator is a linear device and is the optimum detector when the noise is Gaussian, white, and uncorrelated with

the signal [Van Trees, part 3 1971]. When these conditions are met, such as while operating in a noise-limited condition, the performance of the receiver is determined by the type of active signal used. The processing shown in Figure 3.1 leads naturally to using the ambiguity function discussed in Chapter 2 for evaluating receiver performance. Even when these conditions are not met, the performance of the replica correlator may be only slightly less than that of the optimal processor. Because of this, the replica correlator is often used when the optimal processor is too complex for a practical design and the performance degradation is minimal. For example, in most active systems there is a reverberation-limited region, where the noise consists primarily of undesired reverberation from the transmission. In this region, the noise is neither white nor uncorrelated with the signal, nevertheless, the replica correlator is normally used because the optimal receiver is prohibitively complex.

3.2 Receiver Front End Design

Since it is advantageous to implement the demodulator and replica correlator in digital hardware, the receiver front end must be designed to ensure that the expected signal levels are within the dynamic range of the A/D converters. The signal level at the receiver hydrophone can have a dynamic range exceeding 200 dB, while the A/D converter dynamic range may be only 72 dB for a 12 bit A/D converter or 96 dB for a 16 bit converter. There are several methods to reduce the required dynamic range including shielding of the hydrophone from the transmitted pulse, blanking or muting

during the transmission, and varying the front end gain as a function of time.

3.2.1 Receive Hydrophone Isolation and Receiver Blanking

In a conventional sonar, the transmit projector and receive hydrophone are frequently the same physical device, and therefore some method of isolating the sensitive receiver from the high power transmit pulse must be used. Single transducer systems normally isolate the receiver by relays, known as transmit-receive (TR) relays, or a switching diode arrangement. In this type of system it is obviously not possible to process received data during the transmission time, which limits the closest range that the sonar can detect a target.

When a receive hydrophone which is separate from the transmit projector is used, the minimum detection range limitation can be eliminated if the hydrophone can be acoustically isolated from the transmitted pulse. When an acoustic path exists which allows direct path transmitter energy into the receiver, the effectiveness of the system during the transmission will be degraded. In severe cases, this energy leakage from the projector to the hydrophone can overload the front end sufficiently to prevent target detection. Any leakage, however, will degrade the receiver's performance by reducing the dynamic range available for true echoes and creating false targets in the correlator output. Thus, good hydrophone isolation is critical if the receiver is to be used during the transmit cycle.

The projector-to-hydrophone leakage problem is even more difficult if the transmitter is operated near a boundary region which has good reflection characteristics. When operating near a good reflector the sidelobes from the projector can reflect directly back into the hydrophone during and after the transmission. For instance, if the projector and receiver are operated at a depth of 150 meters, the return from the surface will begin about 200 msec after the start of the transmission. These returns can significantly degrade receiver performance.

There are many ways to shield a receiver from the transmitter. In relatively simple systems, the projector and hydrophones can be physically separated and a baffle installed between them. Baffles are also generally installed above and below the receiver to eliminate sidelobe leakage from surface and bottom reflected paths. Unfortunately, it is frequently difficult to identify all of the available acoustic paths and completely eliminate leakage by baffling the hydrophones. A more sophisticated approach can be used if the hydrophone is outside the near-field of the projector. Under these conditions it may be a simple matter to build an array which is steered away from the transmitter. When the projector and receiver are positioned such that the projector peak sidelobes are in the nulls of the receiver sidelobes, the direct path leakage can be substantially reduced. The directivity induced by the receive array is also advantageous since it reduces the ambient noise present at the array output. Obviously when a hydrophone array and its associated beamformer are used, additional hardware is required

which adds to the complexity of the system, particularly if the array main lobe is steerable. In addition to the added complexity, one constraint with this type of system is that the transmitted power must be sufficiently low to prevent driving the receive array into a region of nonlinear performance or saturation. Many systems employ both a receive array and some baffling to improve performance.

Due to the inherent difficulties in completely isolating the receiver from projector leakage, most sonar systems simply blank the receiver during the transmission and do not attempt to detect close in targets. The blanking is normally accomplished by shorting the hydrophone output which allows energy stored in the hydrophone during the transmission to dissipate rapidly. Good hydrophone isolation is still useful, since it minimizes the amount of energy stored in the capacitive elements of the transducer, and therefore the amount of time the hydrophone has to remain shorted after the transmission is complete.

3.2.2 Time Varying Gain

Even after isolating the receiver from the transmitter, the sonar system still needs significant dynamic range. Most of the dynamic range requirement is caused by the variation in target echo strength as a function of range. The attenuation of the transmitted signal, caused by absorption and spreading losses, is significant in the ocean environment and causes the target's signal strength to vary logarithmically with range. When the environment is reverberation-limited, the noise is caused by the active

transmission itself and therefore the noise also varies as a function of range. Since the range is measured as a linear function of time, the reverberation noise input to the receiver will vary with time after the transmission. The noise level from reverberation is determined from the equation [Urick, 1983]:

$$RL = SL - 40 \log r + S_V + 10 \log ((c\,\tau/2)\,\Psi\, r^2) - 2\alpha r$$

where:

RL is the reverberation level in dB re μPa/ 1 meter,

SL is the source level in dB re μPa/ 1 meter,

r is the range in meters,

S_V is the volumetric scattering strength in dB,

c is the sound velocity im meters/sec,

τ is the pulse length in sec,

α is the absorption coefficient in dB/meter, and

Ψ is the beamwidth solid angle in steradians.

For example, consider a 200 dB 180 kHz active sonar with a .33 meter diameter circular transducer (10 log Ψ = -34 dB) using a 50 msec active pulse which is operating in isovelocity seawater of infinite extent. If the volumetric scattering strength is -70 dB, the reverberation level at the receiver will vary from 110 dB at 1 meter (1.3 msec after transmission) to 51 dB at 100 meters (13 msec after transmission). If the sonar frequency were changed to 10 kHz (10 log Ψ = -9 dB), and the source level maintained constant, the reverberation level would be 137 dB at 1 meter and 97 dB at 100 meters. This increase in reverberation level at the lower frequency

is caused by the much larger beamwidth, which results in a larger ensonified volume, and the reduction in absorption loss with frequency.

Once the expected volumetric scattering strength is determined, it is straightforward to compress the dynamic range of the input signal by designing a front end amplifier whose gain varies as a function of time. In fact, by examining the reverberation equation, it can be shown that the time varying gain (TVG) should be simply 20log(r) if absorption losses are minimal. This is because as range increases the ensonified volume becomes larger, increasing the scattering strength by 20log(r), which offsets the -20log(r) spherical spreading loss during the echoes return to the receiver. By employing TVG, the input to that A/D's can be maintained at close to the maximum allowable input level, thereby maximizing the dynamic range.

3.3 Receiver Considerations When a Parametric Array is Used as the Transmit Projector

Although the replica correlator is still the receiver of choice when a parametric array is used as the transmit projector, there are three important points which are unique to a parametric system that should be considered in designing the receiver. First, the transmit frequency can be several octaves above the received frequency. Second, the parametric array has very narrow beamwidths and does not have significant sidelobes. And third, the difference frequency is generated at some distance from the projector.

As shown in Chapter 2, a parametric array works by using nonlinearities in the water medium to mix two high frequency signals into the sum and difference frequencies. The difference frequency is the one used for the active system, since its lower attenuation loss will allow the signal to propagate to long ranges. One advantage of this scheme is the wide separation between the transmit frequency and the difference frequency. If the receive hydrophone does not respond at the higher primary frequency, all of the problems associated with direct leakage of the projector energy into the receiver are eliminated. When the primary and difference frequencies are separated by several octaves it is not difficult to design a hydrophone which is unresponsive at the primary frequency. Good isolation is still desirable to ensure that the leakage is not strong enough to drive the receiver crystal into a nonlinear region, but the design of the isolation can be considerably simplified. The receiver front end can also be easily protected from overloading by using a passive bandpass or lowpass filter immediately after the hydrophone, to filter out any leakage energy which might be present.

The narrow main lobe of the parametric array also impacts the design and performance of the receiver. In a reverberation-limited environment, the narrow beams produce much lower reverberation levels which improves detector performance and reduces the need for TVG in the front end. The reason for the reduction in reverberation level can be seen by referring to the reverberation equation in Section 3.2.2, and noting that Ψ is the solid angle beamwidth. As the beamwidth becomes smaller the ensonified

volume and the reverberation level both decrease. Under some conditions the reverberation may be reduced to the point where the sonar is noise-limited and the replica correlator is again the optimal receiver. Along with the narrow main lobe, parametric arrays have almost no side lobes; a feature which is extremely useful in eliminating boundary reverberations from the surface, bottom, and other strong reflectors. In shallow water there may be numerous reflections between the surface and bottom which can effectively overload a conventional sonar for a substantial period of time. By eliminating the sidelobes, the parametric array can completely eliminate this problem, thus permitting the use of active systems at close ranges in very shallow water.

Another important consideration is that the difference frequency is formed at some distance from the projector. This factor can also impact the close range reverberation levels. The near-field of a parametric array is an area which is still being actively researched, but a simple model, the horn model [R. Mellen,1976], considers the wavefront to be a plane wave within the near-field. Although most of the parametric array energy conversion typically occurs within a Rayleigh length of the physical array, the parametric near-field can extend much farther. Thus, the wavefront does not begin to expand as quickly as it does in the conventional array, which reduces the ensonified volume and therefore the reverberation noise. The source level is lower at very close ranges which also reduces volumetric scattering noise.

3.4 Receiver Considerations When Pseudorandom Broadband Is Used As The Active Signal

There are additional considerations when pseudorandom broadband is used for the active pulse. The unique characteristics of this signal can be useful in reducing volumetric reverberation and eliminate, or at least reduce, echo fading caused by destructive interference. Another consideration is that since this signal may not satisfy the narrow-band criteria, it may not be useful to perform complex demodulation prior to replica correlation. Finally, pseudorandom broadband signals can have excellent range and Doppler estimation characteristics which can simplify the post correlation processing.

As discussed in Chapter 2, pseudorandom broadband signals can have very large bandwidths when a parametric array is used as the projector. Volumetric reverberation is known to be a frequency dependent phenomena caused by distributed scatterers throughout the medium. If the source level at the scatterer resonance frequency is reduced, the volumetric scattering is also reduced. Thus it is possible to significantly reduce the reverberation level, by spreading the energy over a wide bandwidth, thereby reducing the energy at an individual scatterer's resonance frequency.

There can be another significant advantage when pseudorandom broadband signals are used in a reverberant environment. If the reverberation sources are modeled as uniformly distributed independent random variables in range and Doppler, the choice of the

active signal will not affect the detection performance of the correlation receiver when the environment is reverberation-limited. Under most conditions this model is inadequate, since at least in the Doppler direction it is reasonable to expect the scatterers to have limited velocity with zero mean and a small variance. Thus, the reverberation region should realistically be limited to a finite area in the range Doppler plane with most of the distribution contained in a region close to zero Doppler. With this in mind, the ideal signal is the one whose ambiguity function, while centered on the target, encompasses the least amount of the area in the range Doppler plane contaminated by reverberation. Stewart has shown that the receiver performance can be much better when pseudorandom broadband is used, as opposed to CW or LFM, if the extent of the range and Doppler spread of the reverberation can be resolved by the signal [Stewart and Westerfield, 1959].

Van Trees has developed a reverberation model which is useful for determining the performance of the correlation receiver as well as for designing the optimum receiver. The performance degradation can be computed by

$$\rho_r = \frac{E_t}{N_0}\int_{-}^{} df \int_{-}^{} d\lambda \tilde{S}_{DR}(f,\lambda)\theta(\lambda-\tau_d, f_d-f)$$

where :

E_t is the transmitted energy,

N_0 is the additive Gaussian white noise strength,

$\tilde{S}_{DR}$ is the range and Doppler scattering function, and

θ is the signal ambiguity function.

This equation is useful for evaluating whether the sonar is reverberation-limited or noise-limited. When ρ_r is greater than one the sonar is reverberation limited and likewise when ρ_r is less than one the sonar is noise-limited. This model assumes: 1) the distribution of scatterers along the path is a nonhomogeneous Poisson process; 2) the velocity of each scatterer is an independent random variable; and 3) the strength of each scatterer is an independent random variable. The reverberation consists of the summation of the echoes from a large number of scatterers, which are described by independent identically distributed random variables. Because of this, the central limit theorem holds and the resultant reverberation can be described as a nonstationary Gaussian process. It is not difficult to derive the optimum receiver for these conditions [Van Trees, part 3 1971]. Unfortunately, implementing the receiver requires a detailed knowledge of the scattering function which is frequently unavailable and can change from one environment to the next. If the scattering function is not properly modeled, the receiver's performance will degrade and may become much worse than the correlation receiver performance. As a result, the correlation receiver is often used and it is therefore important to optimize its performance in the presence of reverberation. The flexibility in designing pseudorandom signals, due to the independence of the range and Doppler resolution characteristics, as well as the narrow ambiguity function main peak, make this signal well suited for enhancing receiver performance in a reverberation environment.

The wide bandwidth can also be useful in eliminating the fading which can occur as a result of interference from multipath or multiple reflectors from a complex target. Since pseudorandom broadband switches phase frequently at apparently random points, a single interference echo cannot cause complete fading of the signal. In fact, since the phase flips have the characteristics of a Bernoulli random process, there will be only a few bits lost even if some chips in the multipath signal are perfectly out of phase with the direct path signal. The narrow beamwidth of the parametric array also helps reduce multipath interference.

When a wide-band signal is used, it may not advantageous to baseband the signal prior to processing. If the signal does not satisfy the requirements for the narrow-band approximation, basebanding the signal by means of complex demodulation may not result in a significant reduction in the receiver bandwidth requirements. Under some conditions the receiver complexity and the number of calculations may increase since both the in-phase and quadra-phase channels will have to be processed after the complex demodulator. In addition, since most receivers only present the magnitude of the correlator output, all of the phase information is lost. If the complex demodulator is not used the phase, which might contain useful information, is naturally retained

Finally, the high resolution capabilities of pseudorandom broadband signals can simplify post correlation processing. Since the range and Doppler estimates are independent, unlike LFM signals,

no additional sources of information are required to uniquely determine the position of the target in the range Doppler plane. This is in contrast to other signals where after detection the position of the target is estimated by using multiple transmission histories and some form of target tracker. For example, the Doppler can be estimated by tracking the targets range history.

3.5 Conclusion

The conventional correlation receiver's performance can be enhanced by using parametric transmit arrays and pseudorandom random broadband pulses. The parametric array's unique properties of narrow beamwidth and the absence of sidelobes can reduce the volumetric reverberations and eliminate boundary reverberations This effect, combined with the wide separation between the projector frequency and the difference frequency, can simplify the receiver's design and enhance its performance. Pseudorandom broadband pulses can also reduce reverberation and in some cases provide the ability to discriminate against the reverberation. Even though the correlator receiver may not be optimum under reverberation conditions, its performance can be enhanced when these pulses are used.

Chapter 4

Experimental Test Bed System

4.0 Introduction

The experimental test bed system consists of a mechanically steerable array assembly with position indicator, transmitter and receiver systems, analog and digital recording systems, and various test equipment. Figure 4.1 shows a block diagram of the system. The transmitter, receiver, and array positioning systems are discussed separately in the following sections.

4.1 Transmitter System

The transmitter consists of a digital waveform generation system, analog reconstruction filters, power amplifiers, and a sonar transducer. The design of this system allows for arbitrary waveforms to be generated and transmitted as long as the bandwidth and center frequency are within the limitations of the power amplifiers and transducer.

4.1.1 Digital Waveform Generator

The waveform generator software is built around Matlab™, an engineering numeric computation package. Pseudorandom waveforms are created by first calculating the maximal length sequence using the polynomial method [Gold, 1978]. This method calculates the sequence by examining the resultant of the division of two polynomials. The polynomials are determined from the seed values

and register connections of the equivalent shift register. Although the sequence values can be calculated with an algorithm which simulates a shift register via a recursion, the polynomial division method is more efficient. The inputs to this algorithm allow any maximal length sequence to be generated by simply specifying the register connections and the seed value. After calculating the sequence values, leading and trailing zeros are added. These zeros, which are removed at the output of the modulator, are necessary to minimize filter edge effects in the modulator filters.

After the sequence values are calculated the results are supplied to the modulator which phase modulates a complex exponential and digitally filters the signal. Direct sequence amplitude modulation could have been used, but this would have resulted in considerable signal energy at the carrier frequency. Since this experiment endeavored to produce a broadband signal with a flat energy distribution across the bandwidth, phase modulation was more appropriate. The modulation angle was approximately ninety degrees, but was offset slightly for optimal carrier suppression of the spread spectrum signal.

The modulated signal is filtered using a lowpass finite impulse response (FIR) filter having a 10 kHz bandwidth and a very narrow transition band. High order digital filters are necessary so that very sharp roll-offs can be maintained in the filter transition band, limiting the signal bandwidth to the projector bandwidth. Failure to limit the bandwidth results in excessive ringing of the

transducer with attendant signal distortion, and potentially damaging the transmitter due to reflected power.

The filter coefficients were designed using the Parks-McClellan method for an equiripple magnitude response and linear phase characteristics. There are two stages in the filter. Each stage consists of a 513 point FIR filter with identical filter coefficients in each stage. The output of the first stage of the filter is reversed in time and run through the second stage. The output of the second filtering stage is again time-reversed so that the signal maintains its original time ordering. This process results in a signal with zero group delay and very low amplitude distortion.

After filtering the signal is a basebanded, phase modulated, pseudorandom broadband pulse with 10 kHz of bandwidth. This signal is multiplied by a complex exponential to produce the broadband 174 kHz parametric primary component. Finally, the 184 kHz parametric primary CW component is added to the 174 kHz spread spectrum signal and the result stored in a Matlab™ double precision floating point output file. The signal and filter frequency response magnitude are shown in Figure 4.3. Several different pseudorandom broadband waveforms can be generated in this manner and stored for subsequent testing. In addition, other waveforms which can be mathematically described in a Matlab™ routine, such as an FM-chirp, can also be generated and stored.

Once the primary signal has been generated, the Matlab™ output files are read and processed by an interface program, and

then down-loaded to an Analogic 2020 polynomial waveform synthesizer via an IEEE-488 interface. The Analogic 2020 system consists of remote programmable high-speed RAM, several types of waveform generators, and an IEEE-488 (GPIB) interface to the portable computer. The interface software allows for the selection of various clock rates, single shot as well as multi-shot operation, and trigger configurations. In this application, samples are generated in the Matlab™ program for an 800 kHz Analogic 2020 clock rate. For simple waveforms, like the FM chirp, the Analogic 2020 can also be programmed directly, eliminating the need for the portable computer.

4.1.2 Analog Reconstruction Filters

Output signals from the Analogic are set at a 1V peak to peak (P-P) level and supplied to a Wavetek analog reconstruction filter. Two filter stages are cascaded together with each filter stage consisting of a Bessel filter set for a corner frequency of 350 kHz. The resultant reconstruction filter roll-off is 48 dB per octave. This system ensures that smoothed continuous waveforms were supplied to the power amplifiers.

After filtering the analog signal, the output level is boosted to 20V P-P with an HP 467A wide-band power amplifier. The 20V level is based on the design input voltage of the transmitter power amplifier. Unfortunately, the HP 467A amplifier is not exceptionally linear at this output level and introduces harmonic components which are only about 40 dB down. Since these harmonic components

are at the same frequency as the desired parametric sonar difference frequency, they should be avoided if at all possible. During most of the testing the amplifier output was reduced to 5V P-P, significantly reducing the harmonic components at the output, although overall system maximum power was somewhat reduced.

4.1.3 Power Amplifier

The power amplifier section was developed using hardware supplied by Specialty Devices, Incorporated. The system, designated as the NBSS-1, originally operated as either a CW or FM-chirp parametric sonar with a maximum peak power of 4 kW at the primary frequencies. Since the NBSS-1 was designed to operate using the dual signal method of parametric operation, as opposed to the switching method, it is ideally suited for this experiment. Most of the original system's internal modulation and timing circuits are bypassed since these circuits are unnecessary.

The NBSS-1 power amplifiers are class AB push-pull bipolar amplifiers. Some distortion is generated since the specified matched output transistors are no longer available as replacement parts. Acceptable replacement transistors are installed, although there is some crossover distortion, particularly at lower power levels. While this distortion produces energy at the desired parametric difference frequency, the transducer is not acoustically efficient at these frequencies and effectively filters out most of this energy.

Matching the output stages of the amplifier to the transducer was difficult. The problem was complicated by the fact that at the primary frequencies commercially available matching transformers were not available. The matching transformer and its associated series inductor were wound on type 3C8 pot cores which have excellent magnetic characteristics at the primary frequencies. Although the NBSS-1 system was originally designed to use a single matching transformer, the bandwidth required for the experimental signals made this method of matching unacceptable. Instead of a single matching transformer, a transformer and series inductor were used. The transformer boosted the voltage of the amplifier output and matched the resistive component of the load impedance to the amplifier, while the series inductor was tuned to cancel the reactive component. Output distortion was very pronounced with even a slight amount of impedance mismatch.

As a result of the high primary frequencies of the parametric sonar, EMI from the matching system and from the projector feed cable can be a significant problem. Without adequate shielding the EMI will corrupt the receiver inputs and interfere with the control electronics. To minimize this problem, pot core magnetic material is used for shielding the matching network and additional shielding is provided for the projector feed cabling. The projector feed lines are routed through conduit from the transmitter to several feet below the waterline. Further shielding is provided by tying the feed cable internal shield to the conduit which is connected to the transmitter chassis ground.

Electrical power input to the projector is measured with a 100:1 voltage divider to sense voltage and a one ohm resistor in the return from the projector to measure current. Voltage and current can be monitored on an oscilloscope to determine power output and ensure that the transducer matching network is adequate when waveforms with bandwidths larger than 10 kHz are being evaluated.

4.1.4 Acoustic Transducer

The acoustic transducer is a 330 mm (13") diameter piezoceramic circular thickness-expander plate. The reported resonance frequency was 174 kHz with an anti-resonance at 180 kHz. In this system the transducer is excited with the modulated signal centered at 174 kHz and the other primary at 184 kHz. The transducer produces a beampattern mainlobe response of about 1.8 degrees at the primary frequencies.

4.2 Receiver System

The receiver system consists of a hydrophone, passive filters, preamplifiers, active analog filters, analog to digital converters, data storage recorders, correlators, and a display system. The system is designed to operate in either a near real-time mode or a data storage and analysis mode.

4.2.1 Hydrophone and Passive Filters

The receive hydrophone is mounted on the common structure with the transmit projector. The hydrophone is an International

Transducer Corporation (ITC) model 1032, which is a broadband, omnidirectional, piezoceramic device with a receive frequency response of -192 dB at 10 kHz. As discussed in Chapter 3, a receive hydrophone with very low sensitivity at the primary frequency is desirable to ensure that nonlinearities do not occur in the hydrophone and to limit the dynamic range. requirement of the receiver front end. The ITC 1032 is only about 24 dB down at the primary frequencies, but it was the only readily available unit. To provide directivity against directional ambient noise, the hydrophone is mounted at the focal point of a parabolic dish constructed of a closed cell structural plastic foam trade named Rohachell 110. The dish has a focal point of 6.99 cm (2.75 in) and a diameter at the face of 48.26 cm (19 in) which produces a receive beampattern roughly equivalent to a 48.26 cm diameter circular aperture. A baffle is located in front of the hydrophone shielding it from any direct unfocused signals, thus ensuring that all of the received energy is focused by the parabola.

The hydrophone output is first filtered by a passive Chebyshev low pass filter. Since the high primary levels caused by leakage from the projector to the hydrophone could cause nonlinearities in active devices, a passive filter is used so that the primary energy is removed prior to the preamplifiers. In this particular system the primary and secondary frequencies are so widely separated that a simple passive Chebyshev filter is more than adequate. The filter design is a seven element, capacitive input, 600 ohm nominal impedance filter with a cutoff frequency of 39.1 kHz. Although the

Chebyshev filter generally does not have linear phase characteristics, the phase is reasonably linear in the frequency region of the signals of interest.

4.2.2 Preamplifier and Active Filters

After filtering, the received signal is amplified by a Panametrics 5660C preamplifier before further filtering by a Sonar Signal Conditioner unit designed by the Charles Stark Draper Laboratories. This signal conditioner is capable of providing additional gain, signal filtering, blanking, signal conversion, and recording functions. The signal conditioner filters the input with switched capacitive elliptic filters and provides the output to an analog VCR based recording system. The audio tracks of this particular recorder have sufficient bandwidth to support recording the difference frequency signals.

4.2.3 A/D Conversion

Once the signals have been filtered the output is supplied to the analog to digital conversion system. This system consists of an A/D daughter board and a Spectral Innovations array processor hosted by a Macintosh 2ci computer. Two daughter board configurations are available for analog to digital conversion. A 1 MHz, 12 bit, single channel A/D converter allows for analysis and evaluation of both the primary and secondary frequencies. This is particularly useful for experiments designed to evaluate conversion efficiency or transmitter performance. The other A/D converter is a

16 bit dual channel phase synchronous board. This board is generally used in the receiver for high fidelity processing of target echoes.

4.2.4 Data Processing and Storage

After the data is digitized, several processing options are available. Spectral Innovations supplies an analysis package providing digital filtering and spectrum analysis. One of the modes of this package creates a waterfall-like display which can be used for quick visual searches for target echoes and analyzing the spectral content of the detected echoes. This mode is also capable of storing the data in a binary format on a 300 megabyte hard disk which was modified to operate with the Macintosh computer via the SCSI port. The stored data can be replayed for further analysis, but it is not in a convenient format for other processing. Another software package uses an array processor library to control the A/D converters and directly stream the data in a convenient format to the hard disk at high data rates. After storage, the data can be converted to a form readable by Matlab™ for further analysis and processing. Finally, near real-time performance is available by performing all of the receiver functions with the DSP32C array processor.

When operating in the near real-time mode, data is acquired via the dual channel A/D converter after a synchronization pulse from the trigger circuit is detected on channel 2. Data is clocked in at a 62.5 kHz rate using the A/D converter on board clock and streamed directly to the Macintosh memory. After about one second

of data is collected, the software reconfigures the MacDSP board for correlation processing. The correlator is implemented in the frequency domain and uses the overlap-save method of block convolution processing [Oppenheim and Schafer, 1989].

The near real-time system is designed to accept various correlator filter coefficients. The filter values are read from a file which is built by the same Matlab™ routine used to create the transmitted signal. The only changes involve adjusting the modulator routine for the sampling frequency of the A/D board and setting the modulator output frequency at the parametric array difference frequency. Various digital filters can be added by convolving the desired filter coefficients with the correlator coefficients and storing the results in the Matlab™ file. After each block of data is processed, the correlator outputs are loaded back into the Macintosh memory where the data can either be averaged with previous correlator outputs, displayed, or stored for future analysis.

One aspect of this receiver, which is significantly different from many other sonar receiver designs, is that the data is not basebanded prior to correlating. The reason for this is that with the bandwidth and center frequency chosen for this system the difference frequency signal does not meet the narrow-band criteria. While it would be possible to complex demodulate the signal, the bandwidth reduction would be small and two channels of processing for the in-phase and quadra-phase data would be required. In addition to the two channels of processing, some of the FFT's which

are currently implemented as real would have to be implemented as complex, thereby further increasing the processing load. Under these conditions running the correlator at the upband frequency does not significantly affect the processing load and allows phase information to be retained. The actual receiver sampling rate is much greater than the Nyquist rate requirements in order to allow improved range resolution.

4.2.5 Display Processing

The detection display consists of a Tektronix RTD 710 data acquisition system and its associated monitor. The RTD 710 is designed to capture and provide time domain analysis of signals. To supply the correlator outputs to the RTD 710, the digital data is converted back into analog signals by the daughter board digital to analog (D/A) converters and then supplied to the RTD 170 where the signals are again digitized for display. While this system may appear superfluous for displaying data, it allows for considerable flexibility in the data analysis and eliminates the need to write display code for the Macintosh screen. The RTD 710 provides a high resolution monitor along with programmable cursors and other display formating options which aid in data analysis.

4.3 Steerable Array System

Early experiments with this system revealed that accurate array positioning is critical. With a projector beamwidth of only about 1.8 degrees (-3 dB), positioning the system to ensonify and detect a small target can be a major challenge. At the test

locations the temporal variations in acoustic ray path can be quite dramatic, and therefore the array must be remotely steerable to support testing when the ray paths are changing. The mounting structure shown in Figure 4.2 provides this capability. The structure is built out of aluminum scaffolding and couplings. Array position control is provided by linear actuators powered by DC power supplies. The actuator arm position can be easily controlled to within 0.1 in. Actuator position is determined by measuring the resistance of a linear potentiometer which is attached to the drive. One actuator is connected to the tiller arm, 18 in. from the azimuth drive bearing, and is used to steer the array in bearing. The other actuator is connected by a line to the projector and is used to steer the assembly in depression and elevation (D/E) angle.

To ensure positive control of D/E and continuous tension on the control cable, the projector assembly is maintained positively buoyant by floats attached to the projector. The floats have the added benefit of providing an emergency recovery system for the projector and receiver should the support structure fail. To provide accurate array position information, absolute D/E is sensed with an inclinometer which is attached to the array crossmember. With this arrangement absolute D/E is accurate to better than one tenth of a degree. The inclinometer is necessary since there is no physical method available to align the D/E actuator potentiometer to absolute D/E. The azimuth drive can be aligned by visually aligning the tiller arm to a known reference and measuring the associated potentiometer reading.

4.4 Improved Transmitter Design

The experimental program discussed in Chapter 5 identified several problems with the transmitter design. These problems were primarily caused by erroneous calibration data provided with the transducer. When the transducer was recalibrated the resonance frequency was measured at 157 kHz, not the reported 174 kHz. It would have been unreasonably difficult to modify the NBSS-1 power amplifiers to operate at the correct resonance frequency.

Instead of modifying the NBSS-1 amplifier, it was replaced with a Wilcoxin PA8 power amplifier. The PA8 contains two amplifiers which are modified in this unit to operate in push-pull mode. A center-tapped transformer is used to couple the amplifier to the load. This amplifier is exceptionally linear and is rated at 500W continuous power. Because of the low duty cycle required of this sonar system, the amplifier successfully operates at a 1.4 kW output power during the transmissions. The combination of operating the transducer at close to its resonance frequency and an improved amplifier design enormously simplified aligning the matching network. The same transformer and series inductor combination are used, but it is a straightforward process to achieve a satisfactory match. These modifications result in almost 24 dB more power at the difference frequency.

Another benefit of these improvements was a reduction in the problems associated with transducer ringing. With the new configuration extensive prefiltering of the signal prior to

transmission is no longer required. Preliminary testing with this system has shown that it is capable of transmitting the phase modulated sequence without filtering. As a result, the digital waveform generator could be considerably simplified in future systems.

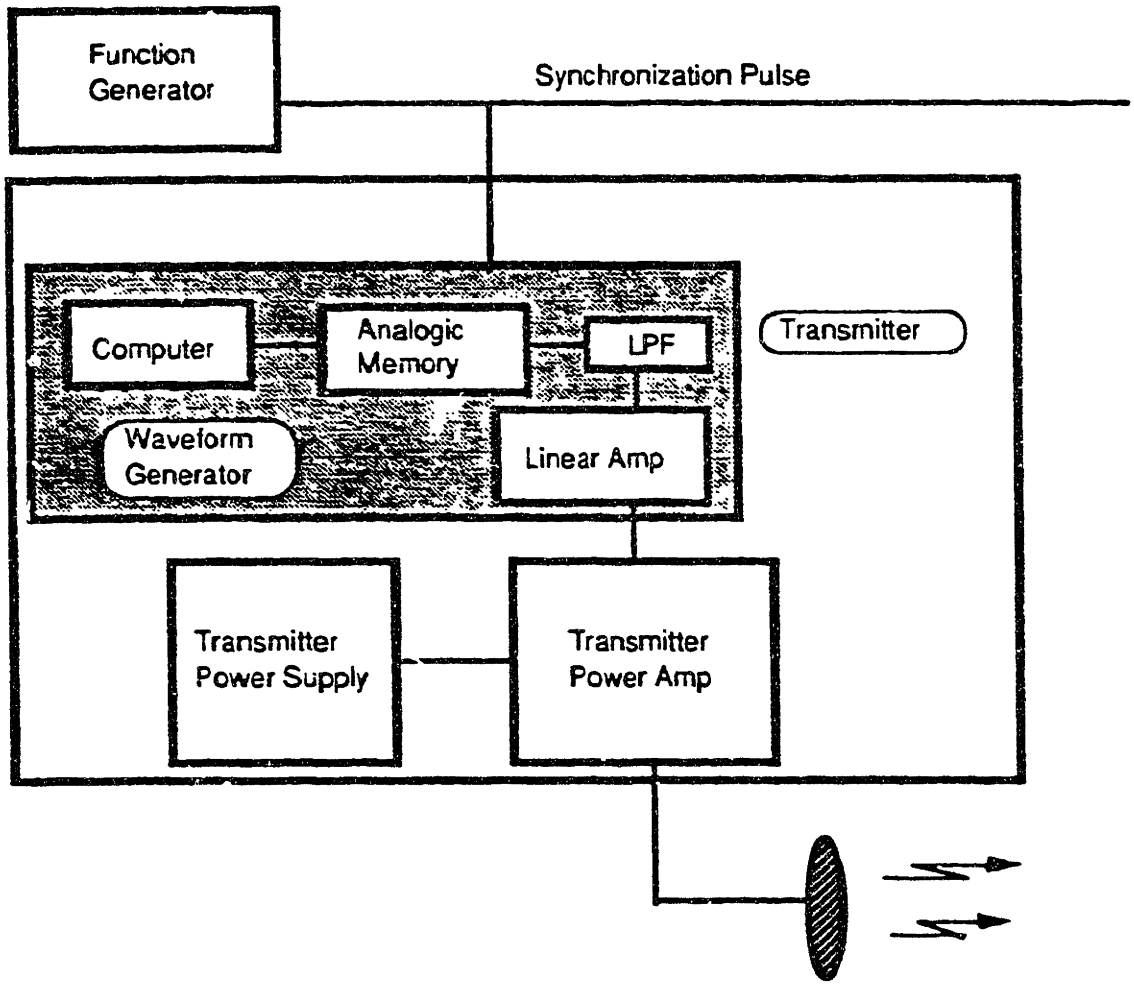

Figure 4.1 a Transmitter Block Diagram

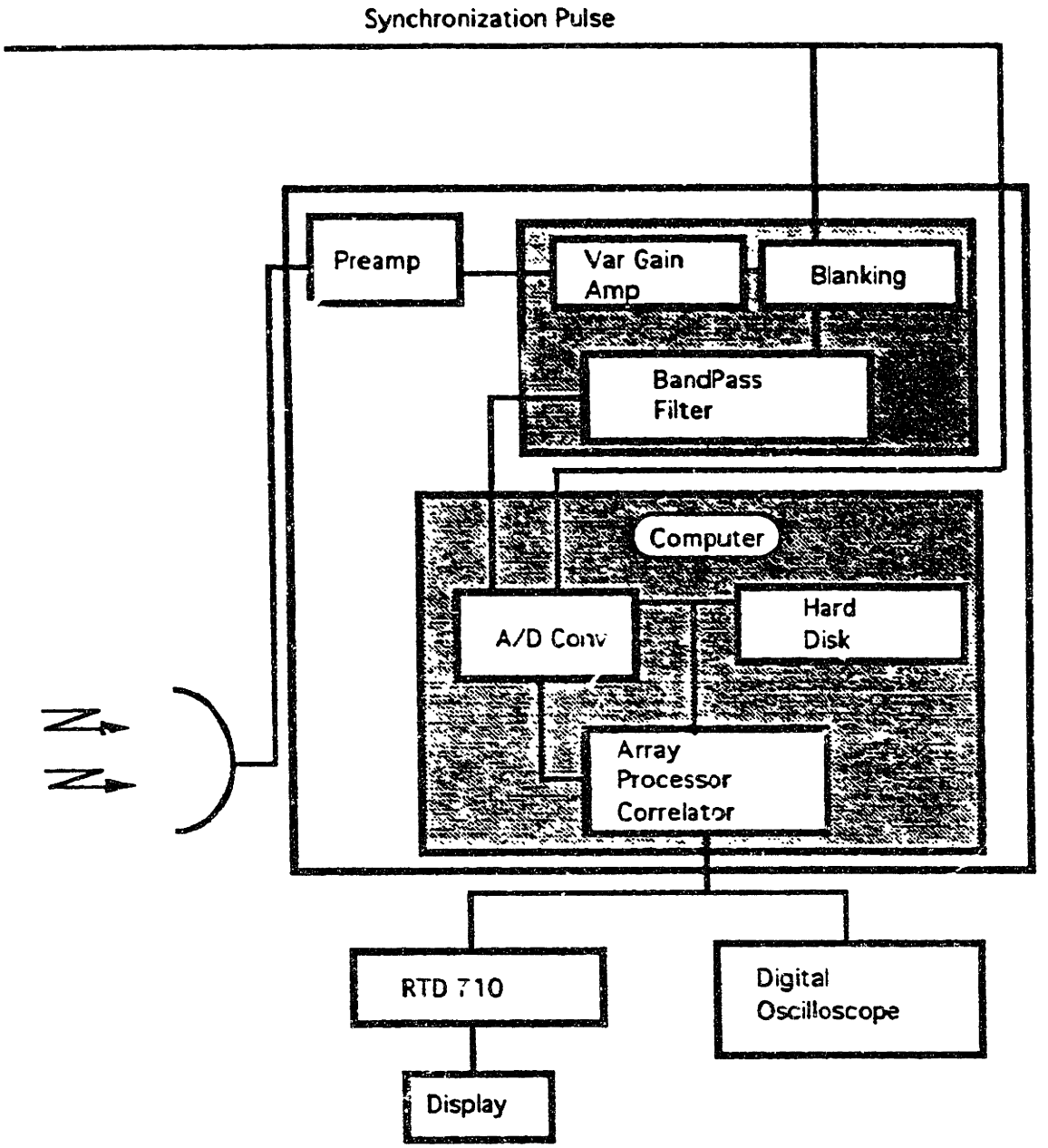

Figure 4.1 b Receiver Block Diagram

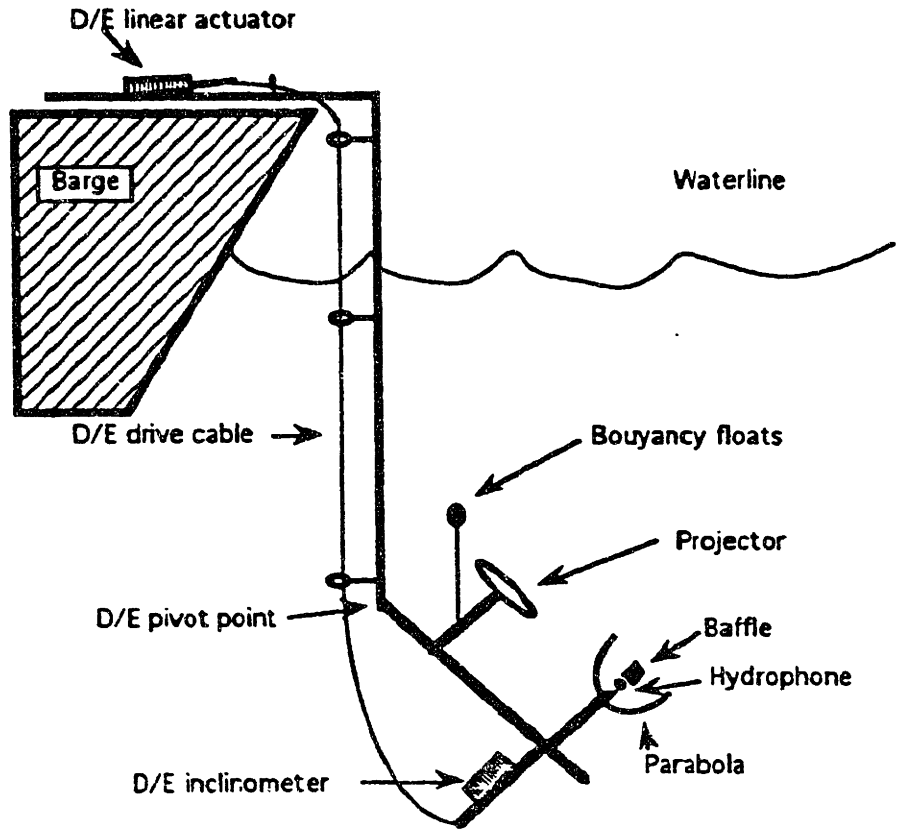

Figure 4.2 a Steerable Array Side View

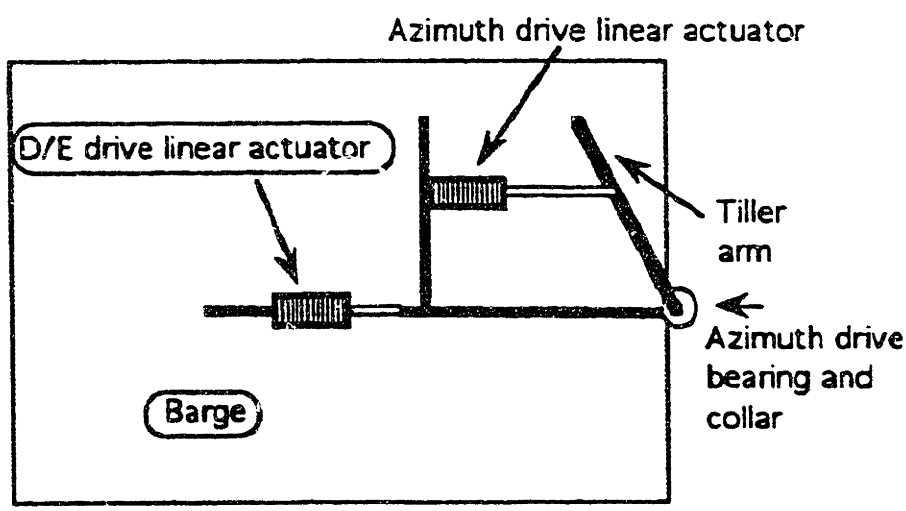

Figure 4.2 b Steerable Array Top View

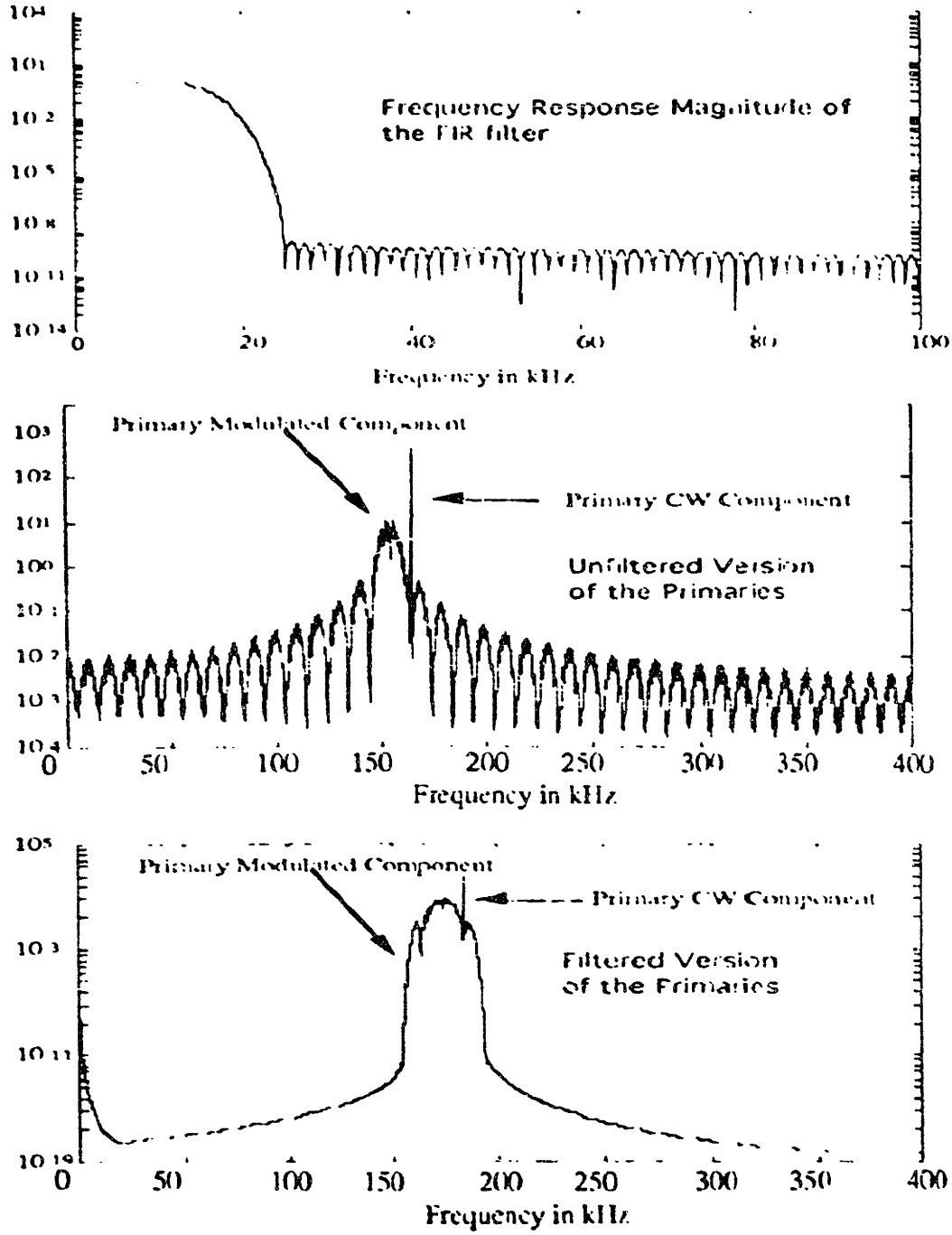

Figure 4.3 Primary Waveform Power Spectral Density.

The top figure shows the frequency response of the 513 point FIR filter used to filter the basebanded broadband component. The middle figure shows the power spectral density of the primaries without filtering the broadband component. The final figure shows the power spectral density with filtering.

5

Experimental Program

5.0 Introduction

The experimental program for this system was divided into three phases. First, to conduct a series of tests designed to ascertain the requirements for a wide-band high resolution sonar system; second, to develop and evaluate the prototype system; and third, to form high resolution sonar images of a sonar target. Most of the experiments were conducted in Boston Harbor at locations shown on Figure 5.1. Boston Harbor was a convenient site which presented a challenging environment for a high resolution experiment. The culmination of the experimental work was the successful imagery of the stern of a U.S. Coast Guard cutter.

5.1 Experimental Program Overview

The experimental program was organized to support the development and testing of a high resolution sonar system. This chapter contains a detailed report of all the important experiments and design decisions made throughout the development program. Conventional sonar design practices had to be modified to support implementing a system which operated at very high frequencies compared to most acoustic systems. Where appropriate, the problems introduced by high frequency operation and the design changes necessary to overcome them are discussed in detail.

The first experiments were conducted in Boston Harbor and were designed to determine the feasibility of transmitting wide-band pseudorandom broadband pulses through a water medium. The waveform generation hardware and receivers were successfully developed and tested. Experiments were conducted to evaluate the utility of the proposed waveforms in estimating time delay for active sonars or communications applications. Receiver data for the pseudorandom broadband and other candidate pulses was recorded for future analysis. The system was also used to investigate the hardware requirements for a parametric sonar. The results of the parametric sonar testing were inconclusive but provided valuable information for future design work.

The next experiments, conducted at Lake Lavon, Texas, tested the ability of a modified commercial parametric sonar to transmit the pseudorandom broadband pulse. Design problems which were detected by the first Lake Lavon test were evaluated and corrected in time to support a second test at this location. These experiments demonstrated that a pseudorandom broadband pulse could be successfully transmitted by a parametric sonar.

At the conclusion of the Lake Lavon tests the system was shipped to Boston Harbor to perform some quantitative measurements. A number of hardware design problems materialized which interrupted the test program. Most of the difficulty was caused by the large bandwidth requirements of this test program.

Extensive effort was required to solve these problems and continue the experiments. Some of these are discussed in detail.

The next experiments were intended to quantify the performance of the system. A commercial hydrophone was calibrated at the primary frequencies and used for acoustic power measurements. Far-field experiments were conducted using this hydrophone. The results of these measurements are presented in a tabular format.

The final experiments obtained high resolution single beam images of a U. S. Coast Guard cutter. A high resolution image of the stern section of the cutter distinctly revealed the propellers, rudders, and skeg.

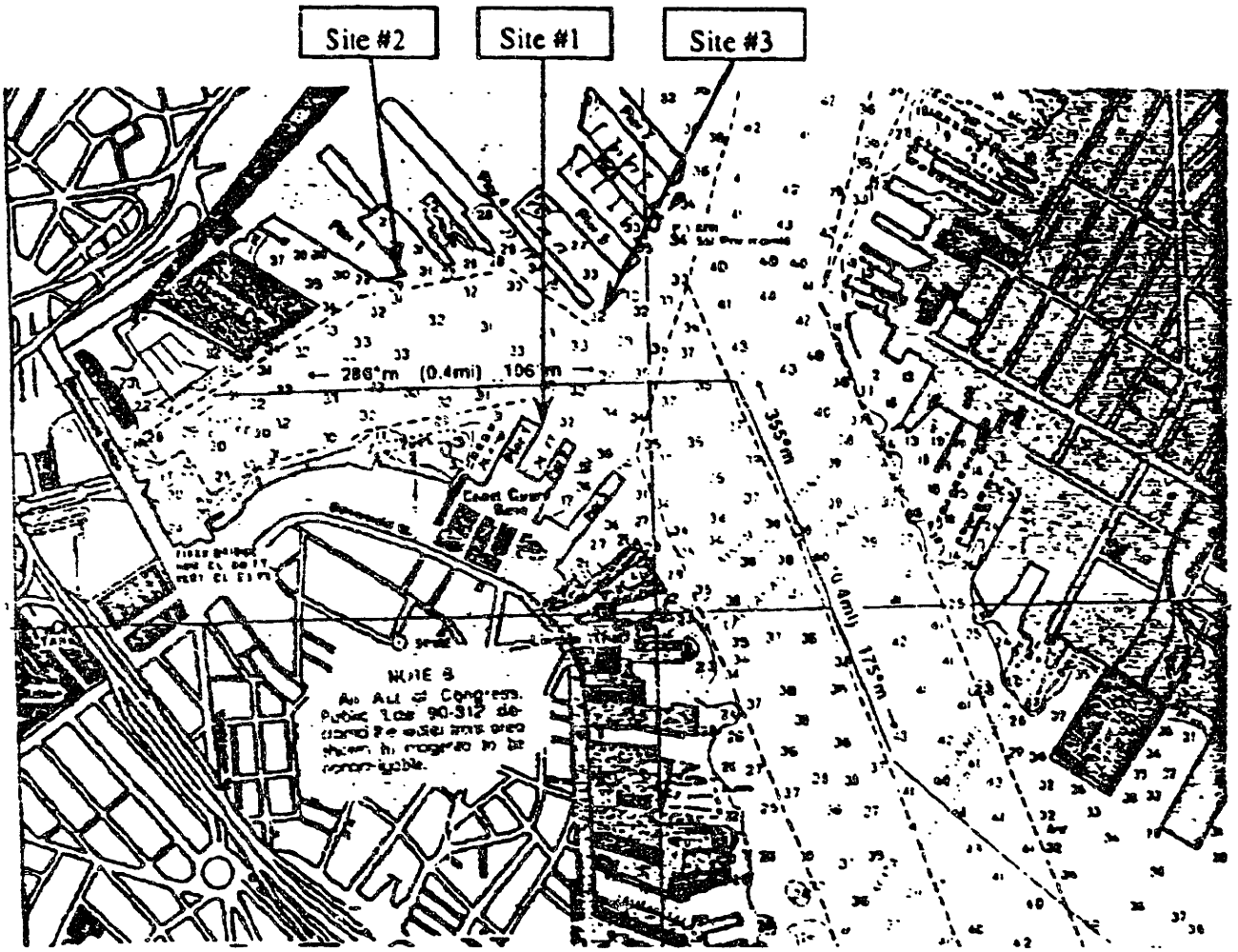

Figure 5.1 Boston Harbor experiment sites

Phase 1: Preliminary System Design Requirements Experiments

5.2.1 Experimental Test Bed Description

The first series of experiments focused on evaluating transmitter and receiver designs which might be used in a high resolution sonar system. The transmitter design work evaluated candidate active waveforms and investigated the problems which might be encountered in implementing a parametric system. During these first experiments, the nonlinear parametric system testing was independent of the waveform evaluation testing. There were two primary reasons for conducting independent tests. First, the nonlinear effect might have unforeseen effects on the waveform and complicate the analysis of the results. Secondly, since at this point in the program the use of a parametric sonar was only one of the many options under consideration, it was undesirable to constrain the experiment such that the results were only valid for a parametric design.

The test bed system for this series of experiments is shown in Figure 5.2. This configuration was designed primarily to support data acquisition for post experiment analysis of the transmitted waveforms and therefore the signal processing was performed off line. The transmitter could produce a wide variety of waveforms with various modulation scheme to facilitate obtaining a waveform

library for further analysis. The Analogic 2020 polynomial digital waveform synthesizer could create any waveform which could be described by a polynomial. This hardware allowed conventional waveforms, such as CW and LFM, to be quickly synthesized or modified. During testing, changes in the signal's frequency, bandwidth, or other significant parameters took only a few minutes for the Analogic to compute before the signal was ready to transmit. More complex signals which could not be described by a polynomial were generated in a digital computer and down-loaded to the Analogic 2020 via an IEEE-488 interface. The digital portion of this system worked so well that it was completely retained in the final design discussed in Chapter 4.

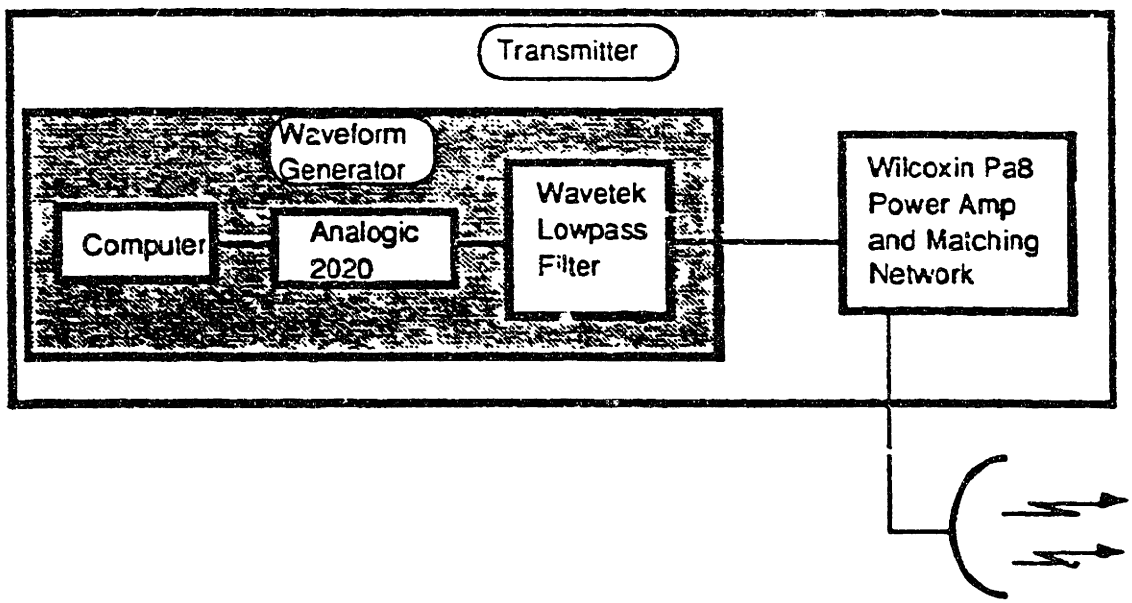

Figure 5.2.a Sonar test bed transmitter block diagram.

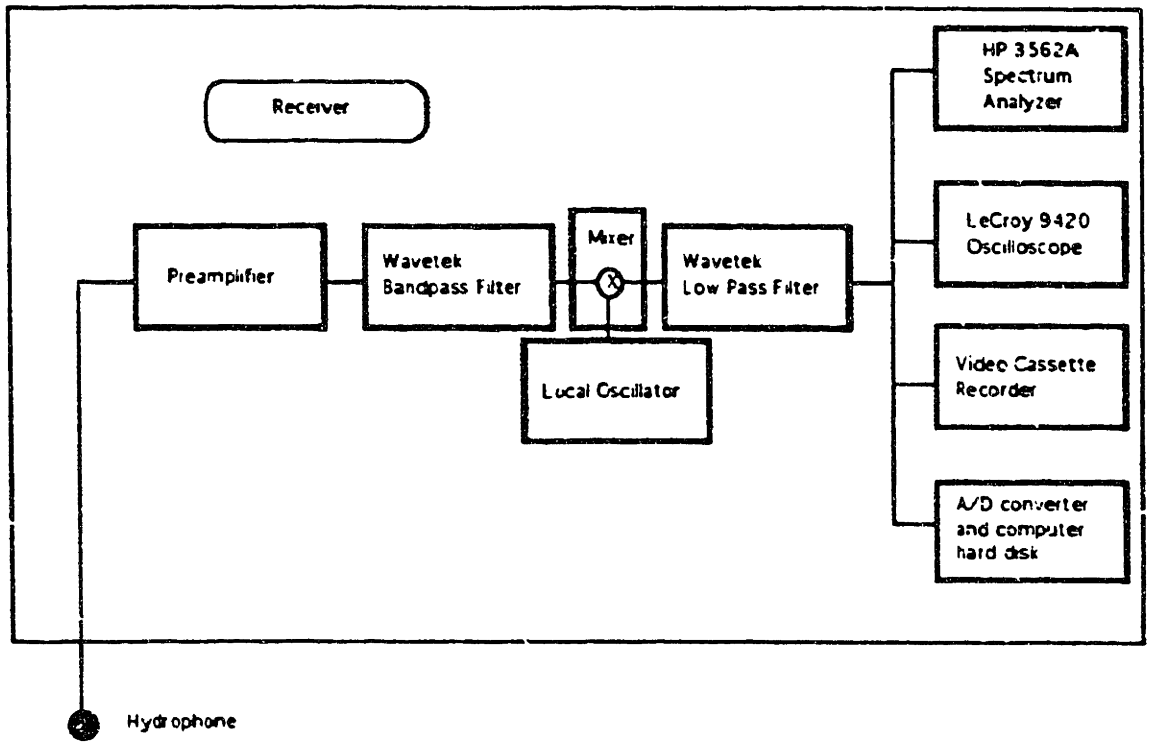

Figure 5.2.b Sonar test bed receiver block diagram.

The receiver system was designed to provide some on-site time domain and spectral analysis ability along with analog recording and digital storage for more detailed future analysis. For analog recordings, the audio tracks of a high fidelity VCR were used. Digital sampling was performed by a high quality dual channel 16 bit A/D converter with a maximum sample rate of 50 kHz and a bandwidth limited to 22 kHz by the antialiasing filters. Since most of the transmitted signals were centered in the 30 kHz to 80 kHz range and both methods of data storage had bandwidth limitations of about 20 kHz, the majority of the received signals were filtered and translated in frequency prior to recording or digitizing. To

maximize the amount of data which could be collected, most of the data was frequency translated to a 10 kHz center frequency and recorded on VCR tape. The analog recording permitted long time records of data to be collected. Selected portions could later digitized for analysis. If a waveform appeared to be particularly interesting it could be digitized at the experiment site, but due to storage limitations only a few minutes of digital data could be collected.

Prior to translating the signal in frequency the data was prefiltered with a Wavetek analog bandpass filter. Prefiltering was necessary to prevent corruption of the data from aliased out-of-band noise. A passive mixer with an external local oscillator was employed to provide the frequency translation. In the first experiment an analog Wavetek function generator was used as the local oscillator for the frequency translator, but after analyzing the data it was clear that the instabilities in the oscillator frequency severely degraded the performance of the receiver. In the second experiment, another Analogic 2020 was substituted as the local oscillator input to the frequency translator. The Analogic 2020 features the ability to precisely set the oscillator frequency which dramatically improved the performance of the prototype receivers.

The data which had been recorded on the VCR tape was played back and digitized with a PC-based data acquisition system. After digitizing, the data was converted from binary to flat ASCII format and then loaded into Matlab™ for processing and analysis. One of the Matlab™ routines implemented a digital receiver which basebanded

the signals, filtered through a replica correlator, and displayed the output as magnitude squared on a time versus amplitude plot. The receiver also had the ability to perform digital filtering prior to replica correlation. FIR filters were used to correct amplitude distortions in the signal from known causes such as transducer roll-off. Most of the filters were created by building an inverse filter for the distortion using the Kaiser Window method [Oppenheim and Schafer, 1989]. For instance, transducer roll-off was compensated for by specifying a filter with the magnitude of the frequency response equal to the reciprocal of the transducer frequency response. The response was smoothly tapered to avoid edge effects and the Kaiser Window technique employed to obtain the FIR filter coefficients.

There were two types of transducers available for this experiment. The ITC 1032 transducer has a resonance frequency of approximately 40 kHz with a diameter of 2.7 inches, while the ITC 1042 has a resonance frequency of 80 kHz and a diameter of 1.4 inches. Generally the 1032 transducers were used for transmitting, since with the larger ceramic volume they were capable of handling higher power levels. Two parabolas, identical to the receive parabola discussed in Chapter 4, were manufactured to provide directivity. The focus of the parabola was designed to accept either an ITC 1032 or ITC 1042 transducer. An acoustic absorber placed in front of the transducer prevented unfocused energy from escaping the parabola in the case of the transmitter or reaching the hydrophone in the case of the receiver. It was hoped that the added

array gain provided by these transducer and parabola assemblies would allow the test bed to radiate enough acoustic power for parametric sonar experiments. These assemblies were mounted on a scaffold structure similar to the one shown in Figure 4.1. In addition to the parabola assemblies, other ITC 1032 and ITC 1042 omnidirectional transducers were available for deployment.

The experiment site was located at the U. S. Coast Guard station in Boston labeled as Site 1 in Figure 5.1. The scaffolding with the parabolic array was deployed at the end of the pier with the parabolas at a depth of either 2.4 meters (8 ft) or 4.9 meters (16 ft). Other transducers could be deployed in the harbor channel at distances of up to 182 meters (600 ft) from the edge of the pier.

5.2.2 Active Waveform Evaluation Experiment

This experiment evaluated the system's ability to transmit a PSK spread spectrum waveform modulated with a pseudorandom sequence through the water column and successfully correlate the data at the receiver. The transmitted signals had a nominal -3 dB bandwidth of 12 kHz, corresponding to a 0.1 ms chipping rate. The maximal length pseudorandom sequences had lengths of 31 bits and 511 bits, resulting in transmission times of 3.1 msec and 51.1 msec respectively. To minimize multipath, the parabola was used as the projector. By steering the parabola in D/E, a signal could be transmitted using either the direct path or the surface-reflected path. The ability to excite only a single eigenray allowed a comparison with previous experiments which had used PSK

waveforms transmitted in a direct path environment [Quazi and Konrad, 1982].

Since the primary objective of this experiment was to evaluate candidate waveforms, it was desirable to ensure that the signal level was adequate for time domain analysis without additional processing. Prior to recording the data for each waveform the transmitter power was adjusted to provide a signal level at the receiver at least 6 dB above the local ambient noise. Due to wide temporal variability in the ambient noise from local shipping and nearby industrial operations, it was not possible to maintain a constant power level for each transmission while simultaneously maintaining a satisfactory signal-to-noise ratio at the receiver.

After completing the transmission of each waveform and eigenray combination, an ITC 1032 transducer was placed 61 meters (200 ft) from the pier and used as a projector. Using this omnidirectional projector excited significant multipath which was used to evaluate waveform performance in a multipath environment. The experiment was abruptly terminated when a harbor cruise ship ran over the small marker buoy and cut the energized projector cables. This successfully tested the power amplifier short circuit protection as well as the test groups ability to dodge whipping cables caught in the vessels screws!

Throughout the experiment the hydrophone response was monitored at a test point located prior to the mixer. Although the

received signal's spectral shape resembled the transmitted spectrum, there was severe envelope distortion evident when viewed in the time domain. This distortion did not change significantly with changes in transmitter power or arrival path. Initially the problem was assumed to be in the power amplifier, but the distortion was not present at the voltage monitor point to the projector. This monitor point consisted of a 60 dB attenuator attached across the projector drive leads. Some time later it was discovered that all of the ITC 1032 transducers were defective due to improper solder joints between the leads and the ceramic. The solder joints had failed and the leads were held against the ceramic by only the encapsulant. This defect resulted in intermittent contact when the projector was loaded which could produce substantial distortion.

Despite the distortion the receiver demodulators were tested using the acquired data. When the spread spectrum signals with a center frequency of 10 kHz were analyzed the demodulator output was within 2 dB of the predicted correlator gain. This was somewhat unexpected because the waveform had appeared to be severely distorted at the receive hydrophone. Surprisingly, the 10 kHz data was the only useful coded waveform data for post experiment analysis.

Initial attempts to process any of the frequency translated signals were unsuccessful. An analysis of the CW and LFM signals revealed that the problem was caused by instability in the local oscillator input to the mixer. This instability resulted in an error in

the translated carrier frequency. Once this was recognized signals which did not have suppressed carriers, such as FM chirps, were analyzed by correcting the receiver local oscillator for the error in the translator oscillator. Analysis of the pseudorandom signals however posed a much more difficult problem, since these signals had been transmitted with a fully suppressed carrier. In addition, because this signal is relatively Doppler intolerant, an accurate setting of the demodulator local oscillator is mandatory. To recover these signals, an estimate of the correct translated carrier frequency was obtained by examining the spectrum of the square of the signal.

After a good estimate of the carrier frequency was obtained and the receiver local oscillator correctly set, the demodulators produced an output which showed the correlation peaks, but with magnitudes which were several dB below the predicted values. The poor performance of the correlators was probably due to short term frequency instabilities in the oscillator. Rather than trying to track the oscillator frequency it was decided to repeat the experiment using a more stable digitally synthesized local oscillator. This demonstrated the importance of using either exceptionally stable analog systems or generating the signals digitally with a stable clock.

5.2.3 Parametric System Testing

Another experiment evaluated the suitability of this system as a test bed for a parametric sonar. Two discrete frequencies

separated by 10 kHz were generated, summed in the digital waveform generator, and then transmitted from the parabola. A receive hydrophone was placed 122 meters (400 ft) away for this portion of the experiment. Although the 10 kHz difference frequency was present at the receiver, the level was inconsistent with the expected conversion efficiency derived from the nomograms in Urick. At these low power levels the effective parametric array length is absorption limited and the Westervelt equations should provide rough performance estimates.

The parametric conversion efficiency measurement was probably in error. The difference frequency was detected at the projector voltage monitor point, indicating that nonlinear mixing was occurring in the amplifier or the projector. If the projector was efficient at the difference frequency, these nonlinearities could substantially contaminate the parametric conversion measurements. Because of the poor agreement between the theory and measured performance and the questionable nature of the measured data, it was determined that this system was inadequate for use as a parametric sonar test bed. Several future experiments with this system incorporated incremental improvements in an attempt to produce a suitable parametric system for low power testing. None of these changes were successful in conclusively demonstrating that the difference frequency signals received by the hydrophone were being generated by nonlinear mixing in the water column and not in the transmitter electronics.

During these experiments it was noted that the difference frequency level fluctuated significantly between transmissions. In retrospect, these fluctuations were probably due to the intermittent projector ceramic connections. The poor impedance match between the projector and the power amplifier also complicated the analysis. These two factors probably caused the actual radiated acoustic power to be much lower than expected. Since for a nonsaturated parametric array conversion efficiency decreases with decrerasing power, the measured conversion efficiency should have been lower than predicted. Clearly it is worth repeating this test in the future. With a better impedance matching network and a properly functioning projector the system should produce a reliable parametric array.

5.2.4 Receiver Design Improvements, Implementation of a Digital Receiver, and Characterization of Transmitter Distortion

The next experiment was designed to reevaluate the demodulators when a stable local oscillator was used to frequency translate the received signals. During this test the waveform distortion observed in the first experiment was still evident. The data was analyzed using the replica correlator demodulator and another system which was used to recover the individual bits of the pseudorandom sequence. Once again transmitter power was adjusted to ensure a positive signal-to-noise ratio at the receiver for each test.

All the transmissions were successfully processed by the receiver despite the apparent distortion. In all cases the correlator actual gain was within 2.2 dB of the predicted values. Individual bits were also easily recovered in the single path cases and recovered by filtering even in the multipath cases. Correlator gain was determined by calculating the average signal-to-noise ratio in the single eigenray cases and then measuring both the peak-to-maximum-sidelobe ratio and peak-to-noise ratio observed in the correlator output. The peak-to-noise ratio was defined as the correlator peak value to average noise value where the noise was defined as the level outside of the pedestal of the signal's ambiguity function.

Since it may be possible to use this type of system for digital communications, some analysis on recovering the individual bits was performed using the multipath data. A schematic representation of the system used is shown in Figure 5.3. In this system, the acoustic channel was modeled as a simple FIR filter with known delays. The filter delays and coefficients were determined by analysis of the output of the correlator.

An examination of Figure 5.4, which is representative of the conditions experienced during this experiment, reveals that there were two predominant paths along with several minor arrival paths. The predominant paths correspond to the direct path and a surface-reflected path. The surface-reflected delay time and the magnitude of the coefficient were easily read from the correlator output. The

only remaining parameter to determine was the sign of the delay coefficient which in this case was negative due to the phase reversal at the interface. Since this receiver does not baseband and compress data, it may be possible to infer the coefficient sign information by examining the phase of the correlation function, although this was not attempted in this experiment. It is interesting to note that the surface-reflected phase reversal results in the poles of the inverse filter residing inside the unit circle and a bounded-input-bounded-output stable filter (BIBO).

Once the filter model was established an inverse filter was constructed to remove the undesirable multipath effects. Of course the inverse filter worked satisfactorily only as long as the channel remained relatively temporally invariant or if the environment was sampled frequently enough and the filter delays and coefficients periodically updated. Prior to filtering the data the bit error rate exceeded 5% in the multipath cases, even with a 20 dB signal-to-noise ratio at the receiver. After filtering 120 seconds of data, 18,396 bits were analyzed and successfully decoded with two errors for an error rate of 1.1e-5. The errors corresponded to the last 2 bits of one transmission which were severely distorted. This test was by no means intended to be a detailed study of the possibilities of using this system to transmit data but these brief results are certainly encouraging.

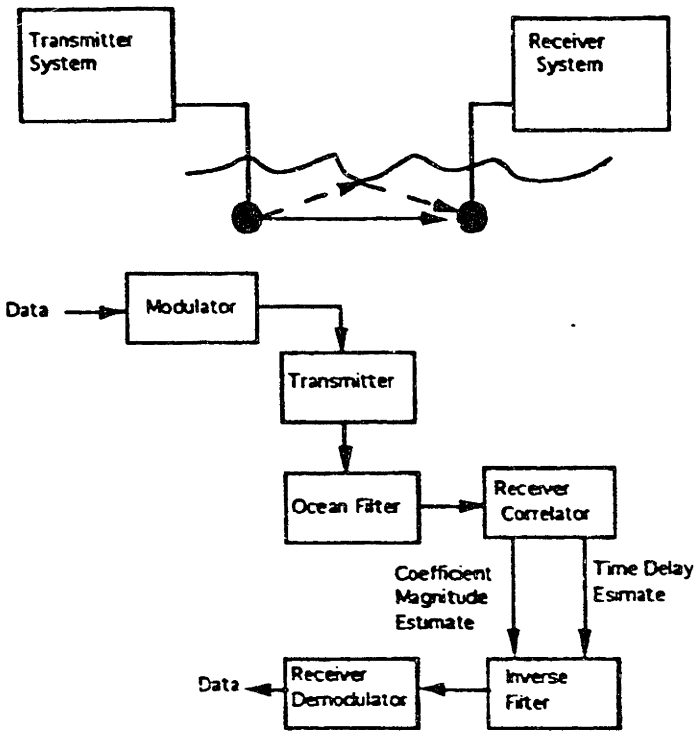

Figure 5.3. Schematic View of Bit Recovery System.
The upper diagram shows the direct and surface reflected paths with the phase reversal in the surface path indicated by a dashed line. The lower diagram is a simplified schematic of the system used to recover the transmitted sequence.

A special set of signals was also transmitted tc investigate the distortion problems. An analysis of several of the previous transmissions revealed there were two types of unexplained distortions present in the received signals. The first type of distortion was an apparent clipping of the higher amplitude signals. In hindsight this problem was probably due to the electrode bonding problems which were later discovered in all of the ITC 1032 transducers used in these experiments. The second type of distortion occurred near the phase transitions of the PSK waveform as well as near the beginning and end of the waveform. The nature

of these distortions, particularly the exponential decay of the distorted signal at the end of the waveform, suggested that the problem might be attributed to ringing in the hydrophone and amplifier circuitry. This was confirmed by transmitting various pulses with different center frequencies and bandwidths. These experiments established that the system was capable of transmitting a pulse with a 10 kHz bandwidth. Much higher bandwidth signals resulted in ringing which was very pronounced in the received signal.

5.2.5 Transmission of Bandlimited Signals

The third experiment used the same waveforms except that all of the signals were bandlimited to 10 kHz prior to transmission. A seperate 0.2 msec chipping rate signal was also evaluated. This signal was prepared in case the bandwidth limit seriously degraded the performance of the 0.1 msec chipping rate signal. Classical spread spectrum systems normally employ a bandwidth which is at least twice the reciprocal of the chipping rate. Utilizing a bandwidth which is less than twice the chipping rate results in some slight reduction in the correlation peak to sidelobe gain and a broadening of the main lobe of the ambiguity function. Another problem with limiting the bandwidth is that the filtering produces substantial amplitude modulation of the signal. This amplitude modulation could result in a reduction in the total energy transmitted and thereby reflected from a target.

The filters for this experiment were Parks-McClellan filters calculated by the Remez exchange algorithm [*Programs for Digital Signal Processing*, algorithm 5.1, 1979]. These filters ranged in length from 255 points to 2013 points and were implemented in two stages, with the output of the first stage time reversed and then filtered by the second stage. The output of the second stage was again time reversed so that the signal retained its original ordering in time. This technique was used to ensure that the signals had zero group delay.

The transmit power was set to provide a positive signal-to-noise ratio prior to correlation at the receiver. Power was set lower than in the previous test in the hopes of eliminating the high amplitude clipping Although occasional instances of higher amplitude clipping were still noted, the received signal was markedly less distorted. The bandwidth limited signals did not exhibit any of the ringing effects noted in the original experiments.

Several sets of correlator coefficients were evaluated during this test. Each set of coefficients had a different bandwidth which ranged from 10 kHz to 400 kHz. The result of this investigation was somewhat surprising as the correlation gain was essentially the same regardless of the filter bandwidth used. In fact no degradation in gain was measurable from the data, although the main lobe was somewhat broadened when the lower bandwidth correlator coefficients were used. Several FIR filters were also incorporated to correct for known transducer and electronic component effects.

These filters did not provide any significant performance improvement.

While satisfactory results were obtained when the matched filter bandwidth was not restricted, this does not imply that the receiver front end bandwidth should be unrestricted. If the receiver front end bandwidth is excessive, there will be little signal information available near the bandwidth edges, but the increase in noise can dramatically degrade performance by consuming the available A/D dynamic range. There may also be cases where it is desirable to limit the bandwidth of the matcned filter coefficients. For example, a strong interfering noise source at a frequency which corresponds to a sidelobe in the matched filter's frequency response would degrade receiver performance. This interference could be suppressed by using a bandwidth limited matched filter which reduced the sidelobe response of the filter. This option was used in some of the later experiments when strong noise sources were present near the signals of interest.

Another point to consider in designing the receiver filters is that although it may be desirable to correct for severe distortion of the waveforms caused by known and quantifiable effects, the consequences of these corrections must be carefully evaluated. Even though the distortion may appear to be severe, particularly when viewed in the time domain, filtering to correct the degradation may not significantly improve the correlation gain. In some cases the extra filtering may introduce computational noise as well as increasing the complexity of the system.

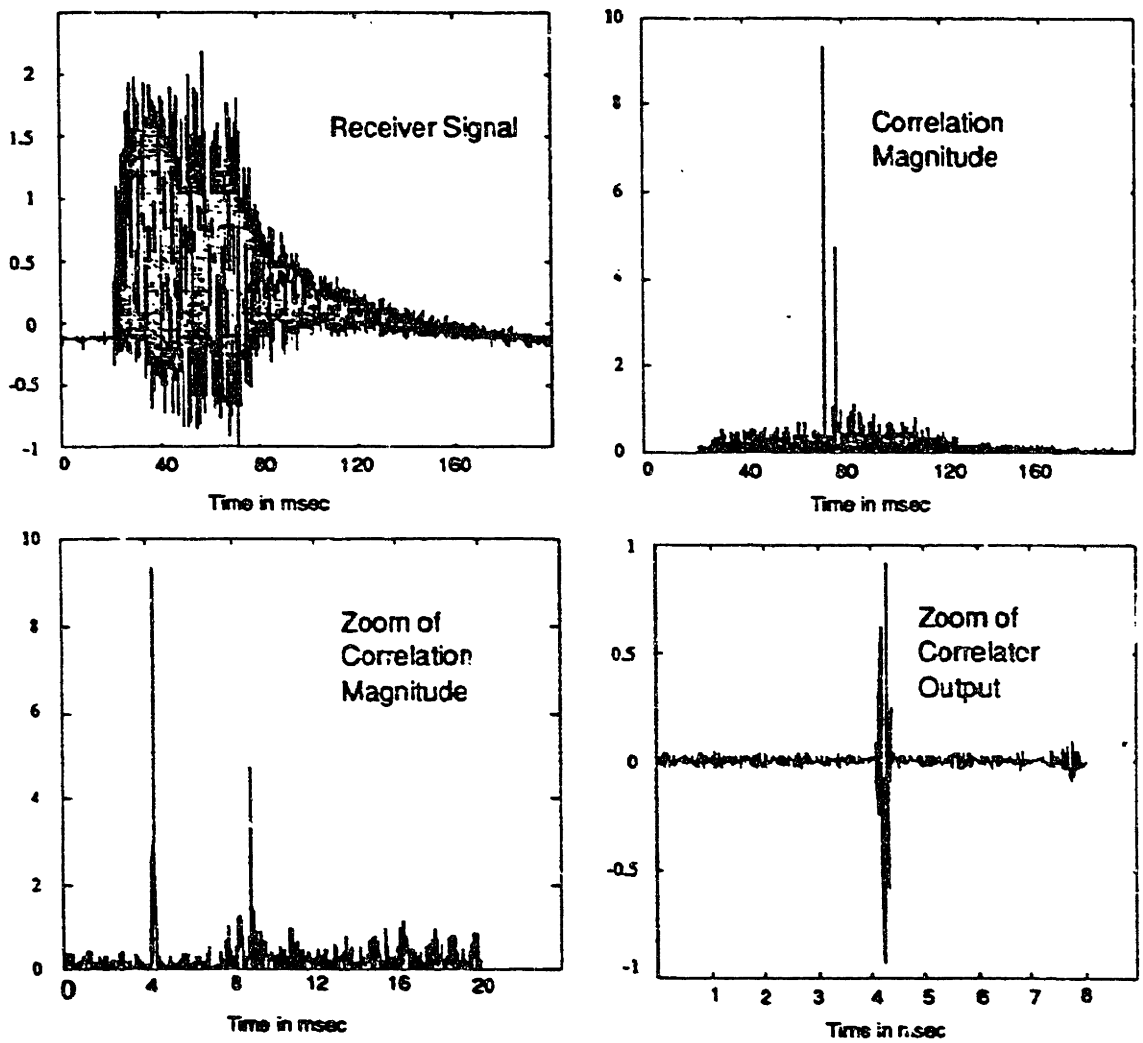

Figure 5.4. Received data from a pseudorandom broadband transmission.

This data was generated using the 51.1 msec pseudorandom broadband pulse with a bandwidth of 10 kHz and a center frequency of 10 kHz. The signal was modulated using a 511 point maximal length sequence and PSK suppressed carrier modulation. The receiver processing used replica correlation, but the hydrophone data was not basebanded. The receiver digital sample rate was 50 kHz which results in an over resolution of the correlator peaks by 5 samples. The upper left plot shows the receiver signal prior to processing by the replica correlator. Distortion of the signal along with the effects of multipath propagation can be seen in the data. The upper right plot is the output of the replica correlator. The ambiguity function pedestal can be seen, along with two correlation peaks. The first peak is from the direct path propagation while the second one is from the bottom bounce path. The bottom left plot is a zoom view of the upper right data showing the two peaks again. Finally, the lower right is a further expansion of the first correlation peak and is plotted without taking the absolute value of the data. The symmetric peak has a well

defined structure, which combined with the over sampling at the receiver front end, provides enhanced resolution for estimation of time delays.

The results of the receiver correlator test are shown in Figure 5.4. This experiment demonstrated that this signal is capable of producing accurate time delay estimates which could be used to determine range to a target. The correlator gain was 25 dB and the peak to maximum sidelobe gain was 13.6 dB, which agrees well with the theoretical value of 13.5 dB.

5.2.6 Conclusions and Design Decisions from Phase 1 Experiments

The following conclusions were drawn from this first series of experiments.

1) High frequency pseudorandom broadband pulses using PSK modulation can be transmitted through a shallow water channel under multipath conditions and still be coherent at the receiver. The PSK modulated data transmitted by A.Z. Quazi and W.L. Konrad used similar frequencies and bandwidths, but their experiment was conducted in a deep water direct path environment and was specifically designed to avoid multipath problems. Deep ocean tomography experiments have also used pseudorandom broadband pulses with PSK modulation, but at a much lower frequency and with considerably less bandwidth.

2) The wide-band nature of this pulse makes deep signal fades caused by multipath interference unlikely. None of the test data, including omnidirectional cases with strong multipath interference

caused by nearby pier structures, showed evidence of significant signal fading periods. This should yield considerably improved performance over conventional active sonar pulses which can exhibit deep signal fades in a multipath condition caused by either multiple eigenrays or from a complex target with multiple reflectors.

3) The PSK pulses can be filtered and bandwidth limited to the reciprocal of the chipping rate and still yield acceptable time delay estimates at the output of the receiver correlator.

4) Successful use of these waveforms requires exceptionally accurate as well as stable clocks and local oscillators in the receiver and transmitter.

5) The existing hardware was inadequate for reliably generating a parametric sonar beam.

6) While these tests were not successful in transmitting the desired signal using a parametric sonar it was clear that to obtain the narrow beamwidth with very low sidelobes desired for shallow water imagery a parametric sonar was necessary. The parabola design worked reasonably well in demonstrating many of the system concepts but the sidelobes of the parabola were only about -17 dB down and the beamwidth was only narrow enough if the pulse frequencies were above 40 kHz. The sidelobes alone would cause significant interference from boundary reverberation in the shallow water environment.

As a result of these conclusions and other lessons learned in working with the test bed system the following decisions were made concerning the system design:

1) The pseudorandom broadband pulse with a 0.1 msec chipping rate and PSK modulated by a 511 point maximal length sequence was selected as the primary waveform.

2) The transmitted pulse would be bandwidth limited to eliminate ringing in the transmitter. If necessary, the bandwidth could be limited to the reciprocal of the chipping rate.

3) A parametric sonar transmitter would be implemented so that the required directivity could be achieved with a reasonable size array.

4) Because of the problems encountered in implementing a new design parametric sonar transmitter an existing parametric sonar would be modified and used for the following experiments.

5) The projector drive electronics would incorporate an accurate method to measure both projector excitation voltage and current simultaneously. This was necessary to provide accurate measurements of transmitter power and to ensure an acceptable impedance match is maintained when wide bandwidth signals were used.

6) The projector bandwidth would have to be at least 10 kHz to transmit the modulated signal plus sufficient bandwidth to include the other CW primary frequency.

7) The transmitter power supply would have to include sufficient energy storage to reduce the peak supply line current and avoid excessive supply voltage droop. While this may seem to be merely a design detail, the failure to adequately address this concern in the test bed design contributed significantly to many of the data analysis problems. Several instances of apparent malfunctions in the receivers could be attributed to poor stability in oscillators, amplifiers, and recorders due to low supply voltage conditions.

5.3 Phase 2: Preliminary Development of the Prototype System

5.3.1 Modifications to an NBSS-1 Commercial System

After identifying the problems faced in implementing a new design parametric system, it was decided to obtain a commercial parametric array system. Although none of the commercially available systems had all of the desired characteristics, one system fulfilled most of the requirements and could be modified to incorporate the rest. This system was the NBSS-1, originally designed by Raytheon Submarine Signal Division, available through Specialty Devices, Incorporated. The NBSS-1 was designed as a dual primary frequency parametric system capable of transmitting either

CW or LFM pulses. The following modifications to the NBSS-1 were performed to meet the requirements for the experiment.

1) The modulator was modified to accept the modulated PSK signal from an external source via a BNC front panel connection. External triggering and clocking connections were also added.

2) The system bandwidth was increased by adjusting the transducer matching network to permit transmission of wide-band acoustic signals.

3) The power supply input was changed from 440V three phase to 120V single phase and additional energy storage was added to prevent voltage droop during long duration pulses. Although this was not absolutely required for the experiment it greatly expanded the number of potential experiment sites.

Modifications to the modulator circuit were reasonably straightforward. An FET switch at the input connected either the existing internal FM-chirp or an external signal to the modulator. In the modulator the selected signal was summed with a 184 kHz CW component, then passed through a low gain buffer amplifier with a passive attenuator network at the output. Transmitter output power was controlled by adjusting the amount of attenuation provided by this network. Although the previous set of experiments had indicated that it was desirable to supply the 184 kHz from the same stable digital source as the modulated signal, this would have required additional modifications to the circuitry. In an effort to minimize the already substantial changes to the original system, the

first parametric experiments were conducted with the 184 kHz CW primary component supplied from the NBSS-1 internal oscillator. The external modulation was supplied from the digital modulator discussed in Chapter 4 and the previous section.

The most challenging part of the modification was the matching network. Although some preliminary test data for the transducer was available, the reported data contained only the essential points required to implement a CW system. These test had been designed to determine the transducers resonance and antiresonance points. Any additional information was unavailable. Unfortunately, this resulted in designing the matching network by trial and error. Based on previous experience Specialty Devices implemented a matching network which used a single transformer to both raise the power amplifier output voltage and cancel the reactive component of the transducer. The impedance match was evaluated by using two CW tones as input signals and measuring the phase of the voltage and current.

The single transformer method of transducer matching has been used successfully in other designs but can be exceptionally difficult to achieve in practice. The difficulty lies in cancelling the transducer's reactive component which, of course, is essential to eliminate reflected energy from the transducer and its deleterious effects on the power amplifier. When a single transformer is used the reactive component of the transducer is cancelled by the leakage reactance of the transformer. This leakage reactance is always present, due to imperfect coupling between the transformer

windings, but its value is not easily predicted. This is particularly true when the transformers are hand wound as they had to be for this application.

The power supply designed for this experiment was a single phase 120V input supply capable of providing regulated +55V at 30A for 100 msec. Voltage regulation was provided by a switching regulator with a nominal 25 kHz switching rate controlling three MOSFET switching transistors. The supply had an 80,000 μF capacitive storage bank.

5.3.2 Low Power Testing

The first test of this system was conducted in Plano, Texas at Lake Lavon, a man made reservoir associated with an Army Corp of Engineers dam. The test was performed at a marina on the lake with the transmitter and receivers separated by about 91 meters (300 ft) in approximately 7.6 meters (25 ft) of water. The purpose of this experiment was to check out the equipment and verify that the receiver could correlate against the difference frequency signal. At this point in the test program the electrical power to the transducer was limited to about 50 Watts due to limitations in the insulation of the matching transformer primary windings. Nevertheless, even at these low power levels the difference frequency signal was clearly discernable at the receiver.

The receiver for this set of experiments, shown in Figure 5.5a, was different from the previous experiments. The receiver system was built around a Spectral Innovations Array Processing card

(MacDsp 256kc) with a 1 MHz 12 bit single channel A/D converter daughter card hosted on a Macintosh 2ci computer. Clocking pulses for the A/D converter were generated by the Analogic 2020 polynomial waveform synthesizer.

Software was provided to digitize and store the received data on a 300 Megabyte SCSI compatible hard disk which had been reformatted and modified to operate with the Macintosh. Once the data was acquired, it was converted to a Matlab™ readable format and processed by a receiver implemented in Matlab™. The data was not basebanded prior to correlation processing and no additional filtering was used to correct for transducer roll-off or other effects. The Wavetek analog filters provided antialiasing filters and were also useful in selectively removing either the primaries or secondaries prior to digitizing the data

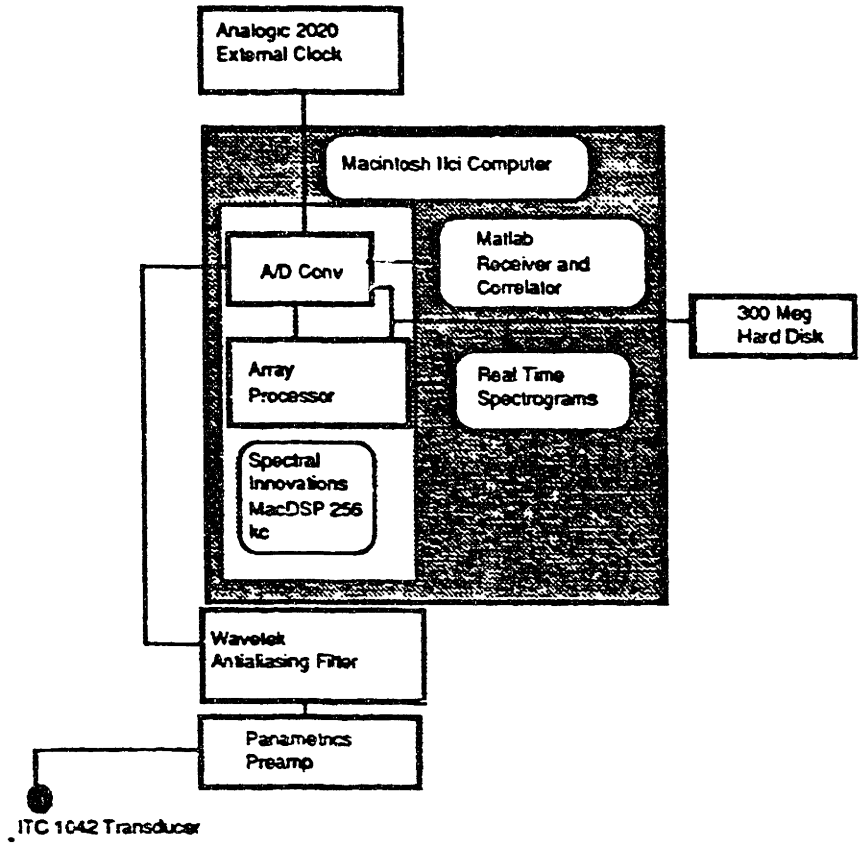

Figure 5.5a. Block diagram of the receiver hardware configuration used for the Lake Lavon experiments.

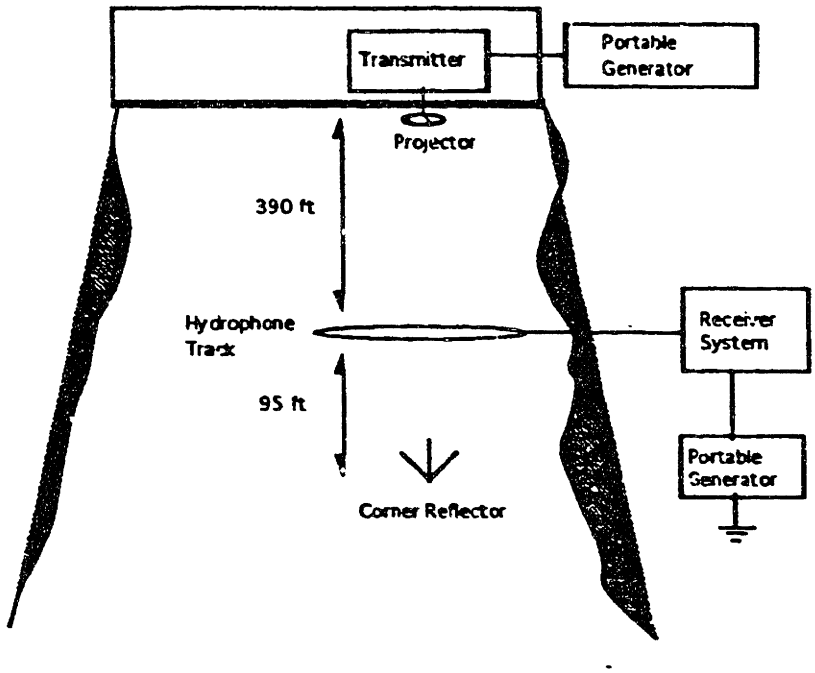

Figure 5.5b. Test site configuration for the Lake Lavon dam experiments.

The plan for the marina test was 1) to verify that parametric difference frequency signals could be formed with this apparatus, 2) that the modulated primary signal was not adversely affected by the transmission process, and 3) that the difference frequency signal could be processed with the receiver. As soon as the system started transmitting the difference frequency signal was visible in the spectrum displays of the receive hydrophone data. The bandwidth and shape of the difference frequency signal corresponded with the bandwidth and shape of the modulated primary.

To verify that the primary modulated signal was not adversely affected by the transmitter hardware, the receive hydrophone data was filtered with an analog bandpass filter with a passband from 140 kHz to 200 kHz. By using a bandpass filter, low frequency noise

was eliminated which permitted translating the primary signals to a lower frequency without contaminating the data with noise. The primary frequencies were translated by clocking the A/D converter at 80 kHz which aliased the 174 kHz modulated primary to a 14 kHz center frequency. While some noise in the 180 to 200 kHz band was also aliased into the signal bandwidth, the aliased noise was insignificant since there was very little ambient noise above 180 kHz and the signal-to-noise ratio was in excess of 15 dB. Once the signal had been digitized it was processed by a replica correlator which had filter coefficients selected for the 14 kHz center frequency. The results of this correlation showed a post correlator gain of 26.8 dB which agrees very well with the theoretical gain of 27 dB.

After verifying the primary signals were transmitted satisfactorily, the Wavetek filter was reconfigured as a lowpass filter with a 30 kHz cut-off frequency. The receiver was then used to process the difference frequency signal. Unfortunately, the correlator output did not contain any discrete peaks. The lack of peaks was suspected to be caused by instability in the transmitter's 184 kHz oscillator. If this oscillator was not set at the correct frequency, the difference frequency signal would be displaced in frequency which would degrade receiver performance. This condition was not necessarily easy to diagnose since the transmitted pulse was 51.1 msec long and therefore, the resolution of a conventional spectral estimator was poorer than the frequency error tolerance of this signal. To evaluate this problem, an

algorithm which searched a selected frequency band for the maximum correlator response was used to process the difference frequency. The Burg 2 high resolution spectral estimation algorithm was used to estimate the actual frequency of the 184 kHz CW component which had been previously digitized. Both of these methods verified that the 184 kHz oscillator was drifting as much as 100 Hz. Later analysis of the data demonstrated a correlation gain of approximately 25 dB was realized when the appropriate frequency corrections were added to the receiver calculations.

Additional modifications to the equipment were performed to correct the oscillator drift problems. The transmitter oscillator circuits were disabled and the Matlab™ modulator program was modified to linearly sum the CW signal with the modulated signal. Another test was scheduled to be performed at Lake Lavon in deeper water. The purpose of this experiment would be to evaluate the performance of the system with the new modulator configuration, record data which could later be used for analysis, and obtain echoes from a set of corner reflector targets.

5.3.3 Low Power Testing with Improved Modulator Stability

The next test at Lake Lavon was conducted by suspending the transducer from the dam to a depth of 4.9 meters (16 ft.). The receiver was located about 119 meters (390 ft) away with corner reflector targets 29 meters (95 ft) behind the receiver hydrophone. The receiver hydrophone and targets were mounted on reelable

assemblies which were aligned perpendicular to the axis of the acoustic beam. This arrangement, shown in Figure 5.5b, allowed the positions of the receive hydrophone and targets to be adjusted with respect to the transmitted beam.

The results of the receiver correlator test are shown in Figure 5.6. This demonstrated that the system was capable of producing a modulated signal at the difference frequency with sufficient fidelity to support accuurate time delay estimation. The correlator gain was 22 dB and the peak to maximum sidelobe gain was 12 dB.

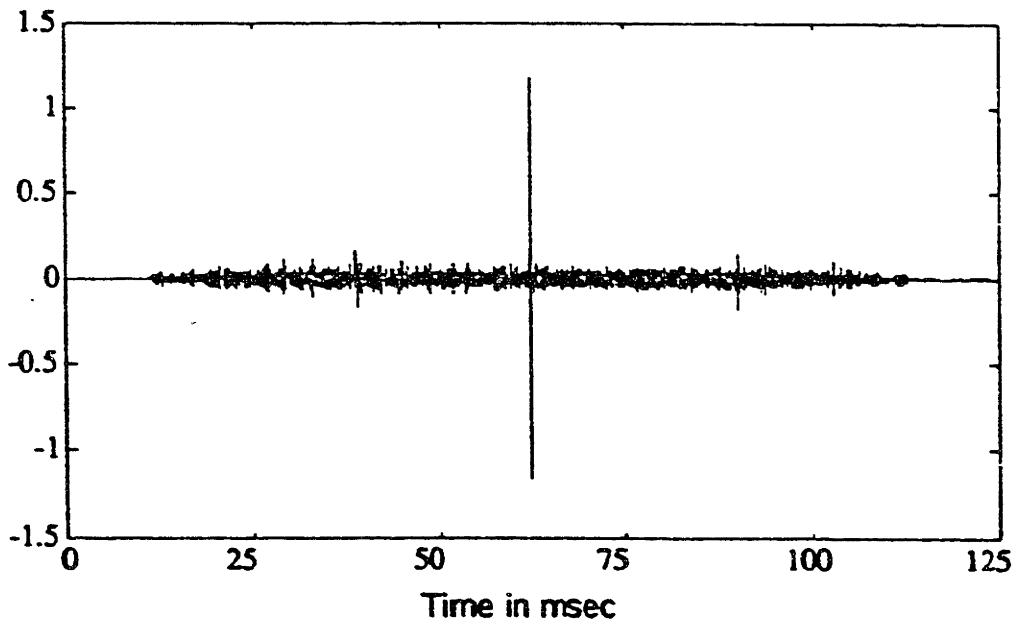

Figure 5.6 Receiver correlator output from Lake Lavon test.
This plot shows the results from processing the difference frequency signal with the receiver. The characterisitic pedestal and correlation peak can be seen in the data. This experiment confirmed that the parametric array could transmit pseudorandom broadband signals with sufficient fidelity to support time delay estimation. Also note that because of the very narrow beamwidth there is only one arrival path evident in the data.

The data recording portion of the test was primarily designed to acquire data for evaluating future receiver modifications. The hydrophone was in the near-field of the parametric array, but the data gathering system was configured so that rough estimates of the conversion efficiency could be made using the recorded data. Normally conversion efficiency is determined by measuring the difference frequency acoustic power at a range greater than the near-field of the parametric array and calculating the primary acoustic power based on the electrical input power to the transducer. Corrections are then applied for the difference frequency spreading loss and absorption.

For this experiment, the acoustic power at the primaries was also measured with the receiver hydrophone. This provided an independent method to compute conversion efficiency and primary power should there be a problem in resolving the measurements by the conventional method. The data could not be analyzed immediately because the receiver hydrophone was only calibrated to 100 kHz. Additionally the hydrophone is not omnidirectional above 100 kHz, but exhibits some directionality at these frequencies since it is large with respect to a wavelength. Despite these limitations the required data was collected so that, once the hydrophones had been calibrated, an estimate of parametric conversion could be obtained.

The corner reflector targets may have been detected but due to uncooperative weather conditions target detection could not be

confirmed. The receiver required about 20 minutes to process two seconds of data. Therefore, unless the target echo had a positive signal-to-noise ratio and could be observed without correlation processing. the time required to position the targets and receivers in the narrow beam was prohibitive. There were some indications that the corner reflector might have been detected on the edge of the acoustic beam, but the test was interrupted by a hail storm which inundated the area. The experiment continued briefly until lighting strikes in the vicinity of the dam convinced the test team (particularly those on the dam) that further testing was imprudent.

5.3.4 Conclusions From Low Power Parametric System Testing

In general these experiments were successful and indicated that the system was capable of supporting the experimental program. The following conclusions were drawn from these experiments.

1) A pseudorandom sequence using PSK modulation could be used in a parametric sonar to produce a signal at the difference frequency with sufficient fidelity to provide accurate time delay estimates using a replica correlator.

2) The importance of frequency stability in any component which directly affects the stability of the signal in its transmission or reception was reinforced. This problem has been solved in the transmit system by digitally synthesizing all the components of the waveform and using a stable accurate D/A converter. The receiver

uses high quality A/D converters with stable clocks to avoid corrupting the signal.

3) The difficulties in transducer matching to accommodate wide-band signals was demonstrated. Several bipolar output transistors failed during the experiments as the matching network was being adjusted.

4) Array positioning with the narrow beamwidth system continued to be a problem. An improved array steering control system was required.

5.3.5 Preliminary Boston Harbor Test Facility Configuration

At the completion of the Texas experiments, the system was shipped to Boston, Massachusetts and assembled at a test site shown on Figure 5.1 as site 2. The projector and hydrophones were mounted on a structure which could be steered in bearing and D/E. This assembly, shown in Figure 4.1, featured precise steering control by linear actuators which could be positioned remotely. The electronics for the system were housed in a heated test shack at the end of the pier provided by the MIT Sea Grant College program. The cables for transmitter power, receiver signals, array positioning control, and D/E indication were routed from the test shack to the array assembly in a semi-permanent fashion.

Approximately one week of testing was devoted to eliminating transmitter RF leakage into the receiver and control systems. The

EMI from the transmitter tended to overloaded both the receiver front end and the array position indicators. To reduce the EMI, the shielded twin lead transmitter cable was placed in conduit which was grounded to the same point as the cable inner shield. The conduit ran down the pier to a point at least six feet below the water line for the lowest tides experienced. Extra cabling, necessary to allow for the tidal motion of the barge and for array steering, was kept well submerged to provide additional shielding. The EMI was further reduced by minimizing the length of receiver cabling. Initially the excess receiver cables were neatly wound on hose reels near the receiver preamplifiers. This arrangement provided an antenna for the RF leakage which resulted in severe receiver overloading. After the cables were removed from the hose reals and stored in a random fashion under the test shack, performance improved dramatically.

5.3.6 Synopsis of the Investigation into Low Radiated Acoustic Power Problems

At this point it is worth deviating from the chronological description of the experiments to provide some insight into the problems encountered and the rational for the following experiments. The NBSS-1 power amplifier and transducer had been functioning for several years in bottom topography measurements and sub bottom profiling modes. In general, CW and narrow-band LFM pulses were used for these operations. Under these conditions system performance was acceptable and, as long as the bandwidth was small, an adequate match to the transducer was achievable.

During the first Boston harbor experiments, it became obvious that there was a fundamental problem in the NBSS-1 design. In several tests, acoustic performance predictions indicated that the echo should have a large positive signal-to-noise ratio prior to correlation, and yet no echoes were detected. Extensive investigations of the harbor environment using both ray theory and the Parabolic Equation (PE) model indicated that even under the most adverse propagation conditions encountered there should have been detectable echoes. There were strong indications that the acoustic output power was in fact much lower expected.

Since some excellent quality returns had been detected from high target strength objects, suggesting that the system was capable of yielding high resolution results, it was decided to continue with the experiments while conducting a parallel investigation into the apparent lack of acoustic power. Experiments intended to quantify the power output and conversion efficiency of the system were added to the planned Boston Harbor experiments. The relatively high ambient noise, shallow water, and rapid temporal variability present in the harbor made these tests difficult to accomplish with a high degree of accuracy, but they revealed that the acoustic power was at least 9 dB below the predicted values. Finally, an impedance bridge was used to measure the transducer's in-water impedance as a function of frequency. These measurements conclusively demonstrated that the transducers resonant frequency was 157 kHz, not 174 kHz as indicated in the calibration data.

A model of the transducer, developed by Mr Ken Rolt of MIT, agreed very closely with the measured transducer impedance values [Rolt and Irza, 1991]. Using the measured data and the model new operating frequencies were chosen. The higher projector efficiency at these frequencies yielded significantly more primary power and a higher parametric conversion efficiency. Because of the difficulty in modifying the original NBSS-1 power amplifiers to operate at the lower frequencies, another off-the-shelf amplifier was used to drive the transducer. The details of this design are discussed at the end of Chapter 4. The modified system was not ready in time to support the planned experiments so all of the results reported in this chapter used the original NBSS-1 system and operating frequencies. The remainder of the chapter will deal with the experiments and design changes in a chronological format.

5.3.7 Transducer Matching Network Improvements

Prior to shipping the system to Boston, the matching transformer was replaced to increase the output power of the system. During the Lake Lavon experiments output power had been limited by the power amplifier output voltage. To correct this, the turns ratio of the output matching transformer was increased to raise amplifier output voltage. Unfortunately, the new transformer caused significant distortion in the output signal. Several transformers were wound and tested but none provide adequated output voltage while simultaneously matching the transducer impedance.

As discussed previously, when a single transformer is used it is often difficult to obtain a satisfactory impedance match. A better approach is to design a matching network with a transformer and a separate tunable inductor placed in series with the transducer. The series inductor can be adjusted to offset the transducer reactance as well as other reactive components such as the inter-winding capacitance of the transformer itself. When this approach was used matching the amplifier to the transducer became a relatively simple matter of adjusting the number of turns on the inductor. The tunable indicator, which was also wound on a 3C8 core, was adjusted to achieve in-phase voltage and current at the transformer. The result of this effort was undistorted output waveforms at about twice the previous power.

Once the impedance match had been accomplished the impedance seen by the amplifier at the secondary of the transformer was 36 Ohms. Attempts to drive a lower impedance load resulted in severe distortion. It was not difficult to show that the output impedance of the NBSS-1 amplifier was approximately 6 Ohms at the primary of the transformer. The transformer was wound with a turns ratio of 1:2.44 which scales the impedance by 1:6. Therefore, with a secondary impedance of 36 Ohms the power amplifier was matched to its load. Unfortunately this resulted in a maximum output voltage of 134 V peak and a maximum output power of only 249 watts, far below the rated 4 kW of the amplifiers. Nevertheless, the system produced signals at the difference

frequency which were capable of detecting targets and resolving complex structures on those targets.

5.3.8 Power Supply Modifications

Some modifications to the power supplies were required due to the poor electrical grounds at the test site. The power supply operated flawlessly in the laboratory or when powered by a gasoline generator grounded with a metal stake driven into the earth. However, when connected to site power, the supply was extremely susceptible to electrical noise including the RFI from the transmitter. When using on-site electrical power, the +55 V regulation became unreliable causing unacceptable signal distortion. Interim grounding improvements were attempted, but were unsuccessful. Catastrophic failure of the regulator finally occurred, resulting in a fire and damage to other power supply components.

The cause of the regulator instabilities was traced to a transformer circuit in the regulator. This switching regulator used MOSFETs, which are susceptible to damage if the gate to drain voltage maximums is exceeded. These particular MOSFETs had a gate to drain maximum of 10 volts. Since the drain voltage was nominally +55 V and the regulator chip output switching pulse voltage was +15 V, a transformer was used to boost the output of the switching to about +55 V. The transformer and other components required for protection of the MOSFETs formed a low Q resonant circuit with a resonance frequency close to the transmitter output frequencies. RFI noise introduced from the transmitter

caused large voltage excursions in the MOSFET gate voltage and loss of regulation.

To eliminate this problem, the power supply was redesigned using the same MOSFET switching regulator concept, but with the transformer replaced by a bipolar transistor common emitter voltage amplifier which boosted the switching regulator pulses to the required +55 V. Additional RFI isolation in the power supply regulation was provided by an optoisolator between the base of the transistor and the output of the regulator chip. The Vcc for the voltage amplifier was supplied from an unregulated point in the power supply. A 200 µF capacitor and an isolation diode were added from Vcc to ground. These components ensured that Vcc was adequate during the entire transmit pulse even while the rest of the power supply voltages were drooping. Finally, although these MOSFETs were designed to be switched in the 200 kHz region, the original power supply switching frequency of 25 kHz was retained to avoid operating the regulator near the transmit frequencies which might introduce further RFI problems. This arrangement worked very well under all the grounding conditions experienced in the subsequent tests.

5.3.9 Development of a Calibrated Hydrophone

To provide the ability to measure acoustic power levels at frequencies above 100 kHz, a calibration experiment was performed on an ITC 1042 hydrophone using the two transducer reciprocity method [Bobber, 1970]. This method requires that both transducers

have the property of reciprocity and identical sensitivities. Hydrophone sensitivity curves provided by the manufacturer indicated that the sensitivities were essentially identical from 10 kHz to 100 kHz.

Reciprocity, of course, requires that a transducer be at least linear, passive, and reversible. As pointed out by Bobber there is no simple method to assure that the *transducers* are in fact reciprocal, but one method of verifying that at least the transmit and receive *systems* are reciprocal is to take a set of measurements and then reverse the role of the transmitter and receiver transducers. If the new set of measurements agrees with the previous set, it is reasonable to assume that the *system* is reciprocal. For this experiment, the roles of the transducers were reversed after each measurement and the results compared. This reciprocity check provided convincing evidence that the system was in fact reciprocal.

The tests were conducted by suspending the two transducers in water at a predetermined depth and with a known distance between the two elements. One of the elements was used as a projector and the other as a hydrophone. The driving current to the projector was measured while it was driven with pulsed CW at the desired frequency for calibration. The hydrophone voltage response was measured after allowing for the propagation time delay. From these measurements, the hydrophone receive response was calculated by using the relationships provided by Bobber. The equations shown below are from Bobber with the appropriate modifications required for the result to be in dB re 1 volt/μPa.

$$M = 20\log\left(\frac{e_{TH}\,J}{i_T}\right)^{1/2}$$

$$J = 2\frac{d_1}{\rho f} \times 10^{-17}$$

where:

M is the hydrophone sensitivity in dB re 1 volt/μPa,
e_{TH} is the measured hydrophone voltage in volts,
i_T is the measured projector current in amps,
J is the reciprocity parameter,
ρ is the density of the test media in gm/cc,
d_1 is the distance in cm, and
f is the frequency in Hz

The equipment setup for this experiment is shown in Figure 5.7. Both transducers were placed at a depth of 4.95 meters (16 ft) and connected to the test equipment with 61 meters (200 ft) of DSS-3 cable. The transducers were placed deep enough for the multipath arrival time to occur after the measurement window and far enough apart to allow for the acoustic propagation time to be longer than the pulse length. Maintaining the pulse length shorter than the acoustic propagation time avoids contamination of the data by induced voltages in the hydrophone cables caused by electromagnetic fields from the projector cables. Transducer drive was supplied from the Wavetek function generator which was operated in a gated trigger mode with the trigger and gate time supplied from the Analogic 2020. This configuration allowed the pulse repetition rate, pulse width, drive levels, and frequency to be easily adjusted.

To determine drive current, the voltage drop across a 10 Ohm resistor in the return line was measured using the LeCroy oscilloscope. On the receive side, the hydrophone output was connected to a Panametrics preamplifier and then to the other channel of the LeCroy oscilloscope for hydrophone voltage measurement. Since the signal-to-noise ratio did not support accurate measurements of the hydrophone voltage in the time domain, the waveforms were examined in the frequency domain. The LeCroy oscilloscope was equipped with a mathematics and FFT package, allowing the oscilloscope to perform many of the functions of a spectrum analyzer. For signals below 100 kHz, the HP 3562A spectrum analyzer was used which provided quick measurements of hydrophone levels at the desired frequencies. All measurements above 100 kHz had to be made with the LeCroy oscilloscope due to the sample rate limitations of the HP 3562A spectrum analyzer. Both instruments were used for measurements below 100 kHz to verify the measurement system.

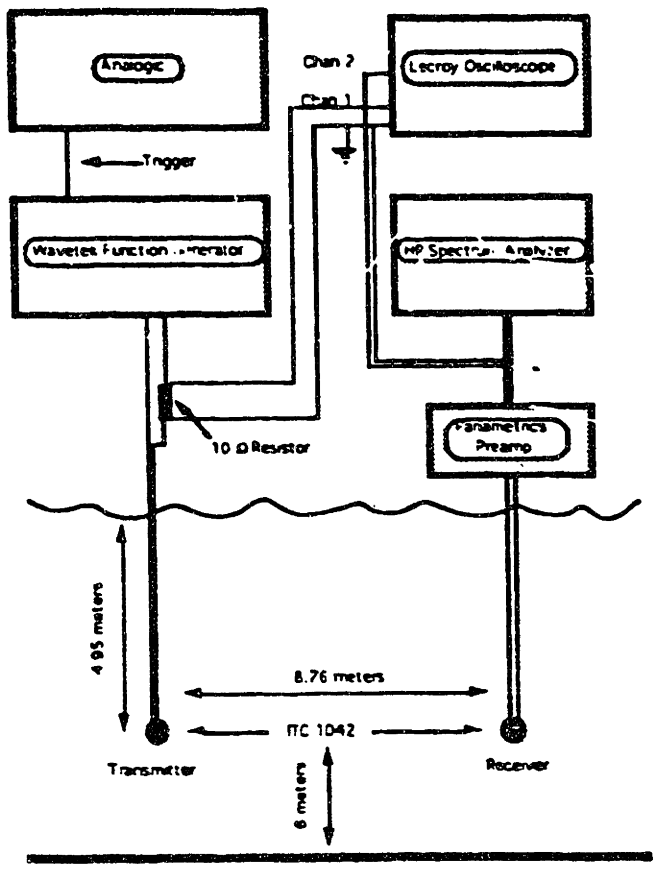

Figure 5.7. ITC 1042 Hydrophone Calibration Experiment Hardware Configuration.

After the hardware was configured, a number of short duration pulses were transmitted to evaluate the optimum pulse length. The first direct path arrival was at 5.9 msec, corresponding to a sound velocity of 1485 meters/sec, with a multipath arrival at about 8.9 msec. Sound velocity was measured and compared with the computed value as a check on hydrophone placement. Based on the desire to measure only direct path signals for this experiment a 1.0 msec pulse was selected as the test pulse. The oscilloscope was then configured to trigger on the Wavetek output with a trigger delay of 5.9 msec and a data acquisition time of 1.0 msec.

Once the effects of the experiment geometry quantified, it was only necessary to measure the receive hydrophone voltage and the transmit current. Receive voltage was measured by applying a flat top window to the hydrophone data and transforming to the frequency domain. A flat top window was used to reduce scalloping loss effects on the amplitude measurements while still providing some side lobe control. Since the oscilloscope was set to display the magnitude of the spectrum in dBm, it was straightforward to convert to volts RMS and apply the correction for the 40 dB of preamplifier gain to determine the hydrophone voltage. The transducer drive current was measured by determining the voltage drop in RMS volts across a 10 ohm resistor in the transducer supply cabling. Traditionally, the voltage and current values have been measured as peak volts and amps but since the quantities appear as a ratio the scaling factor is immaterial.

The results of the calibration experiment are shown in Figure 5.8. The agreement between measured values and the ITC reported values below 100 kHz is quite good. In addition, the agreement between measured values with the source and receiver elements reversed is also very good which supports the claim of reciprocity. The dashed line in Figure 5.8 represents the ITC equivalent circuit model results for an ITC 1042 transducer above 100 kHz, although no previous experimental measurements have been made to confirm the model results. Based on the apparent agreement in this data these measurements should provide a sufficiently accurate calibration for

the ITC 1042 transducers to be used in estimating the performance of the wide-band parametric sonar.

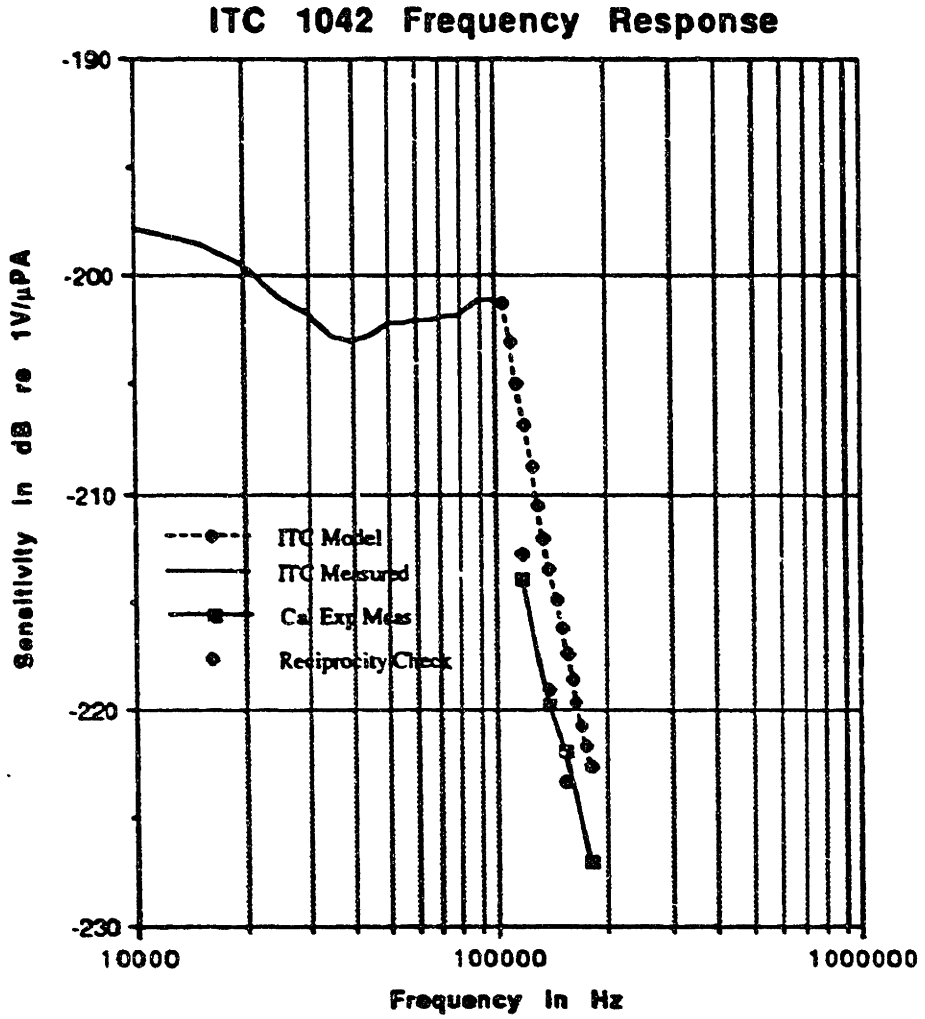

Figure 5.8. Plotted results of the ITC 1042 calibration.

The solid line from 10 kHz to 100 kHz is from the ITC measured data supplied with the hydrophone, including 16 ft of DSS-3 cable losses. The dashed line above 100 kHz is from ITC model data for the same hydrophone and cable length. The solid line and associated data points above 100 kHz is the data measured in the calibration experiment, including 200 ft of DSS-3 cable losses.

5.3.10 Parametric System Characterization: Power Level and Conversion Efficiency Measurements from the Lake Lavon Test

Calibration of the ITC 1042 hydrophone provided the opportunity to evaluate the performance of the parametric sonar. The first experiments in Boston Harbor indicated that the sonar output power was significantly lower than predicted. To quantify the magnitude of the apparent loss in power, the data obtained in the Texas experiments could now be reanalyzed to estimate primary output power as well as conversion efficiency. Although these experiments were not originally designed to provide quantitative measurements of acoustic parameters, sufficient data was available to reconstruct the information required for these measurements. Spectral Innovations provided the necessary technical information on the resource forks of the data file to recover all of the MacDSP data acquisition system settings. The filters and external amplifiers were then calibrated in the laboratory so that the appropriate gain corrections could be applied. The calculations are summarized in Tables 5.1 and 5.2. It is important to recognize that this analysis incorporates all of the corrections determined during the investigation of the apparent lack of transmitter power. Many of these corrections were not determined until the transducer had been characterized at the very end of the experimental program. The very close agreement between the transmitted power estimates calculated by the two different methods indicates that the final model for the transducer was very good and that the other errors in

power calculations were accurately quantified. If these results had been known during the test program the hardware would certainly have been modified to increase output power to sufficient levels.

Parameter	Measured Value
184 kHz Measured Spectrum Level Using Blackman Window 75% Overlap (SL).	+2.2 dB
MacDSP Analog Gain Setting Of 4X (G_{dspa})	+12 dB
Antialiasing Filter Gain (G_{aaf})	-16.5 dB
Preamplifier Gain (G_{pa})	+60 dB
Hydrophone Sensitivity Re µPa @ 1m (M)	-227 dB
Absorption Loss @ 184 kHz 15 °C Fresh Water (α)	.0086 dB/m
Absorption Loss @118m (αR)	1.0 dB
Spherical Spreading Loss @ 118m (PI)	+41.5 dB
Source Level Re µPa @ 1m (L)	216.2 dB

$$L = SL - (G_{dspa} + G_{aaf} + G_{pa}) - M + (\alpha R + PI)$$

Table 5.1 Primary Source Level Computed By Far Field Hydrophone Measurement

Parameter	Calculated Value
Measured Power Input To Projector at 184 kHz re 1 W (PI)	+13.9 dB
Computed Projector Efficiency at 184 kHz (ε)	-9.2 dB
Projector Directivity Index (DI)	+40 dB
Source Level of 1 W re µPa @ 1m (L_{ref})	+170.8 dB
Source Level @ 1m Re µPa (L)	214.9 dB

$$L = Pi + \varepsilon + L_{ref}$$

Table 5.2 Primary Source Level Computed By Input Power To The Projector

Most of the entries in Tables 5.1 and 5.2 are self explanatory but a few require some explanation. The correction for transducer efficiency used in Table 5.2 was determined by employing the model developed by K. Rolt. The transmitting voltage response (TVR) at the resonant frequency of 157 kHz is 200.4 db while at 184 kHz it is 187.1 dB. This corresponds to a difference of -13.3 dB in the TVR; some of which is due to a reduction in transducer efficiency at 184 kHz. To determine how much of the change in TVR is due to losses in transducer efficiency, it is necessary to convert from a TVR at these frequencies to a normalized transmitting power response at the same frequencies. The ratio of the real part of the impedances at 157 kHz and 184 kHz is .197 which corresponds to a difference in input power of -7.1 dB for a 1V input at both frequencies. Therefore, the transducer losses are 6.2 dB greater at 184 kHz than at resonance. Since this transducer is 50% efficient at resonance, the total loss due to transducer efficiency at 184 kHz is 9.2 dB. The

absorption loss used in Table 5.1 was calculated from the equation by Schulkin and Marsh as discussed in Chapter 2. The low absorption value is due to the fact that the experiment was conducted in fresh water. Finally, the data in the tables shows significant attenuation attributed to the antialiasing filter. To maximize the amount of data which could be collected, the A/D sample rate was only 484.8 kHz which required a filter cutoff frequency of 200 kHz. At the time the data was acquired it was intended to be used to test the correlator and therefore, a flat delay was selected to prevent signal dispersion. The flat delay mode exhibits considerable roll-off in the amplitude response near the cut-off frequency of the filter. Since the 184 kHz signal was very close to the edge of the filter passband it suffered considerable attenuation.

Another parameter of considerable interest is the conversion efficiency of the parametric sonar. Although the recalculated acoustic power in the Lake Lavon experiments was extremely low, it is useful to estimate the conversion efficiency from the measured data. The measured conversion efficiency along with necessary intermediate values are shown in Table 5.3, while the predicted efficiency and the parameters necessary for the prediction algorithm are summarized in Table 5.4. The prediction method used is discussed in Chapter 2.

Parameter	Measured Value
Spectrum Level @ 174 kHz	-3.0 dB
Spectrum Level @ 10 kHz	-21 dB
Δ Spectrum Level	-18 dB
Antialiasing Filter Loss @ 174 kHz	-14.4 dB
Antialiasing Filter Loss @ 10 kHz	0 dB
Δ Filter Loss	-14.4 dB
Hydrophone Sensitivity with 400 ft DSS-3 cable @ 174 kHz	-226 dB
Hydrophone Sensitivity with 400 ft DSS-3 cable @ 10 kHz	-203.3 dB
Δ Hydrophone Sensitivity	-22.7 dB
Conversion Efficiency (G)	-55.1 dB

G=Δ Spectrum Level+Δ Filter Loss+Δ Hydrophone Sensitivity

Table 5.3 Measured Parametric Conversion Efficiency

Parameter	Computed Value
Absorption Loss (α)	.0086 dB/m
Rayliegh Length (Ro)	10.5 meters
Scaled Frequency (L^*)	259 dB
Frequency Ratio (f_r)	1 8
Far-field Conversion Efficiency	-52.5 dB
Far-field Range	400 meters
Near-field Correction	-3 dB
Conversion Efficiency @ 118 meters	-55.5 dB

Table 5.4 Predicted Parametric Conversion Efficiency

When evaluating the data in Tables 5.3 and 5.4 it is interesting to note that the receive hydrophone was not in the far-field of the parametric array. The far-field of the physical transducer starts at 10.5 meters, but the far-field of the parametric array does not start until about 400 meters. Thus, the receive hydrophone was well inside the near field and therefore a correction for the truncated array length was required. Due to the exponential nature of the parametric array shading, the correction is relatively small even though the hydrophone was located only about one quarter an array length from the source.

5.3.11 Parametric Array Far Field Conversion Efficiency Measurement

Another conversion efficiency experiment was conducted in Boston Harbor to more accurately determine the parameters necessary to compute performance estimates for the sonar system. This experiment was also constructed to verify that nonlinear mixing in the transmitter power amplifiers or projector was not contaminating the beampattern at the difference frequency. One difficulty in designing a parametric system is ensuring that the power amplifiers and projector remain linear. If significant nonlinear components are generated in either the power amplifier or projector, the beamwidth at the difference frequency will not be the narrow beamwidth of the parametric array but instead will have the beamwidth predicted for the physical array.

Prior to performing this test the spectrum of the voltage excitation to the transducer was monitored with an HP 3562 dynamic signal analyzer. This analyzer is limited in frequency to 100 kHz but was very useful in examining the amplifier output for the presence of low frequency components caused by nonlinearites in the system. There were some nonlinearities present in the amplifier as shown by a weak signal at the difference frequency, but the signal was about 80 dB below the primaries. In many systems, the difference frequency formed by nonlinearities in the amplifier is not radiated as acoustic power due to the low efficiency of the transducer at the these lower frequencies. Unfortunately, 8 kHz is

the resonance frequency of the first radial mode of this transducer, so it was possible that some acoustic energy might be radiated.

The experiment was conducted with the transmitter at site 1 and the receivers set up at site 3 as shown Figure 5.1. The receiver consisted of an ITC 1042 hydrophone moored 43 meters (140 ft) from the end of the pier, a Panametrics preamplifier, a Macintosh computer with the MacDSP hardware and receiver software, and an analog VCR recorder for recording the difference frequency signals. The sample rate for the data acquisition system was 941.2 MHz which eliminated the need for antialiasing filters since there was no significant acoustic energy at these frequencies. Measurements were made in real time, although some of the digitized signals were stored for future analysis. Communications between the test sites for array steering and power level adjustments were provided by VHF marine radios.

The results of this experiment are shown in Table 5.5. The measured conversion efficiency is in very close agreement with the predicted performance. Further analysis of the data also showed that there was no appreciable degradation of the modulated signal caused by the nonlinear process. There had been some concern that the lower frequencies might be significantly attenuated due to the increase in the difference frequency to primary frequency ratio across the bandwidth of the signal. As explained in Chapter 2, this ratio is a key factor in the performance predictions of parametric systems using two discrete primaries. In general, the lower the ratio the better the conversion efficiency. In this system, the ratio

varies from 11 at the high frequency end of the modulation to 45 at the low end. Under the conditions of this experiment, the conversion efficiency would have varied from -65 db at the low end to -42.5 dB at the high end if this signal was affected by the change in the ratio. Obviously this would have been a significant problem which would have severely degraded the performance of the system. However, this experiment confirmed that due to the nature of the phase modulation scheme used in this system, large bandwidths can be obtained without significant shading of the signals amplitude across the bandwidth.

Parameter	Measured Value
Spectrum Level @ 174 kHz	-16.1 dB
Spectrum Level @ 10 kHz	-22.4 dB
Δ Spectrum Level	-6.3 dB
Hydrophone Sensitivity with 200 ft DSS-3 cable @ 174 kHz	-226 dB
Hydrophone Sensitivity with 200 ft DSS-3 cable @ 10 kHz	-200.9 dB
Δ Hydrophone Sensitivity	-25.1 dB
Absorption Loss of Primary @293m (αR)	-20.3 meters
Conversion Efficiency (G)	-51.2 dB

G=Δ Spectrum Level+Δ Hydrophone Sensitivity+αR

Table 5.5 Measured Parametric Conversion Efficiency

Parameter	Computed Value
Absorption Loss	.0692 dB/meters
Rayliegh Length	10.28 meters
Product of Absorption Loss and Rayliegh Length	.7116 dB
Frequency Ratio	1 8
Frequency Scaled Source Level	274.8 dB
Far-field Conversion Efficiency	-51.3 dB
Approximate Far-field Range	180 meters
Actual Range	293 meters

Table 5.6 Predicted Parametric Conversion Efficiency

Figure 5.9 is a copy of one of the MacDSP displays which was used to perform the calculations of conversion efficiency. The difference frequency is visible as are the two primary components. Considerable harbor ambient noise is also evident. The components between 60 kHz and 120 kHz must have been related to industrial activity since these would abruptly disappear at 5 PM local time. The higher frequency discreet components were caused by EMI aliasing into this regime. This EMI was removed in later experiments by using a different preamplifier with differential inputs for the hydrophone.

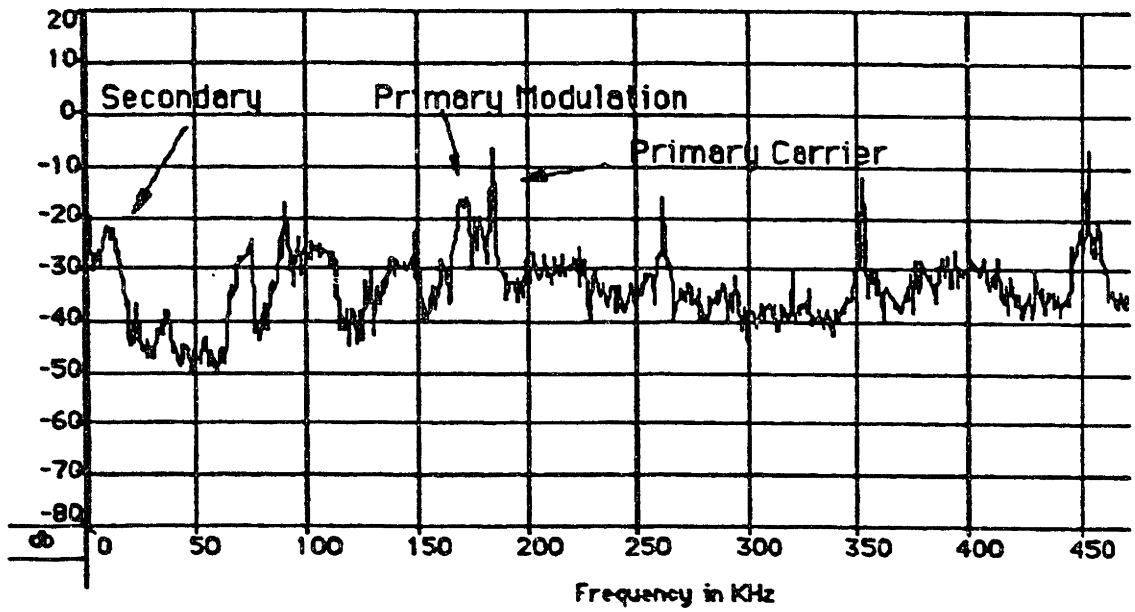

Figure 5.9. Frequency domain plot of the receiver signals during the conversion efficiency experiment.

Both of the primary components are visible between 150 kHz and 200 kHz. The difference frequency data, centered at 10 kHz, is also visible with the same overall spectral shape as the modulated primary. This plot is representative of the acoustic conditions frequently experienced while testing in Boston Harbor. Strong broadband and narrow-band components, such as those shown here from 50 kHz to 150 kHz, were often present. This figure is a copy of the computer screen while using the spectrum mode of the MacDSP Signal Analysis Package.

5.4 High Resolution Sonar Returns From a Bear Class Medium Endurance Coast Guard Cutter

The close proximity of the test site to the Boston Coast Guard Station provided the opportunity to use moored Coast Guard vessels as complex targets for system testing. Medium endurance cutters were frequently present in port at Site 1, pier 2 as shown on Figure 5.1 These vessels were ideal acoustic targets with two rudders and screws as well as a large skeg mounted amidships. Figure 5.10 is a

sketch of the aft end of the version of the Bear class cutters which were based in Boston. These cutters were normally moored starboard side to the pier with the stern section in the line of sight of the sonar system.

For this experiment the transmitted signal was a pseudorandom broadband pulse. The pulse was generated using fully suppressed carrier PSK, modulated with a 511 point maximal length sequence. To minimize ringing in the transmitter and transducer electronics, the signal was limited to a 10 kHz bandwidth prior to transmission. The modulated signal power to the transducer was 75 Watts which corresponds to 222 dB @ 1m Re μPa of acoustic power after accounting for a transducer efficiency of 16% (-8 dB) and directivity gain of 40 dB. Acoustic power at the difference frequency was 171 dB @ 1m Re μPa based on a conversion efficiency of -51 dB between the primary and difference frequencies. The range from the transducer to pier 2 was 366 meters (1200 ft) which results in a two way spherical spreading loss of 103 dB. At 10 kHz the ambient noise as measured on an omnidirectional hydrophone was 48 dB re μPa in a 1 Hz band. Assuming the noise was flat across the 10 kHz spectrum of the signal this produces a total noise in the bandwidth of the signal of 88 dB. The actual noise seen by the receiver was 69 dB due to the 19 dB of directivity provided by mounting the receive hydrophone in a parabola. Using these calculated values a 0 d B target strength object at pier 2 would have a -1 dB signal-to-noise ratio at the receiver prior to processing by the replica correlator.

Only the stern portion of the vessel was in the path of the sonar beam so it would be incorrect to use the integrated target strength reported for ships of this class to predict the systems performance. Because the diameter of the sonar beam 366 meters (1200 ft) from the transducer was approximately 13 meters (43 ft) only a small section of the stern was in the beam. To estimate the target strength as seen by this sonar, the calculations assumed simple geometries for the major reflectors and that all of the echoes added incoherently. Assuming that one edge of the beam was located on the aft edge of the rudder, and using smooth convex shape approximations for the geometry of the rudders and skeg, the ensonified surface of a Bear class cutter should have an integrated target strength of about -3 dB. This would yield a calculated precorrelation signal-to-noise ratio of -4 dB. The actual signal-to-noise ratio at the input to the correlator varied from 5 dB to less than 0 dB which is consistent with the values calculated above.

Figure 5.11a-d shows the results when the Bear class cutter Seneca (WMEC 906) was used as a target of opportunity. Figure 5.11a is a plot of the received signal prior to processing by the replica correlator. The uncorrelated receiver data is not particularly useful for target detection. The large peak at approximately 146 meters (80 ft) is a noise spike and not an actual target while the Seneca echoes are weak and barely visible at 366 meters (1200 ft). Figure 5.11b shows the output of the receiver correlator for this transmission. There is no peak present at the location of the noise spike, but the large peaks from the targets at

the Coast Guard station can be seen clearly. Figure 5.11c is an expanded view of the correlator output showing the peaks from the entire Coast Guard Station while the remaining plots show enlargements of the peaks from the Seneca. To provide a convenient scale for estimating the spacing between the various objects on the expanded plots, the zero point on the abscissa is not referenced to the transducer location, but instead is referenced to an arbitrary point near the group of echoes. The ordinate is also scaled to provide an indication of the relative size of the correlator peaks.

Figure 5.11c shows pier 1, the cutter Seneca, and another peak believed to be from the cutter moored on the opposite side of the pier. An examination of the individual correlator peaks reveals that the echo from the pier structure is broad and diffuse in nature, consistent with a pier supported by numerous pilings and underwater trusses. The next set of peaks consist of returns from various structures on the Seneca itself. The boxed area in Figure 5.11c indicates the region that was expanded in Figures 5.11d-e. The structure of the stern section is clearly evident in the correlator output. A schematic view of the stern is shown in Figure 5.12 along with the locations of the corresponding peaks from the sonar output. In this figure the correlation peaks are locally aligned to the schematic by assuming that the first one is from the center of the starboard screw. Table 5.7 shows a comparison between the location of the centerline of the major stern structures, as obtained from the ship's plans, and their positions as determined from the sonar data. The echoes are not expected to be exactly at the position

of the centerline since all of the detected objects have thicknesses greater than the width of the correlation function. The actual echo location then should be before the centerline location. It is difficult to predict the exact location where the echo should appear since the rudders and skeg are curved faired surfaces which cause the apparent thickness as seen by the sonar to change with the orientation of the surface. As expected, the locations of the majority of the echoes suggest that most of the reflected energy is concentrated at a point midway between the surface and centerline of these faired objects. Table 5.8 shows the thickness of the rudder and skeg at the widest points obtained from the drawings versus the extent of the echoes associated with these objects.

One interesting point to observe from Figure 5.11e is that the closest screw and rudder have a lower peak amplitude than the pair on the other side of the vessel. This was consistently observed from all of the data analyzed from that target during this experiment. Since this ship class uses variable pitch screws, a possible explanation is that the blade pitch and the screw orientation were different between the two screws. The port screw may have been in a position where the blades were more normal to the sonar beam thereby producing a stronger echo. Similarly, the rudders may have been at slightly different angles which would cause them to have different target strengths. The correlator outputs corresponding to the rudders and screws have multiple peaks, indicating that these objects are not acting as a simple point specular reflector. As a result, additional information about the geometry of the rudders and

screws may be present in these outputs and further investigation of the data's fine grain detail is warranted.

The skeg is a large, essentially planar, structure extending down from the keel to the baseline of the vessel and terminating just forward of the screws. While the skeg is partially filled with lead ballast, the rest of it is filled with air, which should provide a high target strength reflector. This object corresponds to the largest peak shown in Figure 5.11d-e along with additional smaller peaks trailing the primary one. Again this indicates that more information about the geometry of the structure producing the echo may be available in the data.

There are two other strong sonar returns present in Figure 5.11d-e. The last peak probably corresponds to the bow of another cutter which was moored on the far side of pier 2. The closer peak is a relatively strong echo with a very symmetric correlation function in contrast to the other echoes. Unfortunately this peak is 10.2 meters (33.4 ft) from the Seneca's starboard screw which places the return far to the port of any known structure. The echo does appear to be associated with the ship since it was not detected in subsequent experiments when the ship was underway. One possibility is that the echo is from an air-water interface in an internal tank, but this can not be confirmed with the available ship's plans.

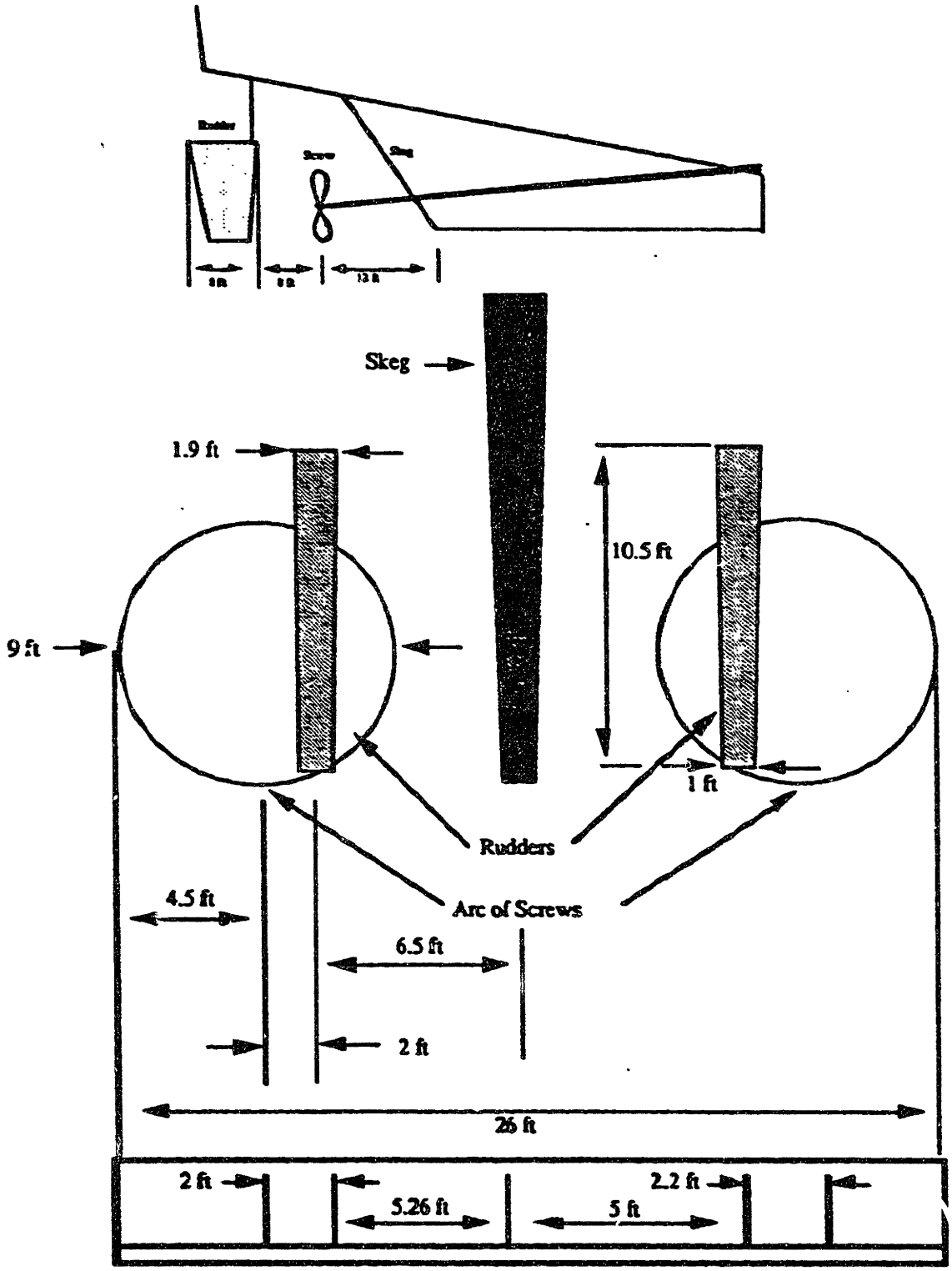

Figure 5.10a-b

Figure 5.10a. Side view of the Seneca which shows the locations of major stern structures and their relative orientation to each other.

Figure 5.10b. Stylized stern view of a Bear class medium endurance Coast Guard Cutter. Distances are shown in feet to correspond to the vessel drawings. The box at the bottom indicates the locations of the correlator peaks shown in Figure 5.11d-e. The first peak is assumed to be generated at the centerline of the starboard screw. Note that the positions of the objects inferred from the correlator peak locations are in very close agreement to the actual structure positions. The distances between the correlator peaks were calculated by assuming an average sound velocity of 1463 meters/sec (4800 ft/sec).

Component	Actual Distance	Distance as Measured from Correlator Output
Starboard Screw	0 meters	0 meters
Starboard Rudder	0.6 meters (2 ft)	0.6 meters (2 ft)
Skeg	2.6 meters (8.5 ft)	2.2 meters (7.3 ft)
Port Rudder	4.6 meters (15 ft)	4.4 meters (14.3 ft)
Port Screw	5.2 meters (17 ft)	5.0 meters (16.5 ft)

Table 5.7 Distances from various components on the Seneca referenced to the center of the starboard screw.

The actual distance is to the centerline of the object as determined from the vessel's plans. Measured distance is calculated from the maximum correlator output location for the particular component. The sound velocity was assumed to be 1463 meters/sec (4800 ft/sec).

Component	Actual Maximum Thickness	Extent of Correlation Peaks
Starboard Rudder	0.58 meters (1.9 ft)	0.42 meters (1.4 ft)
Skeg	0.76 meters (2.5 ft)	0.64 meters (2.1 ft)
Port Rudder	0.58 meters (1.9 ft)	0.3 meters (1.0 ft)

Table 5.8 Extent of correlation peaks from the Seneca echoes

A comparison of the thicknesses of the rudder and skeg on the Seneca as determined from the vessel's plans versus the extent of the sonar correlator output peaks identified with these structures.

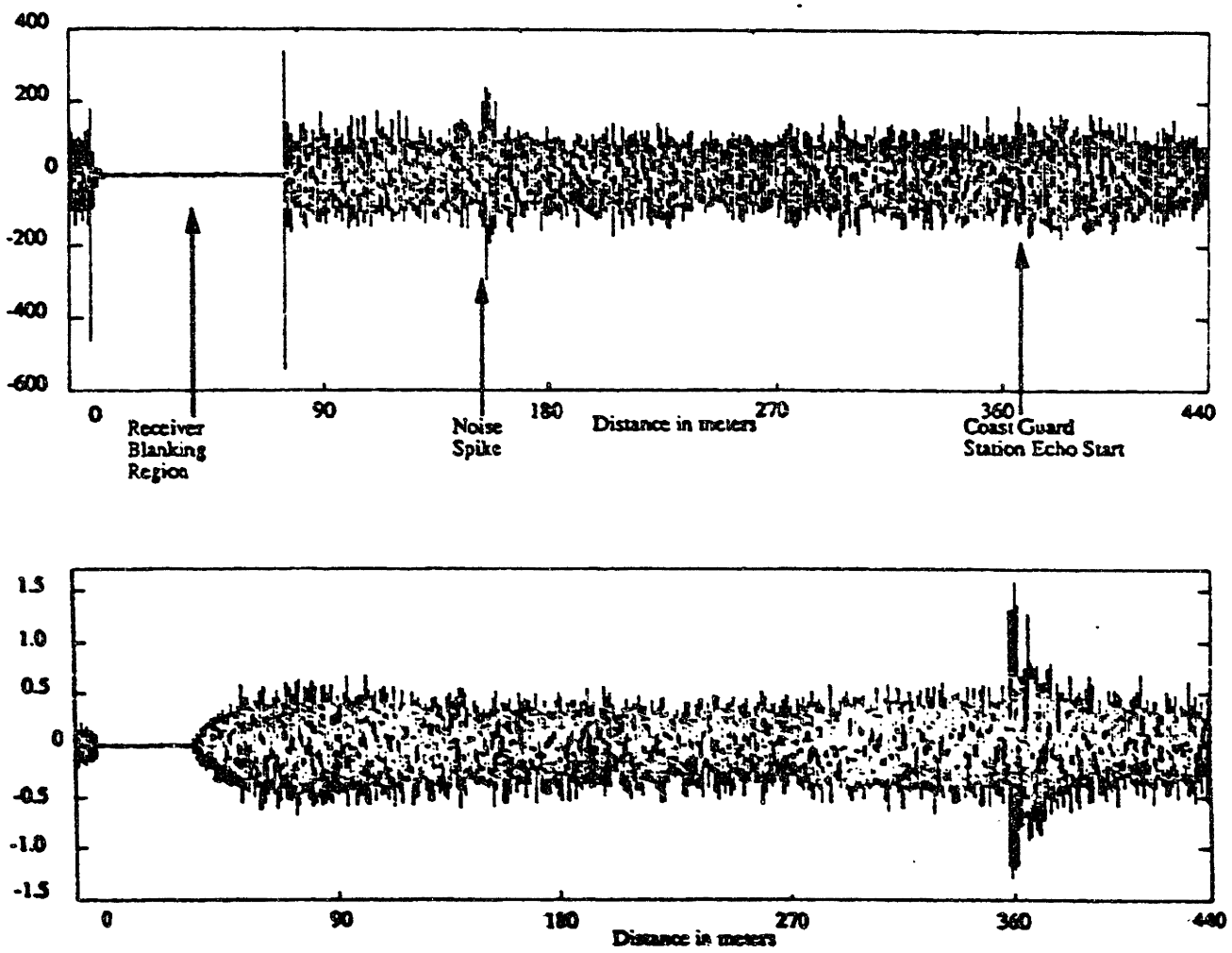

Figure 5.11a-b. The upper plot is the received signal prior to processing with the replica correlator. The signals from the Coast Guard base targets are buried in the noise. The lower plot shows the same data after replica correlation. Now the targets are clearly visible. The scale has been adjusted to correct for the correlator group delay.

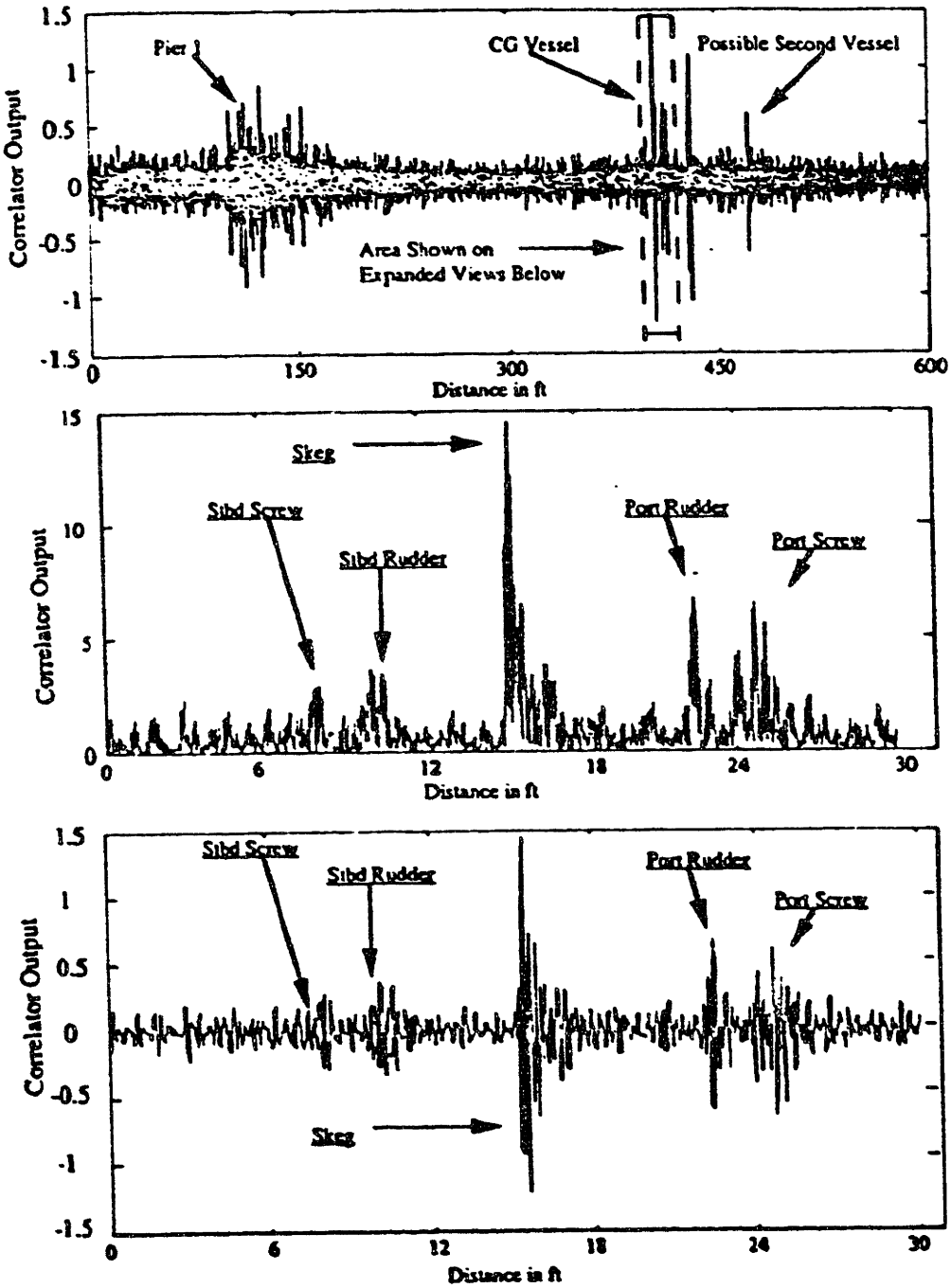

Figure 5.11c-e. The top figure is an expanded view of the echoes seen in figure 5.11b. The area in the rectangular box is further expanded in figure 5.11d to show only those echoes associated with the Seneca. Echoes from prominent structures on the stern of the Seneca are visible in this plot. 5.11e is the same plot except the signal is plotted without taking its absolute value.

These results also indicate the ability of this sonar to directly measure target range and speed. The measurement of absolute range is primarily limited by uncertainties in the exact propagation path and sound velocities between the sonar and the target. However, the difference in range between objects on the same target can be measured very accurately. This data could be used to infer target course from a single sonar transmission by measuring the range difference between widely separated points on the same vessel such the bow and stern. The ambiguity surface for this signal has a Doppler uncertainty of .73 meters/sec (2.4 ft/sec) or 1.4 kts. When the data was processed through a bank of replica correlators corrected for Doppler the measured velocity was .6 kts which is consistent with the motion of the test barge supporting the sonar arrays. There are many contact motion analysis algorithms that would quickly converge to a solution with independent range and speed measurements of this quality.

This experiment conclusively demonstrates the high resolution capabilities of this system. The combination of a signal designed to provide very precise time delay measurements with a parametric array which produces very narrow sonar beams results in a capability to resolve individual structures from a complex target. The information available from the processed receiver data is sufficient to significantly assist in classifying sonar targets. In addition to providing detailed information on the location of the major components comprising the stern of this ship, the correlator

output associated with each object also appears to have fine grain structure which could provide additional classification information.

Finally, these results were obtained at a realistic range, in a noisy environment, and in extremely shallow water using very low power sonar signals. The acoustic power produced at the difference frequency was only 1 Watt. While the low power operation was unintentionally caused by design problems in the transmitter, these results show that a low powered parametric sonar can be useful. Besides the low transmit power, the receivers were hampered by considerably more noise than would be present in most environments. The temporal variability of the noise was dramatic, routinely varying through a 20 dB range throughout the day Since the water depth was always less than 13 meters (43 ft), boundary reverberations from the surface and bottom would have made it impossible for many conventional sonars to operate in this environment. The parametric array's narrow beams along with it's lack of sidelobes dramatically reduced the reverberations. In fact, a later experiment at the same site using 250 Watts of acoustic power at the difference frequency did not have significant boundary reverberation.

Chapter 6

Conclusions And Recommendations For Future Work

6.0 Conclusions

Pseudorandom broadband pulses used in conjunction with parametric transmit arrays can significantly improve the performance of high resolution active sonar systems. This project successfully designed, constructed and tested a wide-band active sonar system employing pseudorandom broadband pulses and a parametric transmit array. The experimental program demonstrated that this system was capable of generating exceptionally high resolution images of complex targets.

Parametric arrays are capable of transmitting pseudorandom broadband signals generated by PSK modulation. There was no significant degradation in the active signal caused by the parametric array. By using PSK modulation the potential for the array gain to vary over the bandwidth of the signal is eliminated. This avoids problems such as the attenuation of the low frequency portion of wide-band LFM pulses that occurs when swept frequency signals are transmitted by parametric arrays.

The parametric array's narrow beamwidth and absence of detectable sidelobes can be used to achieve high azimuthal resolution. The narrow beamwidth allowed selected portions of a sonar target to be imaged. Multipath interference problems can be substantially reduced by steering the narrow beam to exploit the

optimum eigenray and minimize the excitation of undesirable eigenrays. In addition, these features allow the system to operate in very shallow water by reducing volumetric and boundary reverberations.

The small size of the parametric array permits low frequency wide-band systems to be constructed without prohibitively large transmit arrays. This could greatly extend the achievable range of high resolution systems by exploiting the lower attenuation loss at low frequencies. Throughout these experiments a two degree beam was formed at 10 kHz using a transducer which was only 330 mm in diameter. Wide-bandwidths are also easily achievable with a parametric array.

There is a substantial conversion efficiency loss associated with parametric arrays. Nevertheless, this penalty can be more than offset by the advantages offered by this system. The high resolution images of the U.S Coast Guard cutter Seneca in shallow water could not have been obtained with conventional systems.

6.1 Future Work

At the completion of the experimental program a new transmitter system was designed and briefly tested. This new system is capable of transmitting 250 Watts at the difference frequency when operating at a low duty cycle. Preliminary experiments with this new transmitter have been very promising. The current environmental conditions preclude conducting a quantitative assessment of the system's performance due to a sharp

negative sound velocity gradient which limits the maximum range to less than 50 meters. As winter approaches and the harbor sound velocity profile becomes more isovelocity the test program will resume.

Initial testing with the new transmitter will focus on obtaining quantitative performance estimates. Permits have been issued to moor sonar test targets in Boston Harbor in order to conduct this investigation. These targets will include spheres, cylinders, and other simple geometries. The echoes from these targets will also be used to evaluate the possibility of using this type of system to extract target classification information. These experiments will attempt to exploit the wide-band nature of this system in determining the target's form function. The high resolution in estimating time delay will also be used to evaluate nonspecular echoes from the target.

After the quantitative performance assessments are complete another experiment is planned to evaluate the use of this sonar in a synthetic aperture application. By exploiting the coded waveforms it might be possible to increase the speed of the vehicle and enhance the performance of a synthetic aperture sonar. Additionally the high quality time delay estimates can be used to assist in focusing the aperture.

A major limitation in the current system is that it is restricted to a single beam which must be mechanically steered. The feasibility of building a multibeam parametric system which

can be steered electrically should be investigated. Previous work has shown that steerable systems are practical when the primary frequencies are relatively low but there is no evidence of a steerable system operating with the primaries in the hundreds of kilohertz region.

Additional work is required to determine the utility of this system at longer ranges. The effects of internal waves, multipath propagation, and boundary interactions must be investigated.

Appendix A

Computer Code for Near Real-Time Correlator and Waveform Generator

Near Real-Time Correlator

/ * A Think C routine designed to perform near real time correlation of active sonar signals. Any active signal which has the correlator coefficients stored in a file can be used as long as there is sufficient memory for the filter coefficients, the input data, and the final results. The system is designed for a Macintosh computer and stores the input data along with the correlator output results in the Macintosh heap. The correlator is implemented in the frequency domain using the overlap-save method. The FFT size used should be adjusted to optimize the efficiency of this system. In general the maximim size which will fit in the available memory should be used assuming the data record is much larger than the FFT size. In order to keep the flowpath of this algorithm as simple as possible to permit rapid modifications no attempt was made to optimize this code in terms of computation efficiency other than the basic concerns of FFT size. Since the input data is real, symmetry rules could be used in order to significantly reduce the number of complex multiplies. The trade of would be a significant increase in the number of memory manipulations required to provide the symmetric portion of the result. There is a time penalty associated with implementing this using the Array Processing Library which would offset much of the gain in reduced complex multiplies. Most of the time used by the routine is in acquiring and displaying the data. The final results are converted to analog using the daughter card and output to a display device such as a storage oscilloscope or an Tektronix RTD 710.

This routine uses the Spectral Innovations MacDsp hardware along with the Array Processing Library to perform near real time correlation of the received sonar

signal. The hardware configuration requires a dual channel A/D and D/A daughter board (model SIAD2C) and a MacDSP motherboard (model 256-KC). The only additional software required is the Spectral Innovations Array Processing library. This code was compiled using Think C versions 4.0 and 4.05. Other compilers may require changes to the code particularly in the use of type "short double" which has a size of 8 bytes in Think C and corresponds to type "double" used in many other C compilers. Another change is in forcing the result of "sizeof" to type "size_t" since Think C implements the result of "size_of" as "integer" instead of "size_t".

The correlator is written assuming that the input signal is on A/D channel 1 with a trigger present on channel 2. The trigger should be a +3V pulse and last for a minimum of two clock cycles on the A/D card.

The clock for the A/D is set using variable "sampleRate." The correlator results are output on D/A channel 1 using the same clock rate specified for the A/D.

The correlator expects a file containing the correlator coefficients to be present in the same folder as the correlator routine with the file name "signalno1.fil". This file should contain the filter coefficients in Matlab format. Note that if this file is generated on the Macintosh it must have the resource fork removed or the file will not be correctly opened by fopen. One method of doing this is to generate the file in Matlab using a routine like "Replicagen" and then run the file through the file translator routine using the MS-DOS conversion. This will strip the resource fork and put the file in a form where it will be correctly interpreted. The coefficient file is only read when the routine is initializing.

The output is scaled such that a 3V input signal which correlates perfectly with the replica produces a 3V output peak. This is done by reading in the replica from the Matlab file at initialization and correlating against the same coefficients reversed. The

scale factor is determined from this result. This routine is not limited to a 3V A/D card but will work with any daughter board which represents maximum voltage as 32767.0.

There is an error in the Spectral Innovations Array Processing Library which causes the result of the function A_Input_2ch to store the input from A/D channel 2 in the buffer allocated for channel 1. This routine is used to search for the trigger pulse on channel 2 of the A/D card. The code is patched to correct for this problem. When the Array Processing Library is updated and this problem corrected the line:

test=V_Sum(myDSPPtr1,10);

should be changed by replacing "myDSPPtr1" with "myDSPPtr2".

```
#include "APLib_dsp.h"

extern   void InitDSP(void);
extern   void FreeDSP(void);

main()

{

        InitDSP();
        Correlator();
        FreeDSP();

}


/ *     The primary routine. This routine performs all of the MacDsp operations and
implements the correlator   */


#include "APLib_dsp.h"
#include "tcuvlib.h"

void exit(int);

void InitDSP(void);
void FreeDSP(void);

void Init_Windows(void);
```

```
void ScalePlot_DSP(long DSPPtr, long size);

short           err, myMacDSPRefNum, IOBOARD, averages;
long            myDSPPtr1, myDSPPtr2, Corrbuffer, ioBuffDSPPtr, myReturnDSPPtr1;
long            DSPChansArr[2],nfft;
double          sampleRate, antiAliasFilter, gain;

/* Initialize DSP board */
void InitDSP(void)

{
        err = InitAllDSPMemMgrs();


        err = GetMacDSP(&myMacDSPRefNum, 0, 0, 0);

        printf("myMacDSPRefNum = %d \n", myMacDSPRefNum);

        err = LoadCode(myMacDSPRefNum);

        sampleRate = 62500.0;
        antiAliasFilter = sampleRate / 2.0;
        gain = 1.0;

        err = Set_DataAcqReg(myMacDSPRefNum,
                        &sampleRate, &antiAliasFilter, &gain, 0, 0, 0);


}

/* Free DSP arrays */
void FreeDSP(void)

{
        err = FreeDSPPtr(myDSPPtr1);
        if (err) printf("FreeDSPPtr1 err = %d \n", err);
        err = FreeDSPPtr(myDSPPtr2);
        if (err) printf("FreeDSPPtr2 err = %d \n", err);
        err = FreeDSPMemMgr(myMacDSPRefNum);
        if (err) printf("FreeDSPPtr2 err = %d \n", err);

}


/* Correlator */
void Correlator(void)
{
        FILE *fp;
        char name[20];
        int type, mrows, ncols, imagf, mn, numsave;
        short double *xr, *xi;
        float  xrconv[4088], xiconv, Scale, test;
        int     choice,inc;
        long    frameCount, frameSize;
        long    count;
        Ptr     MacPtrResult, MacPtr;
```

```
/*Initialize important parameters. Obtain memory space for the two Macintosh arrays. MacPtr is the pointer to the
* storage location of the acquired data. MacPtrResult is the pointer to the correlator results.*/

        frameCount = 20;
        frameSize = 4096;
        nfft=8192;

                        count = frameSize * frameCount * sizeof(short);

                        MacPtr = NewPtr(count);
                        if (MacPtr == 0) {
                                printf("Could not allocate Mac Array \n");
                                return;

                        }
                                MacPtrResult = NewPtr(count+2*nfft);
                        if (MacPtr == 0) {
                                printf("Could not allocate Mac Result Array \n");
                                return;
                        }
                        err = NewDSPPtr(myMacDSPRefNum, frameSize * 10, &ioBuffDSPPtr);
                        if (err) printf("New ioBuffDSPPtr err = %d \n", err);


/*Read in the coefficient data from the Matlab file "signalno1.fil."                                        */
        fp = fopen("signalno1.fil","rb");
        if (loadmat(fp, &type, name, &mrows, &ncols, &imagf, &xr, &xi)) {
                printf("\nRead error\n");
        }
        fclose(fp);

/* Convert the coefficients from double to single precision
        */
        for(inc=0;inc<mrows*ncols;inc += 1)
   xrconv[inc]=(float)*(xr+inc);
   mn=ncols*mrows;

   /*Get pointers to DSP memory to load the data and trigger pulse into also get the dispalaced pointer
  for the first good data point without circular convolution affects                                      */

              numsave=nfft-mn+1;
             err=NewDSPPtr(myMacDSPRefNum,8*nfft,&myDSPPtr1);
             if(err) printf("NewDSPPtr1 err = %d \n",err);
              err=NewDSPPtr(myMacDSPRefNum,40,&myDSPPtr2);
             if(err) printf("NewDSPPtr2 err = %d \n",err);
              err=NewDisplacedDSPPtr(myDSPPtr1,4*(mn-1), 4*(numsave), &myReturnDSPPtr1);
             if(err) printf("NewDSPPtr1 err = %d \n",err);



/* Get memory on the DSP card for the correlator filter coef                                               */
   err = NewDSPPtr(myMacDSPRefNum, 8*nfft, &Corrbuffer);
                        if (err) printf("New Corrbuffer err = %d \n", err);

/*Initialize the buffer by preload with zeros                                                             */
                        V_Fill(Corrbuffer, 2*nfft, 0.0);
```

```
/* Load the coefficients, scale to A/D range */
                                PutDSPFloat (&xrconv, Corrbuffer, mrows*ncols);
                                if ( err = GetLastErr() )
                                        printf("PlaybackFromArray err = %d \n", err);
                                Scale = 32767.0/(Scale = V_AbsMax_Value(Corrbuffer, nfft));
                                SV_Mult(Corrbuffer, Corrbuffer, nfft, Scale);
                                printf("Loading coefficient done \n");
                                V_RtoC(Corrbuffer ,Corrbuffer , nfft);

        free(xr);
        free(xrconv);
        if (imagf) {
                free(xi);
        }


/*Compute the scale factor for D/A conversion later */
                        V_Fill(myDSPPtr1, 2*nfft, 0.0);
                        CV_ROrd(Corrbuffer, myDSPPtr1, mrows*ncols);
                        C_FFT (Corrbuffer, nfft);
                                if ( err = GetLastErr() )
                                        printf("C_fft err = %d \n", err);
                                printf(" coefficient fft done \n");
                        C_FFT (myDSPPtr1, nfft);
                                if ( err = GetLastErr() )
                                        printf("C_fft err = %d \n", err);
                                printf("reverse coefficient fft done \n");

                        CVV_Mult(myDSPPtr1,Corrbuffer,myDSPPtr1,nfft);
                        C_IFFT(myDSPPtr1, nfft);
                        V_Real(myDSPPtr1, myDSPPtr1, nfft);
                        Scale = 32767.0/(Scale = V_AbsMax_Value(myDSPPtr1, nfft));

        do{

                printf("enter the number of averages <enter>: \n");
                scanf("%d", &averages);

  for(averages; averages >0;averages--){

/* Find the trigger on channel 2 then start. Read in 10 values and ensure the sum is =>6 to eliminate first
value read problem                                                                              */
        test=0;
        while(test < 6.0){
        A_Input_2ch(myDSPPtr1, myDSPPtr2, 10);
        test=V_Sum(myDSPPtr1,10);
        }


/*Get the sonar data and load it into Mac memory*/
                                CaptureToArray(MacPtr, frameCount, frameSize, ioBuffDSPPtr);
                                if ( err = GetLastErr() )
                                        printf("CaptureToArray err = %d \n", err);
/*                              printf("CaptureToArray done \n");                       */


                                for(inc=0;(inc*(nfft-mm+1))<=(frameSize*frameCount)-mm;inc++)
```

```
{

/*Load the data from Mac Memory onto the MacDsp card and convert to complex floating point format*/

                                PutDSPInt(MacPtr+2*(inc*(nfft-mn+1)-mn+1),myDSPPtr1,nfft);
                                if ( err = GetLastErr() )
                                        printf("PlaybackFromArray err = %d \n", err);
/*                              printf("Loading array done \n");*/
                                V_ItoF(myDSPPtr1,myDSPPtr1,nfft);
                                V_RtoC(myDSPPtr1,myDSPPtr1,nfft);

/*Take the fft of the data, multiply by the filter coef, inverse fft, scale, and send back to the Mac*/

                                C_FFT (myDSPPtr1,nfft);
                                if ( err = GetLastErr() )
                                        printf("R_fft err = %d \n", err);
/*                              printf("fft done \n");                  */
                                CVV_Mult(myDSPPtr1,Corrbuffer,myDSPPtr1,nfft);
                                C_IFFT(myDSPPtr1,nfft);
                                V_Real(myDSPPtr1,myDSPPtr1,nfft);



                                SV_Mult(myDSPPtr1,myDSPPtr1,nfft, Scale);

                                if(!(inc)) V_Fill(myReturnDSPPtr1, 100, 32500.0);

                                V_FtoI(myReturnDSPPtr1, myReturnDSPPtr1,numsave);

                                GetDSPInt(myReturnDSPPtr1,MacPtrResult+2*inc*(nfft-
mn+1),numsave);
}

/* Get the correlator results from Mac memory and send it to D/A channel 1                      */
        PlaybackFromArray(MacPtrResult, frameCount, frameSize,myDSPPtr1);


}

                printf("enter your choice then type <enter>: \n");
                printf("go on correlator:    1 \n");
                printf("quit correlator:     0 \n");
                scanf("%d", &choice);

        } while ( choice );

        DisposPtr(MacPtr);
        DisposPtr(MacPtrResult);

        err = FreeDSPPtr(ioBuffDSPPtr);
        if (err) printf("Free ioBuffDSPPtr err = %d \n", err);

                err = FreeDSPPtr(myDSPPtr1);
        if (err) printf("FreeDSPPtr1 err = %d \n", err);
}
```

```
/*Routine to read in correlator coefficient data from Matlab file                * /

/* From the file provided by Matlab.  Modified to function with Think-C
* by changing the type "double" to "short double" and forcing the result
* of sizeof to size_t.        Mods by JA Halsema:*/
/* Author J.N. Little 11-3-86  */


#include <stdio.h>

typedef struct {
    long type;  /* type */
    long mrows;  /* row dimension */
    long ncols;  /* column dimension */
    long imagf;  /* flag indicating imag part */
    long namlen; /* name length (including NULL) */
} Fmatrix;

loadmat(fp, type, pname, mrows, ncols, imagf, preal, pimag)
FILE *fp;       /* File pointer */
int *type;      /* Type flag: see reference section of guide */
int *mrows;     /* row dimension */
int *ncols;     /* column dimension */
int *imagf;     /* imaginary flag */
char *pname;    /* pointer to matrix name */
short double **preal;  /* pointer to real data */
short double **pimag; /* pointer to imag data */
{
        char *malloc();
        Fmatrix x;
        int mn, namlen;

        /*
         * Get Fmatrix structure from file
         */
        if (fread( (char *) &x,  (size_t)sizeof(Fmatrix), 1, fp) != 1) {
                return(1);
        }
        *type = x.type;
        *mrows = x.mrows;
        *ncols = x.ncols;
        *imagf = x.imagf;
        namlen = x.namlen;
        mn = x.mrows * x.ncols;

        /*
         * Get matrix name from file
         */
        if (fread(pname,  (size_t)sizeof(char), namlen, fp) != namlen) {
                return(1);
        }

        /*
         * Get Real part of matrix from file
         */
        if (!(*preal = (short double *)malloc(mn* (size_t)sizeof(short double)))) {
                printf("\nError: Variable too big to load\n");
                return(1);
```

```
        }
        if (fread(*preal, (size_t)sizeof(short double), mn, fp) != mn) {
                free(*preal);
                return(1);
        }

        /*
         * Get Imag part of matrix from file, if it exists
         */
        if (x.imagf) {
                if (!(*pimag = (short double *)malloc(mn*(size_t)sizeof(short double)))) {
                        printf("\nError: Variable too big to load\n");
                        free(*preal);
                        return(1);
                }
                if (fread(*pimag, (size_t)sizeof(short double), mn, fp) != mn) {
                        free(*pimag);
                        free(*preal);
                        return(1);
                }
        }
        return(0);

}
```

Waveform Generator Matlab Code Example

%%Built from Replica Generator to allow waveform generation in the Mac Replica Generator built after hard disc failure from pulse modulator. This program generates the correct correlator replica for the specified receiver sample rate. Code is provided for an FIR filter in order to correct for analog processing of the received signal prior to digitization. Also added pulse1.m to front so the program would be stand alone.

```
L=9;
slength= (2^L)-1 ;
%%sequence order
aout=zeros(1,slength);    %%initialize the output vector
F=zeros(L);               %%size the matrix
f=fliplr([1 0 1 1 1 1 1 0 0 1]);   %%f polynomial
a=[0 0 0 0 0 0 0 0 1];     %%sequence initialization
for n=0:L-1;
F=F+f(n+1)*diag(ones(1,L-n),n);%%make the matrix to compute G
end

G=a*F;                    %%compute G polynomial


%%now compute the sequence
```

```
f=f((L+1):-1:2);          %%put f and g into a decending powers order
G=G(L:-1:1);
rot=[L (1:L-1)];
for n=1:slength
aout(n)=G(L);              %%write to the output vector
G=G(rot);G(1)=0;           %%shift g one bit right

if aout(n)==1
G=(G | f)-(G & f);
end                        %%exclusive or f into g
end
```

```
%pulse modulator
%modified from mod5jan to include fftfilt and dyadic product to
compute signal which removed 'for' loop. Deleted aexpand changed
to signal everywhere deleted f2 Recovered after hard disc failure
8Jun91. Modified again to include 10April91 mods for arbitrary
sample rate. 9Jun91 Removed data computed in pulse1.m which was
added to the beginning of the program.

f1=174e3;
fs=800.0e3;
t=1/fs;
ang=atan(sqrt(slength));
BW=5e3;
dtime=1/(2*BW);
plength=dtime*(slength+5);

%%build the array for a sample rate with an integer number of
sample points per digit. Round up. Set the first column to NAN since
these have the wrong values. It is just a placeholder column.

ncols=ceil(dtime*fs);
signal=ones(1,ncols);
signal(1,1)=nan;
signal=[aout 0 0 0 0 0]'*signal;
%%Now remove the incorrect samples.
%First calculate which rows have a value in column 1 that should be
kept.

keep=1/(1-(ncols-dtime*fs));
```

```
signal(1:keep:length(signal),1)=signal(1:keep:length(signal),2);
signal=signal';
signal=signal(:)';
signal=signal(signal~=nan);
signal=2*ang*(signal- .5);
signal=exp(-i*signal);

%% These steps are used if filtering is desired.

%edge=BW*2*(t);
%bandstop=.05+edge
%f=[0 edge bandstop 1];
%m=[1 1 0 0];
%M=((-20*log10(.01))-13)/(2.324*.1);
%M=512;
%b=remez(M,f,m);
disp('Im here');
signal=fftfilt(b,signal,2^14);
signal=fftfilt(b,fliplr(signal),2^14);
signal=fliplr(signal);
%N=64
%M=(1 ./[1.5 1 .5 .25 .158 .079 .063 .0316 .0079]).^.5;
%F=[0 5/25 8/25 10/25 12/25 13/25 14/25 15/25 1];
%b=fir2(N,F,M,blackman(N+1));
%signal=filtfilt(b,1,signal);
disp('Im here');
%% Generate the upband signal and take the imag part

signal=exp(i*2*pi*f1*(0:t:plength-t)).*signal;
signal=imag(signal);
signal=signal(1:(length(signal)-5*dtime/t));
signal=signal + sin(184e3*2*pi*(0:t:(dtime*slength)-t)+ang-pi);


%%Plot and store
%p=spectrum(signal,1024);
%specplot(p,1/t);
%signal=signal(length(signal):-1:1)';
signal=signal/(max(signal));
%save sigmod signal
```

References

Bobber, R., *Underwater Electroacoustics*, Peninsula Publishing, (1988).

Berktay, H., "Possible Exploitation of Non-Linear Acoustics in Underwater Transmitting Applications," *J. Sound Vib.*(2) 435-461 (1965).

Berktay, H.O., "Nonlinear Acoustics," *Signal Processing, Proc. of the NATO Advanced Study Institute at Loughborough, Eng.*, Academic Press (1973).

Carlton, L. F., "Electrical Beamsteering of the TOPS Parametric Source," NUSC Tm No. TD124-105-75, 19 January 1976

Gold, R., "Optimal Binary Sequences for Spread Spectrum Multiplexing," *IEEE Trans. on Info. Theory*, Oct., 619-621 (1967).

Glisson, T.,*et al*, "On Sonar Signal Analysis," *IEEE Trans. on Aero. and Elec. Systems*, Jan., 37-49 (1970)

Hermand, J. and Roderick, W., "Delay-Doppler Resolution Performance of Large Time-Bandwidth-Product Linear FM Signals in a Multipath Ocean Environment," *J. Acoust. Soc. Am.* 84(5), 1709-1727 (1984).

Mellen, R. and Moffett, M., "Parametric Sonar Characteristics for Circular and Square Piston Projectors," *Scientific and Engineering Studies Nonlinear Acoustics 1954 to 1983*, Naval Underwater Systems Center (1984).

Muir, T.G., and Golsberry T.G., "Signal Processing Aspects of Nonlinear Acoustics ," Tech. Report, Univ. of Texas at Austin ARL, ARL-TR-80-38 (1980).

Muir, T.G., "Nonlinear Acoustics: A new Dimension in Underwater Sound," *Science, Technology, and the Modern Navy*, (E.I. Salkovitz, Ed.) U.S. Govt. Printing Office (1977).

Novikov, B.K., Rudenko, O.V., Timoshenko, V.I., *Nonlinear Underwater Acoustics*, Acous. Soc. Am.(1987).

Oppenheim, A., and Schafer, R., *Discrete-Time Signal Processing*, Prentice Hall (1989).

Programs for Digital Signal Processing, IEEE Press, John Wiley and Sons, (1979).

Quazi, A.Z., Konrad, W.L., "Underwater Acoustic Communications," *IEEE Communications Magazine*, March, 24-30 (1982).

Rolt, K. and Irza J., "Sonar Transducer Electro-Acoustic Equivalent Circuit Models for CSDL Sound Gear," Charles Stark Draper Lab. (1991).

Skolnik, M. I., *Radar Handbook*, McGraw-Hill Publishing (1990).

Stewart, J.L., Westerfield, E.C., "A Theory of Active Sonar Detection," *Proc. IRE*, vol. 47, May, 872-881(1959).

Schulkin, M. and Marsh, H., "Sound Absorption in Sea Water," *J. Acoust. Soc. Am.* 34, 864-865 (1962).

Urick R., *Principles of Underwater Sound*, McGraw-Hill Publishing (1983).

Van Trees, H.L., *Detection, Estimation, and Modulation Theory*, John Wiley and Sons, (1971).

Van Trees, H.L. "Optimum Signal Design and Processing for Reverberation-Limited Environments," *IEEE Transactions on Military Electronics*, July-Oct, 212-228(1965).

Westervelt P., "Parametric Acoustic Array," *J. Acoust. Soc. Am.* 35(4), 535-537 (1963).